Fourth International Workshop

Computational Experiment in Aeroacoustics CEAA2016

September 20-24, 2016

Svetlogorsk, Kaliningrad region
Russia

Book of abstracts

MOSCOW – 2016

УДК 533:534.2
ББК 26.233

Computational Experiment in Aeroacoustics. CEAA2016: Fourth International Workshop, Svetlogorsk, Kaliningrad region, Russia, September 21-24, 2016: Book of abstracts. – Moscow: Keldysh Institute, 2016. – 150 p.
ISBN 978-5-98354-026-2

The Book of abstracts represents the talks of participants of the Fourth International Workshop “Computational Experiment in Aeroacoustics” (CEAA2016) which is organized by Keldysh Institute of Applied Mathematics of Russian Academy of Sciences, Moscow, Russia, with assistance of Central Aerohydrodynamical Institute (TsAGI), Zhukovsky, Russia, and Immanuel Kant Baltic Federal University, Kaliningrad, Russia, under financial support by the Russian Foundation of Basic Research (Grant No. 16-01-20500) and official sponsors. The Workshop is held in Svetlogorsk, Kaliningrad region, Russia, September 20-24, 2016. The Book consists of abstracts of invited lectures and technical presentations.

УДК 533, 534.2
ББК 26.233

Makeup: *L.V. Dorodnitsyn*
Cover: *A.V. Gorobets*

ISBN 978-5-98354-026-2

ORGANIZER

Keldysh Institute of Applied Mathematics of Russian Academy of Sciences (KIAM), Moscow, Russia

with assistance of

Central Aerohydrodynamical Institute (TsAGI), Zhukovsky, Russia

Immanuel Kant Baltic Federal University, Kaliningrad, Russia

FINANCIAL SUPPORT

Sukhoi Aviation Holding Company

Russian Foundation of Basic Research (Grant No. 16-01-20500)

Russian Helicopters

Central Aerohydrodynamics Intstitute (TsAGI)

Central Institute of Aviation Motors

TESIS

International Commission for Acoustics

ORGANIZING COMMITTEE

Chairmen

Boris CHETVERUSHKIN, Prof., Full member of RAS, Keldysh Institute of Applied Mathematics of RAS, Russia
Tatiana KOZUBSKAYA, D.Sci., Keldysh Institute of Applied Mathematics of RAS, Russia

Members of Organizing Committee

Michael DUMBSER, Prof., University of Trento, Italy
Vladimir GOLUBEV, Prof., Embry-Riddle Aeronautical University, USA
Charles HIRSCH, Prof., Vrije Universiteit Brussel, Belgium
Jerome HUBER, Dr., AIRBUS OPERATIONS SAS, Toulouse, France
Marc JACOB, Prof., ISAE-SUPAERO, Toulouse Area, France
Sergey KARABASOV, D.Sci., Queen Mary University, London, UK
Viktor KOPIEV, Prof., Central Aerohydrodynamics Intstitute (TsAGI), Moscow, Russia
Alexey KUDRYAVTSEV, D.Sci., Khristianovich Institute of Theoretical and Applied Mathematics of SB RAS, Novosibirsk, Russia
Ulf MICHEL, Prof., Dr.-Ing., CFD Software E+F GmbH, Berlin, Germany
Alexey MIRONOV, Dr., Central Institute of Aviation Motors (CIAM), Moscow, Russia
Mikhail STRELETS, Prof., Peter the Great St.Petersburg Polytechnic University, Russia
Vladimir TITAREV, Dr., Dorodnicyn Computing Center of FRC CSC RAS, Moscow, Russia
Xin ZHANG, Prof., Hong Kong University of Science and Technology, HONG KONG

LOCAL ORGANIZING COMMITTEE

Anatoly ALEXANDROV, KIAM
Vladimir BOBKOV, KIAM
Ludwig DORODNICYN, Lomonosov Moscow State University
Alexey DUBEN, KIAM
Andrey GOROBETS, KIAM
Tatiana KOZUBSKAYA, KIAM (Coordinator)
Larisa SOKOLOVA
Mikhail SURNACHEV, KIAM

LECTURES

SIMULATION OF AIRCRAFT INSTALLATION NOISE – A KEY TO LOW NOISE AIRCRAFT DESIGN

Jan Delfs

DLR – Deutsches Zentrum für Luft- und Raumfahrt e.V.
Institute of Aerodynamics and Flow Technology, Technical Acoustics Branch
38108 Braunschweig, Germany, Jan.Delfs@dlr.de

Introduction

Classically, aircraft component noise research has been conducted (i) to identify a link between local flow features, component design parameters and the resulting aerosound generation and (ii) to derive means for noise reduction at the source. Component sources traditionally have been categorized into engine noise on the one hand and airframe noise on the other hand as depicted in Fig. 1.

The ACARE acknowledges that restricting R&T to single a/c components will furtherly not suffice to meet the objective of -10dB per aircraft operation in 2020 as set out by the strategic paper "Vision 2020" of the EU in 2001. In addition, these so called 1st and 2nd generation noise reduction technologies have to be considered in combination with low noise aircraft architectures [1]. This is even more valid for the longer term view, described in the document "Flightpath 2050" of ACARE. In view of noise, another aspect of the development of transport aircraft is of concern, which is driven by fuel savings and environmental requirements. This aspect concerns the increase in size of the aeroengines of modern conventional aircraft: one will see classical sources of noise diminish, while new sources, related to the close integration of engines and wing, will occur. In order to either include the consideration of novel aircraft architectures or the closer integration of components for conventional aircraft both bring a new category of noise into the picture, namely installation noise.

Installation noise has two important aspects, one related to sound generation and one related to sound radiation, although in special cases this distinction may be difficult to make.

Installation sound sources are characterized by the fact that two aircraft components, which may or may not be sources themselves in isolated situation, generate a source as a result of their particular arrangement at the aircraft. In this case typically one of the components exerts an aerodynamic effect onto the other component which results in a strongly increased radiation from the latter.

Fig. 1. Installation related sources of aerosound at transport aircraft

There are situations, in which the mentioned aerodynamic effect of the first component may even reduce the sound radiation of the second component (beneficial effect). In a way the (tonal) sound radiation of the (subsonic) fan of a turbofan engine may be regarded as an installation source because neither fan rotor nor fan stator in isolation would radiate tonal sound while only in their respective combination sound would be radiated out of the fan duct. The most important installation related sources and source effects are sketched in Fig. 2 for a conventional transport aircraft.

Acoustic installation refers to the effect the airframe or parts of it has on the radiation of some noise sources on the aircraft. As depicted in Fig. 3 acoustic installation occurs as a result of sound reflection, diffraction at the aircraft body and also sound refraction in the associated shear- and boundary layers. In comparison with the radiation from the isolated sources of noise at an aircraft the related acoustic installation effects may increase or decrease the sound amplitudes reaching the observer at the ground. This depends again on the arrangement of the source with respect to the rest of the aircraft.

It is to be mentioned that installation noise is not only an issue for community noise of aircraft but as well for cabin noise. Any source noise increase due to installation (e.g. due to boundary layer ingestion of the engine intake) will potentially also negatively affect cabin noise excitation. The same is true for acoustic installation issues, i.e. any engine noise reflected off the fuselage will potentially increase cabin noise excitation as well. Also in this case refraction and even turbulent scattering may heavily influence amplitudes and phases of the pressure on the fuselage skin, which causes it to vibrate and generate cabin noise.

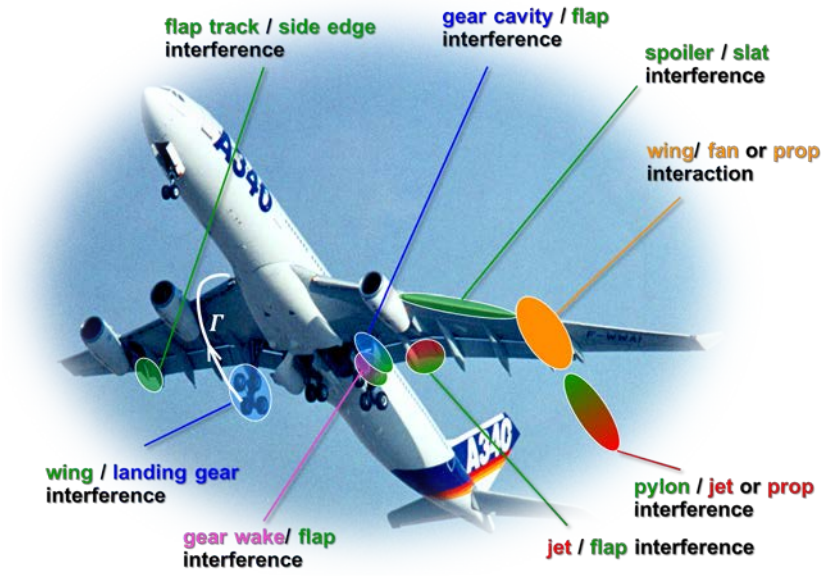

Fig. 2. Installation related sources of aerosound at transport aircraft

Challenges

Considerable difficulties are involved in simulating installation noise experimentally and computationally. On the other hand the above discussion shows that installation noise represents a non-negligible issue if overall aircraft noise is of concern. In comparison to studying single component sources installation sources generate extra difficulties due to the necessity to take into account at least two a/c components in their unsteady aerodynamic interaction, which requires either relatively large wind tunnels and/or large computational resources.

The simulation of realistic acoustic installation effects at complete aircraft pose considerable challenges as well. Experimental simulation in acoustic wind tunnels suffer from the difficulty that necessarily complete aircraft models are required, which necessarily leads to considerable downscaling and corresponding upscaling of frequencies, which are hard to measure. Also Reynolds numbers may become unrealistically small. Moreover, realistic turbofan engine sources at this small size are not available today. The computational side is challenging as well. A full scale aircraft acoustic installation noise simulation up to relevant frequencies of –say 5kHz- is beyond the capabilities of today's computers if all viscous mean flow effects are to be taken into account, by solving e.g. the Linearized Euler Equations.

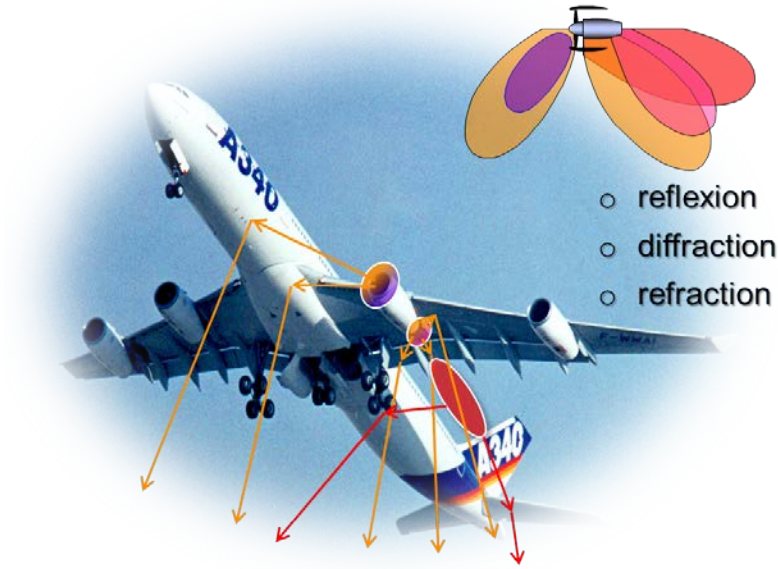

Fig. 3. Acoustic installation effects at transport aircraft

Current conventional aircraft represent configurations at which a relatively clear distinction exists among the various components as e.g. the engine, the pylon, the wing system, the fuselage and the empennage. The classical design philosophy of aircraft has been implying that the overall aircraft system is understood as a synthesis these distinct aircraft components each of which represent a distinct function. In such case the overall aircraft noise may be looked at as superposition of single component noise sources.

However, even for conventional aircraft of the most modern generation installation sources will be important contributors to the overall aircraft noise, and therefore need to be described appropriately. Most notably the (efficiency driven) required increase of the turbofan engine size (UHBR engines) for a given airframe necessarily leads to a much higher degree of integration between engine nacelle and the wing. In fact, the integration may become so close that nacelle and wing locally merge into one aerodynamic system, where no distinction between engine on the one hand and wing on the other hand may be made anymore. This situation naturally carries over to the aeroacoustics of engine and wing, leading to new sources as e.g. the jet flap interference source (neither being engine nor airframe noise). For “modernized” current aircraft even today acoustically important questions naturally arise as e.g. whether the jet noise reduction achieved by using UHBR engines will be over-compensated by a noise increase which is expected due to increased levels of JFI, see e.g. Fig. 4.

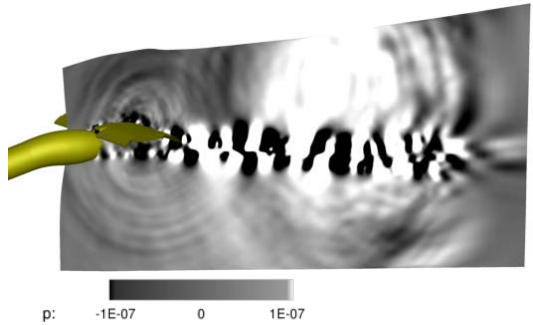

Fig. 4. 3D CAA simulation of jet flap interaction noise experiment in DLR's acoustic wind tunnel AWB (dual stream cold jet and high lift airfoil)

Objectives

From the above reasoning installation noise cannot be neglected for the assessment of modern conventional aircraft and more intensive research in prediction and design is required. Moreover, according to [2] one of three requirements of ACARE on future noise research is to "very significantly increase the effort dedicated to Low Noise Aircraft configurations". This particularly implies to develop means to experimentally and computationally study installation effects and complete aircraft noise. The new quality is that such prediction methods have to be raised to high fidelity computation methods because one is venturing into unknown terrain. Experience with low noise aircraft cannot be gained by flight test like for conventional aircraft; also semi-empirical prediction models are naturally not available.

Content of lecture

The paper will discuss some results of experimental and recent computational studies of DLR on installation sources from which estimates for the relevance of installation sources at conventional aircraft are drawn. Based on these, first thoughts are derived on variations to potentially more silent tube and wing aircraft configurations. Some computational results on noise shielding are discussed in detail, combined with the warning that for certain conditions, the usual neglect of viscous flow effects may lead to very large errors in predicting the attenuation even at low flight Mach numbers.

References

1. http://www.xnoise.eu/about-x-noise/projects/generation-2-projects/openair/
2. ACARE "Activity Summary 2014-15" http://www.acare4europe.com/documents/acare-annual-report

AIRFRAME NOISE MODELING AND PREDICTION

Yueping Guo
NEAT Consulting, Seal Beach, California, USA,
yueping.guo@neat-consulting.com

While numerical simulation methods have progressed significantly in the past few decades [1], they still face difficult challenges in large scale realistic applications. In the aircraft industry, physics-based modeling is currently the dominant approach for acoustic design and prediction, where robustness, accuracy and quick turn-around time are some of the necessary features required for prediction tools. This paper discusses the development of physics-based methods for airframe noise modeling and prediction, and presents models for airframe noise components including the leading edge slats, the flap side edges, the landing gears, and the trailing edges. The technical approach includes analyzing and understanding the physical mechanisms of noise generation in the unsteady flows around the airframe, which is necessary to capture the dominant features of the flow process that are responsible for the noise generation. Noise sources for each airframe component are identified and analyzed to reveal their respective characteristics. The prediction models are then developed based on the fundamental theory of aerodynamic noise generation, by using a combination of statistical analysis, asymptotic expansion, dimensional scaling, and functional correlation. The prediction models are developed for each airframe noise component, including spectral features, far field directivity patterns, Mach number dependencies, and component amplitudes that are correlated to geometric and operational parameters. The total noise is then found by incoherent sum of the components. For each noise components, as well as for the total airframe noise, extensive validations are presented, covering a wide range of configurations from small scale component tests in wind tunnels to full configuration aircraft flight tests, to demonstrate the accuracy and robustness of this physics-based approach.

For large commercial transport airplanes, the major noise sources for the airframe are the leading edge slats, the flap side edges, the landing gears, and the trailing edges. The relative ranking order of the sources depends on the detailed design of the aircraft. For each of the four major sources, the physical mechanisms that are responsible for the noise generation are shown in Fig. 1. These individual source mechanisms are identified by analyzing various data from experiments [2–4]. Since noise components from different source mechanisms usually have different characteristics, the analysis of the far field noise functional trends can reveal the features of the sources. An example of the source and far field analysis is illustrated in Table 1, which lists various salient features associated with slat noise and its sources.

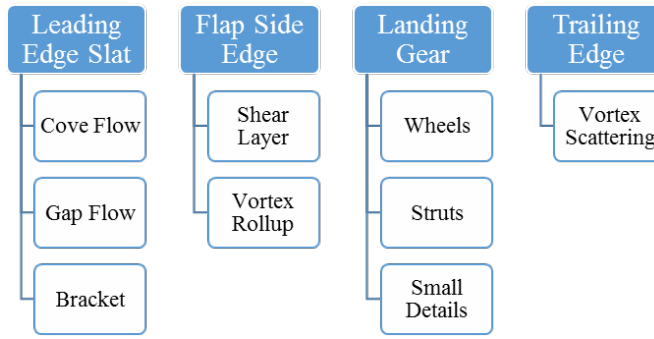

Fig. 1. Source mechanisms of airframe noise

Table 1. Slat noise source mechanisms and noise characteristics

	Cove	**Gap**	**Bracket**
Mechanism	Flow Separation and Vortex Oscillation	High Speed Flow and Edge Scattering	Bluff Body and Vortex/Strut Interaction
Directivity	Dipole Normal to Chord	Half Dipole	Dipole Normal to Strut Length
Spectrum	Broadband in Low and Mid Frequency Domain	Hump in Mid and High Frequency Domain	Narrow Hump in Mid and High Frequency Domain
Mach Scaling	5^{th} to 6^{th}	5^{th} to 6^{th}	6^{th} to 7^{th}
Amplitude	Slat, AOA, Gap, M	AOA, Gap, M	Local Flow, Strut, M
Length Scale	Slat Chord	Gap Width	Strut Size
Source Size	Chord × Span	Width × Span	Size × Length

The understanding of the source physics is the essential starting point for the modeling and prediction of the far filed noise. The technical approach is illustrated in Fig. 2. It starts with the theory of aerodynamic sound generation, either in the original form of the Lighthill acoustic analogy [5] or in its formal solutions in the form of the Ffowcs-Williams/Hawkings equation [6]. The latter is of particular relevance to airframe noise because of the low Mach number and high Reynolds number associated with flows at aircraft landing and takeoff conditions. The left part of the figure shows a path for the theoretical approach where explicit models are derived for the far field noise spectrum. This mathe-

matical derivation has been documented in detail in [7–9], which leads to the result

$$\Pi(\mathbf{x}) = \rho_0^2 c_0^4 A(\alpha,\gamma,\Lambda,b,S) W(M) F(f_d, M) D(\theta,\varphi) \frac{S}{\Delta^4 r^2} e^{-\alpha_0 r}. \qquad (1)$$

In this solution, the left hand side is the far field noise spectrum and the right hand side contains various symbols, each representing a parametric feature of the noise field, including spectral shape, directivity, Mach number dependence, amplitude correlation, and other parametric trends.

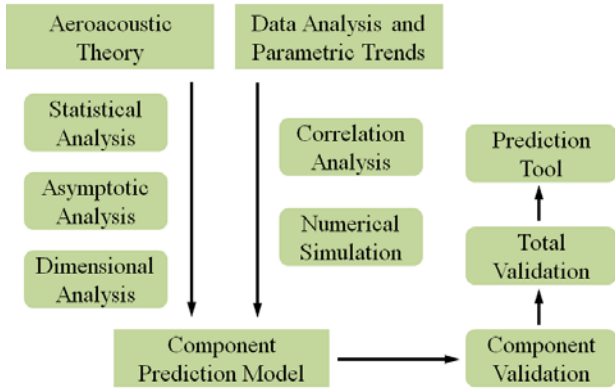

Fig. 2. Illustration of physics-based modeling approach

Table 2. Functional dependencies of physics-based noise model

Feature	Model	Modeling Approach
Ambient Medium	$(\rho_0 c_0^2)^2$	Dimensional Analysis
Amplitude	$A(\alpha,\gamma,\sigma,b,S)$	Correlation
Mach Number	$W(M)$	OASPL Scaling
Spectral Shape Function	$F(f_d,M)$	Source Statistics
Doppler Shift	f_d	Analytical
Directivity	$D(\theta,\varphi)$	Source Integration
Source Dimension	S	Dimensional Analysis
Convective Amplification	Δ^{-4}	Analytical
Spherical Spreading	r^{-2}	Analytical
Atmospheric Absorption	$e^{-\alpha_0 r}$	Empirical

A brief explanation for the parametric trends in Eq. (1) is given in Table 2, where the physical features of the far field noise are listed in the first column, their respective mathematical models are shown in the second column, and the approaches to derive these functional dependencies are explained in the last

column. These functional trends are derived by various methods, including analytical derivation, correlation analysis, and empirical data. The theoretical derivation and correlation analysis lead to prediction models for the airframe components, which are then validated by experimental data. The component validation includes the functional trends and the absolute amplitudes. The validated component models are finally integrated to total noise prediction tools which are further validated by aircraft system noise.

It is important to emphasize the critical step of validation in the modeling. The validation should be systematic, including both functional dependencies and the absolute amplitudes to achieve sufficient accuracy. Furthermore, the validations should include enough variations in the database to cover various configurations and flow conditions, to ensure the robustness of the prediction models. As an example, Table 3 shows the databases for the validation of landing gear noise models, covering a wide range of aircraft configurations, gear designs, and test conditions.

Table 3. Datasets for landing gear noise model validation

Gear Model	Configuration	Number of Wheels	Scale	Test Facility	Reference
Boeing 777	Isolated	6	6.3%	QFF	IJA 8(5)
Regional Jet	Isolated	2	40%	RTRI	AIAA 2010-3973
Airbus 320	Isolated	2	Full Scale	DNW	AIAA 1997-1597
Airbus 320	Isolated	4	Full Scale	DNW	AIAA 1997-1597
Boeing 737	Isolated	2	Full Scale	LSAF	J Aircraft 43(2)
Airbus 340	Isolated	4	Full Scale	DNW	AIAA 2000-1971
Boeing 777 QTD1	Installed	6 & 2	Full Scale	Flight	NASA Report 2002
Boeing 777 QTD2	Installed	6 & 2	Full Scale	Flight	AIAA 2007-3457
Boeing 747	Installed	4 & 2	Full Scale	Flight	J Aircraft 19(12)
Boeing DC-10	Installed	4 & 2	Full Scale	Flight	AIAA 1976-0525

It can be seen from the table that the smallest scale in the validation database is 6 percent, for a high fidelity Boeing 777 main landing gear, tested as an isolated gear in the NASA Quiet Flow Facility [10]. For this configuration, examples are given in Fig. 3, showing the comparisons between predictions and test data for the noise spectrum at 90 degrees emission angle in the flyover plane, as a function of frequency for four different Mach numbers. Apparently, the agreements between the two are good, both in the functional trends such as the spectr4al shape and Mach number variations, and in the absolute amplitudes. The accuracy of the prediction model shown in this figure is representative of all the other test cases for isolated gears.

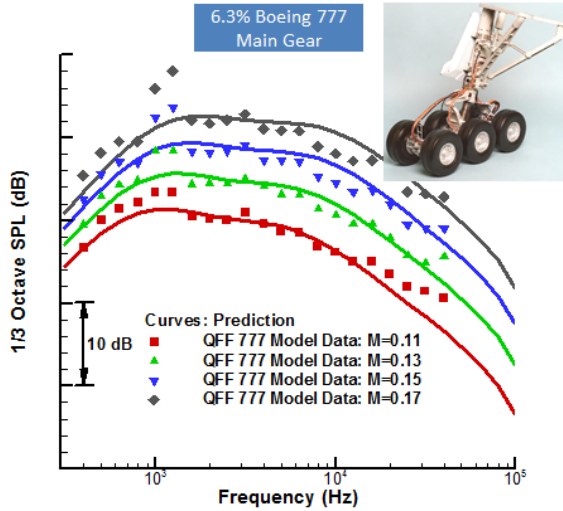

Fig. 3. Validation of landing gear noise model by wind tunnel test data

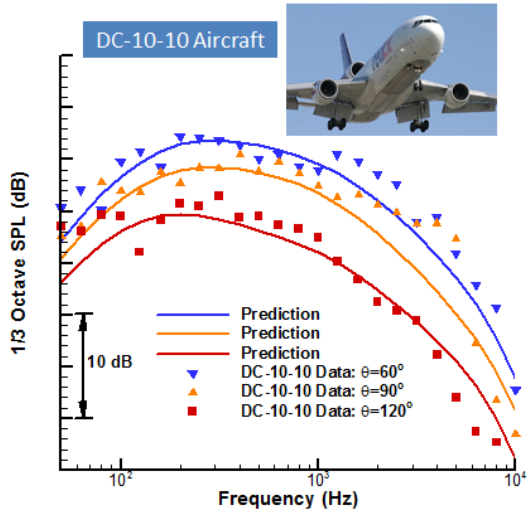

Fig. 4. Validation of landing gear noise model by flight test data

The table for the landing gear noise model validation also includes various full configuration aircraft flight tests, which not only contains both the nose and the main gears at full scale, but also accounts for various installation effects such as the local flow variations, convective amplification, and the noise reflection from the aircraft [11, 12]. These effects can significantly affect the

noise from the landing gears, and thus, need to be correctly modeled. Examples of full scale validation are given in Fig. 4, for the DC-10-10 aircraft [13]. The comparisons in the figure is the spectra at three different emission angles in the flyover plane, showing good agreements between the predictions and data. In comparison with wind tunnel test data for isolated gears, flight test data show more scatter, which is due to the fact that landing gear noise data in flight tests are derived by the difference between gear-up and gear-down flights, a feature present in all the flight test data.

References

1. Singer B.A. and Guo Y.P. Development of CAA Tools for Airframe Noise Calculations. International J. Computational Fluid Dynamics. **18**(6), 455–469, 2004.
2. Guo Y.P., Joshi M.C., Bent P.H. and Yamamoto K.J. Surface pressure fluctuations on aircraft flaps and their correlation with far field noise. J. Fluid Mech. **415**, pp.175–202, 2000.
3. Guo Y.P. and M.C. Joshi. Noise Characteristics of Aircraft High Lift Systems. AIAA Journal. **41**(7), 1247–1256, 2003.
4. Guo Y.P., Yamamoto K.J. and Stoker R.W. A Component Based Empirical Model for High Lift System Noise Prediction. Journal of Aircraft. **40**(5), 914–922, 2003.
5. Lighthill M.J. On sound generated aerodynamically I. General theory. Proc. Roy. Soc. Lond. **A211**, 564–587, 1952.
6. Ffowcs Williams J.E. and Hawkings D.L. Sound Generation by Turbulence and Surfaces in Arbitrary Motion. Phil. Tran. Roy. Soc. Lond. **A264**, 321, 1969.
7. Guo Y.P. Aircraft Slat Noise Modeling and Prediction. AIAA Paper 2010-3837.
8. Guo Y.P. Aircraft Flap Side Edge Noise Modeling and Prediction. AIAA Paper 2011-2731.
9. Guo Y.P. A statistical model for landing gear noise prediction. Journal of Sound and Vibration. **282**, 61–87, 2004.
10. Humphreys W. and Brooks T. Noise Spectra and Directivity for a Scale-Model Landing Gear. International Journal of Aeroacoustics. **8**(5), pp. 409–443, 2009.
11. Guo Y.P., Burley C. and Thomas R.H. Landing Gear Noise Prediction and Analysis for Tube-And-Wing and Hybrid-Wing-Body Aircraft. AIAA Paper 2016-1273.
12. Guo Y.P. Effects of Local Flow Variations on Landing Gear Noise Prediction and Analysis. Journal of Aircraft. **47**, 383–391, 2010.
13. Munson A.G. A Modeling Approach to Nonpropulsive Noise. AIAA Paper 76-525.

PECULIARITIES OF COMPUTATIONAL EXPERIMENT VALIDATION IN AEROACOUSTICS

V.F. Kopiev

Central Aerohydrodynamic Institute, Moscow, Russia, aeroacoustics@tsagi.ru

The problem of aviation noise reduction, which is studied within the field of aeroacoustics, is one of the most formidable one in aviation science, because major noise sources correspond to different types of turbulent flows around a flying vehicle (turbulent jets and wakes, turbulent boundary layer on the fuselage surface, etc.) for which there exist, in principle, no dynamical models allowing the description of subtle non-stationary processes responsible for noise generation. Investigation of these problems requires a unique experimental base that can provide the non-reflection conditions simultaneously with modeling the turbulent characteristics of flows. In this situation, numerical simulation could be a promising tool. Often, the studied problems cannot be modeled with using even the most modern experimental base, for instance, when the cruise conditions should be reproduced. Numerical simulation then becomes the only direct method of acquiring the necessary knowledge.

However, application of numerical methods for solving aeroacoustic problems encounters significant challenges that have no analogies in solving traditional problems of aerodynamics. The necessity to simultaneously resolve many characteristic space-time scales with numerical methods that have small dispersion and small dissipation renders these problems very expensive from the viewpoint of required computational resources. An important peculiarity of aeroacoustic problems consists in the necessity to perform non-stationary simulation for long physical times to collect the sufficient statistics for describing the random processes. The difficulties in achieving the compromise between the accuracy of the results and the required resources make numerical solution validation one of the key problems in aeroacoustics.

It is possible to distinguish three significantly different situations when attempting solution validation that take place in aeroacoustics now. In the first, and most typical situation for validation problems in general, there is an aeroacoustic experiment, while the numerical situation is absent. Such problems are represented, for instance, by isolated vortex noise. If turbulence is considered as a combination of isolated vortex structures, this problem becomes basic for aeroacoustics of turbulence. The recent results of the role played by intermittency in the turbulence structure show that it is desirable to understand the noise generation in this way, avoiding traditional representations of the structure of small-scale turbulence. However, even the problem of isolated vortex noise (e.g., vortex ring) requires computational resources that exceed the available capabilities. The presently available numerical results cannot be considered as

satisfactory. It is possible to formulate a hierarchy of intermediate problems that should be resolved numerically before approaching the modeling of vortex noise itself. At different stages there exist analytical results, and only the final stage of validation requires comparison of the final solution with physical experiment in an anechoic chamber. However, it would be desirable to validate not only the final solution, but also intermediate results obtained at preliminary steps for simplified model problems. That is, a counter problem arises, namely, to formulate and perform experiments that would enable validation not only of the final simulation of turbulence but also of the numerical modelling of the key mechanisms responsible for turbulization of an isolated vortex.

In the second situation, on the contrary, there is a high-quality numerical simulation which is quite difficult to validate by the experiment due to high costs of the experiment, and for the case of Russia due to the absence of the required experimental base. This primarily concerns turbomachinery noise, including aircraft propellers and helicopter rotors. The results obtained in large-scale facilities such as DNW, CEPRA-19, QinetiQ, OS-5 are rarely focused on the validation problems, with the exception of dedicated projects (e.g., ESWIRP project). Beside the problem of validation of numerical methods, a new problem of validation of small-scale experiments by the results of large-scale tests may arise. This may in turn allow validation of numerical methods using the validated small-scale experiments. The situation becomes significantly more complicated when one considers broadband rotor noise, when the main part of noise is related to turbulence characteristics of the flow around blades.

The absence of the required experimental base also gives rise to difficulties in validation of turbulent jet noise simulations in the cruise conditions, when the laboratory experiment cannot be performed at all. It can be hoped that the simulations validated by jet noise tests in an anechoic chamber (takeoff and landing conditions) will be able to predict jet noise in the cruise conditions as well.

In the third situation, validation of numerical methods allows formulating new problems aimed at identification of noise generation mechanisms. In a sense, both directions, experimental and numerical, support each other and help formulating the next steps in each of them. Therefore, despite seemingly well-developed methods of turbulent jet noise measurements, further development of the experimental techniques is required that aim at more accurate measurement of nearfield and farfield structures, including the jet excited conditions when it is possible to directly see in the experiment the objects responsible for noise generation. Numerical methods that use parallel computing and most significantly developed in this field of aeroacoustics, in their turn should allow determining the structure of noise sources for validation of theoretical ideas, including further development of correlation theories.

It can be expected that numerical simulation of this top-priority problem has reached the quality that is sufficient not only for engineering objectives, but also for obtaining the answer to many fundamental questions, including determination of the structure of noise radiating turbulence, determination of space-time and correlation characteristic peculiarities of noise sources etc.

Indeed, it can be attempted to validate many results by flight test measurements; however, it implies that there are software adapted to the conditions of aircraft flyover when noise is coming from a combination of different sources. In this case, preliminary validation can use the measurements in different frequency bands and directions that are known beforehand to be dominated by a specific type of noise sources. Use of multichannel methods and microphone arrays enabling, with certain reservations, localization of different noise sources at aircraft flyover and obtaining quantitative information about each of them is even more promising. In this sense, the problem of validation for developed engineering software when it is required to predict the number with the accuracy of 1-3 dB may significantly differ from an accurate numerical simulation tool for which validation is aimed rather not at quantitative comparison but at the correct prediction of physical mechanisms of noise generation.

Therefore, validation peculiarities of numerical simulation in aeroacoustics are related to the fact that the processes under consideration are at the top limit of the state-of-the-art capabilities in experiment and computational resources. Thus, it requires mutual coordination and support in problem formulation and results interpretation between numerical and experimental approaches in aeroacoustic researches.

COMPUTATIONAL AEROACOUSTIC METHODS FOR INDUSTRIAL APPLICATIONS

Philippe Lafon
IMSIA UMR EDF-CNRS-CEA-ENSTA, Palaiseau, France, Philippe.lafon@edf.fr

1. Introduction

In a wide range of technical fields such as aircrafts, automotive engineering, trains, turbomachinery, power plants, turbulent flows generate noise [1]. Moreover, particularly in confined configurations, strong acoustic feedback mechanisms are often involved [2]. These non-linear interactions between the turbulent flow and the acoustic field produce undesirable high pressure levels that may cause structural excitation and fatigue. To numerically predict this kind of aeroacoustic oscillations, the calculation of both the unsteady flow and the associated sound must be performed in the same computation. This is referred as Direct Noise Computation (DNC) in the literature of Computational AeroAcoustics (CAA) [3]. For carrying out such computations, a numerical tool called *Code_Safari* has been developed.

2. Computational methods

The governing equations and the computational methods are extensively presented in [4]. The compressible Navier-Stokes are solved using high order finite difference schemes [5] on cartesian curvilinear grids. In order to be able to compute complex configurations, an overset capability [6] is available using the Overture library [7]. LES simulations are carried out following the approach presented in [8] that makes no use of subgrid scale model. A shock capturing capability is available using the methodology presented in [9].

3. Application to self-induced transonic flow oscillations behind a sudden duct enlargement

The flow oscillations downstream a sudden flow enlargement have been experimentally studied in reference [10]. It is a configuration typical of the phenomena occurring in high pressure valves on industrial loops. Depending on the ratio between the downstream pressure over the upstream pressure of the reservoirs, several regimes of flow oscillations can be highlighted. Numerical computations have been carried out and most of the physical features have been retrieved [11]. In Fig. 1, the numerical Schlieren fields are given for two different pressure ratios: 0.15 for the top pictures and 0.3 for the bottom picture. In the top one, the downstream pressure is lower and the flow is mostly supersonic and nearly steady. In the bottom one, the flow is transonic and highly unsteady

as the plane shock appearing in the duct can be locked with the longitudinal acoustic mode of the duct and then become the source of strong oscillations.

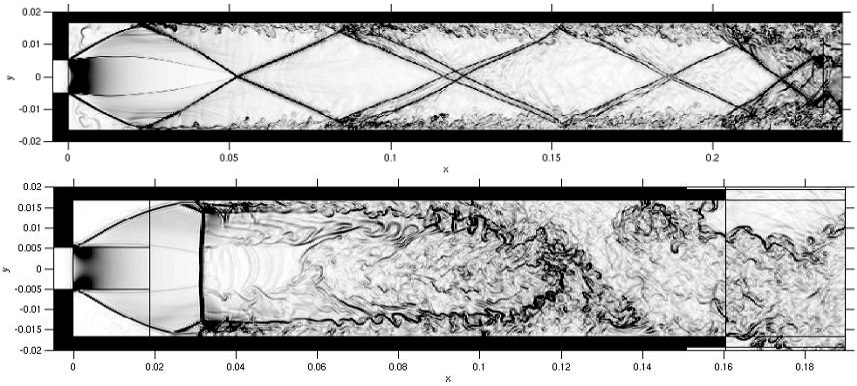

Fig. 1. Numerical Schlieren fields for pressure ratio of 0.15 (top) and pressure ratio of 0.3 (bottom)

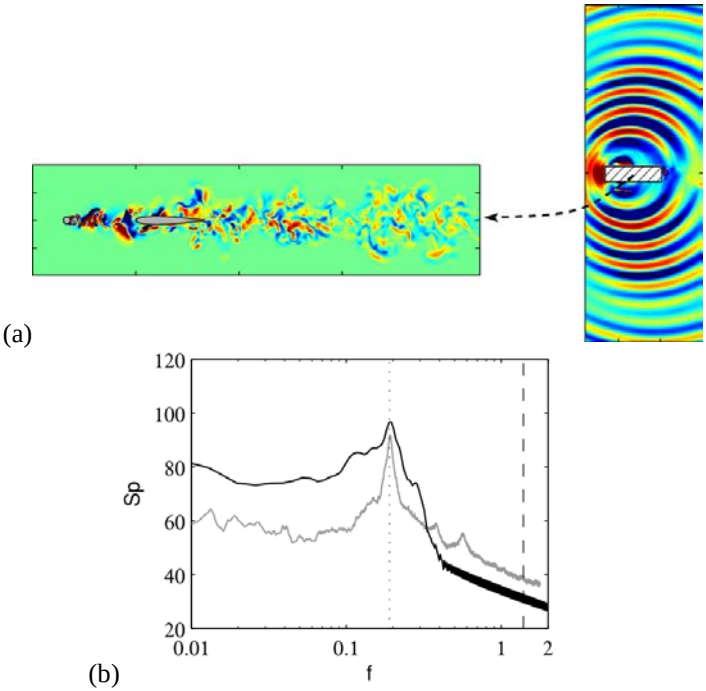

Fig. 2. Spanwise velocity field associated with far-field fluctuating pressure (a); comparison of PSDs of computed and experimental far field pressure view (b)

4. Application to the noise radiated by a rod airfoil configuration

The rod-airfoil configuration has become a classical benchmark for the modeling of broadband noise modeling [12]. This case has been simulated and detailed analysis is presented in [13]. Fig. 2 shows two results. The left pictures display a snapshot of the spanwise velocity field associated with a snapshot of the fluctuating pressure field that is radiated. The right picture displays a comparison of the computed PSD of the far field pressure compared to the experimental one. The main peak is well retrieved but the low frequency domain is overestimated.

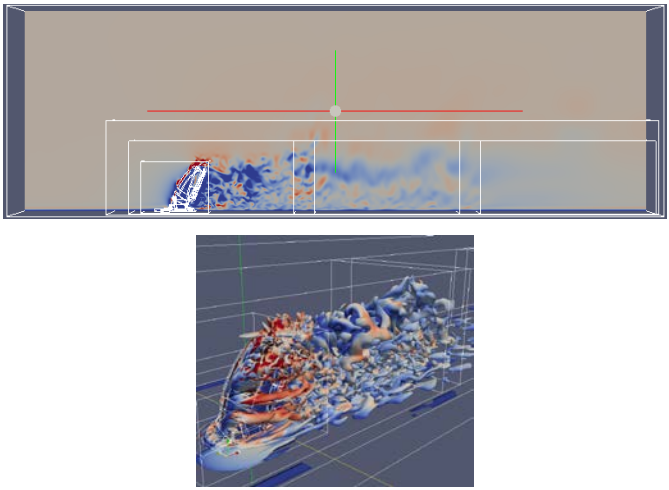

Fig. 3. Velocity magnitude field and overset grid boxes (top); swirl field around the car side mirror (bottom)

5. Application to the noise radiated by car side mirror

This application has been carried out with the collaboration of PSA Peugeot-Citroen (Dr F. van Herpe). This case involves a complex 3D geometry that implies extensive use of the overset approach for building the grids. Surface and volume grids have been constructed on the CAD structure of the car side mirror and these grids have been immersed in grid boxes defining the whole computational domain. Fig. 3 displays the velocity magnitude field in all the computation domain and a zoom on the swirl field around the car side mirror.

The main objective of this computational study is to analyse the pressure fluctuation field on the plate supporting the car side mirror and to try to separate in the pressure field the convective part and the acoustic part. This separation is essential in order to identify the different vibroacoustic transmission

mechanisms through the side glass of the car. So the pressure field has been analysed by taking the space Fourier transform in both directions. Fig. 4 displays some results that are obtained after such treatments. The two pictures present K_x-K_y diagrams for two frequencies. The acoustic "spot" is clearly visible around $K_x = 0$, $K_y = 0$. The convective (vertical) line is also clearly visible. As expected, the two contributions are more separated for the higher frequency.

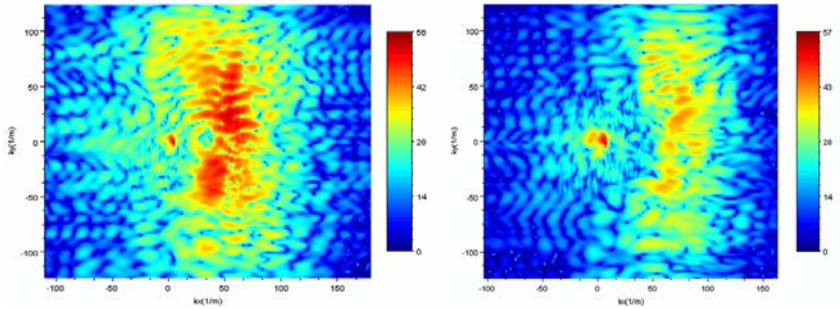

Fig. 4. K_x-K_y diagrams at 2 kHz (left) and 3 kHz (right)

6. Outlooks

Section 2 presented flow acoustics phenomena in the transonic flow regime. But interactions between the flow field and the acoustic field can also happen in the subsonic flow regime and undesirable whistling problems can appear on industrial installations. For studying such situations, a collaboration with McMaster university has started [2] and a simplified configuration involving a cylindrical duct and a rectangular 3D cavity is being studied as displayed in Fig. 5.

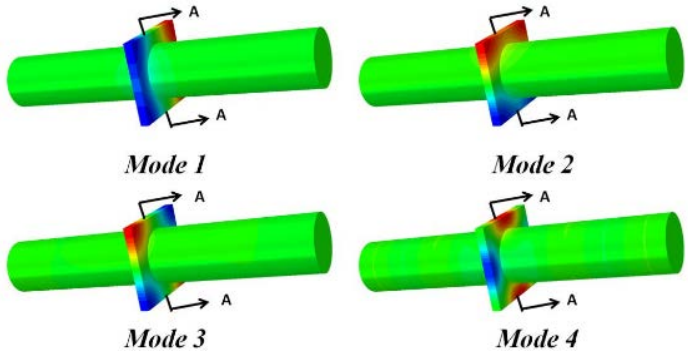

Fig. 5. Different mode shapes present in the cylindrical duct and rectangular cavity configuration

In the next steps, aeroacoustic computations will be carried out for improving the numerical capabilities of the code with new validation cases and for giving new insights to the physical analysis of the phenomena. The main objective is to put into evidence which modes are going to be excited by the flow.

The moving grid capability is not parallelized at the moment. As a new parallel version of the Overture Library is available, next step should be to upgrade its implementation in Code_Safari in order to take advantage of the new parallel features.

New applications have led to the development of a new algorithm in the software. High order finite difference are very accurate and efficient methods for aeroacoustic computations but it is not easy to control the growth of spurious disturbances. Indeed such errors are quite unwanted when the positivity of variables are required, as in two phase flow computations. So, a new algorithm based on WENO finite difference schemes and Weigthed Compact Nonlinear Schemes (WCNS) has been implemented [15].

7. Conclusion

A numerical tool for aeroacoustic simulations has been developed in order to deal with configurations of industrial interest. In this paper, the computational methods that have been used are summarized and several applications illustrating aeroacoustic problems for different flow regimes are briefly presented.

Acknowledgments

Most of these results have been obtained with the contributions of J. Berland, F. Crouzet, Frédéric Daude at EDF R&D and with the collaboration of Ecole Centrale Lyon (Pr C. Bailly), of PSA Peugeot-Citroen (Dr F. van Herpe) and of McMaster University (Pr S. Ziada). Many thanks to Dr Henshaw (LLNL) for his valuable recommendations concerning the overset-grid strategy

References

1. T. Colonius, S.K. Lele. Computational aeroacoustics: progress on nonlinear problems on sound generation. Prog. Aerospace Sci., v.40, 2004, pp.345–416.
2. M. Bolduc, S. Ziada, P. Lafon. On the modal behavior of trapped diametral modes in a ducted cavity. AIAA Paper 2016-2883.
3. C. Bailly, C. Bogey, O. Marsden. Progress in direct noise computation. Int. J. Aeroacoust., v.9, 2010, pp.123–43.

4. F. Daude, J. Berland, T. Emmert, P. Lafon, F. Crouzet, C. Bailly. A high-order finite-difference algorithm for direct computation of aerodynamic sound. Computers & Fluids, vol.61, 2012, pp.46–63.
5. C. Bogey, C. Bailly. A family of low dispersive and low dissipative explicit schemes for flow and noise computations. J. Comput. Phys., v.194, 2004, pp.194–214.
6. J.W. Delfs. An overlapped grid technique for high resolution CAA schemes for complex geometries, AIAA Paper 2001-2199.
7. W.D. Henshaw. Ogen: an overlapping grid generator for overture, Tech. Rep. UCRL-MA-132237, Lawrence Livermore National Laboratory, 1998.
8. C. Bogey, C. Bailly. Turbulence and energy budget in a self-preserving round jet: direct evaluation using large-eddy simulation. J. Fluid Mech., v.627, 2009, pp.129–160.
9. J.W. Kim, D.J. Lee. Adaptive nonlinear artificial dissipation model for computational aeroacoustics. AIAA J., v.39, 2001, pp.810–818.
10. G.E.A. Meier, G. Grabitz, W.M. Jungowski, K.J. Witczak, and J.S. Anderson. Oscillations of the supersonic flow downstream of an abrupt increase in duct cross section. AIAA J., v.18, 1980, pp.394–405.
11. T. Emmert, P. Lafon, C. Bailly. Numerical study of self-induced transonic flow oscillations behind a sudden duct enlargement. Phys. Fluids, v. 21(106105), 2009, pp.1–15.
12. M.C. Jacob, J. Boudet, J. Casalino, M. Michard. A rod-airfoil experiment as benchmark for broadband noise modeling. J. Theoret. Comput. Fluid Dyn., v.19, 2005, pp.171–196.
13. J. Berland, P. Lafon, F. Crouzet, F. Daude, C. Bailly. A parametric study of the noise radiated by the flow around multiple bodies: direct noise computation of the influence of the separating distance in rod-airfoil flow configurations, AIAA Paper 2011-2819.
14. F. Van Herpe, M. Bordji and D. Baresch. Wavenumber-frequency analysis of the wall pressure fluctuations in the wake of a car side mirror. AIAA Paper 2011-2936.
15. T. Nonomura, S. Morizawa, H. Terashima, S. Obayashi, and Kozo Fujii. Numerical (error) issues on compressible multicomponent flows using a high-order differencing scheme: weighted compact nonlinear scheme. J. Comput. Phys., v.231, 2012, pp.3181–3210.

DUCT MODES IN SHEAR FLOW: PROPERTIES AND APPLICATIONS OF THE PRIDMORE-BROWN EQUATION

Sjoerd W. Rienstra
Technische Universiteit Eindhoven, The Netherlands, s.w.rienstra@tue.nl

In a duct of constant cross section, with an acoustic medium and boundary conditions *independent* of the axial position, the wave equation for time-harmonic perturbations of an inviscid mean flow may be solved by means of a series expansion in a particular family of *self-similar* solutions, called modes [1].

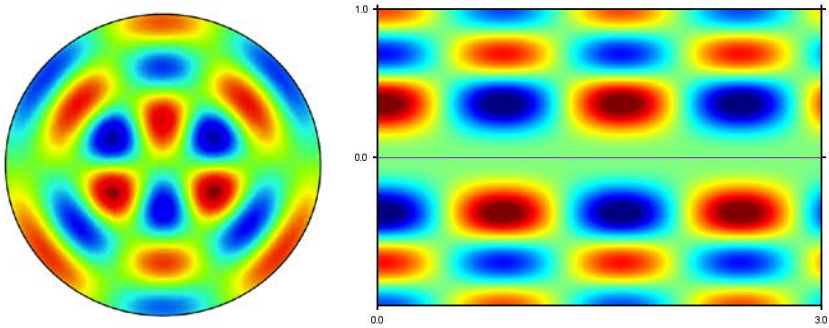

Fig. 1. Snap shot of a duct mode (front and side)

They are related to the eigensolutions of the two-dimensional operator that results from the wave equation on a cross section of the duct. For the common situation of a uniform medium without flow, this operator is the well-known Laplace operator and the equation to be solved is the Helmholtz equation. For a (cross-wise) non-uniform medium, and in particular with mean flow (*i.e.* parallel flow), the details become more complicated, but the concept of duct modes as self-similar solutions remains by and large the same. Although there is no generalization of the Laplace operator (at least, not directly; only in the form of a system of equations), there is a generalization of the Helmholtz equation in the form of an equation which has become known as the **Pridmore-Brown equation** [2]. This equation has been studied for almost 60 years, but little analytical results have been reported. We will consider some recent results and applications of sound in shear flow in general and Pridmore-Brown modes in particular.

Modes are interesting mathematically because they form, in general, a complete basis by which any solution can be represented. Physically, modes are interesting because they are solutions in their own right - not just mathematical building blocks. Moreover, by their simple structure the usually complicated

behavior of the total field is more easily understood. The concept of mode can be formulated rather generally. We have modes in ducts of arbitrary cross section, with any boundary condition and medium, with or without mean flow, as long as medium and boundary condition are constant in axial direction. However, to obtain insight *and* because it is technically relevant it is useful to simplify the geometry of the duct to a cylinder, and obtain modes of simpler shape. To set the various possible models in perspective, we will consider a hierarchy of equations from a very general mean flow to uniform and no mean flow [1].

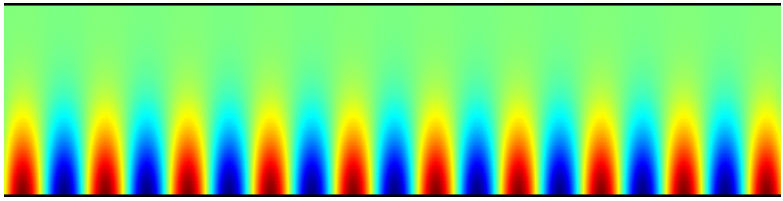

Fig. 2. Pridmore-Brown mode in strong linear shear flow

In its simplest form (no or uniform flow, uniform medium), modes satisfy certain orthogonality properties with explicitly available inner-products of integral type. This enables us to solve transition and reflection problems at geometrical discontinuities by the technique of mode matching. For the more general Pridmore-Brown modes in non-uniform mean flow this is not possible anymore. There exist no analytically exact innerproducts between the modes and they are not orthogonal. There are, however, particular integrals (not exactly equal but close to innerproducts) which can be used very effectively instead [3].

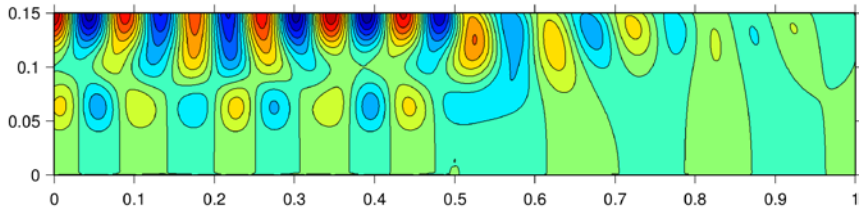

Fig. 3. Result of mode matching along a sectioned duct with shear flow

In potential mean flow, a mass source does not produce vorticity; this is only possible for a force-like source. This is not the case for vortical mean flow. Both mass and force sources may produce trailing (*i.e.* convected) vorticity [4]. A Green's function for example, with its source located in a region with mean shear, will include downstream vorticity which is absent if the source is located elsewhere. If the Green's function is constructed from a series of Pridmore-Brown modes[5], we will have to make sure to include the associated non-acoustic vortical modes. These modes exist only near the wall (a.k.a surface

modes [6,7]). Under certain conditions these modes may constitute a convected instability [5].

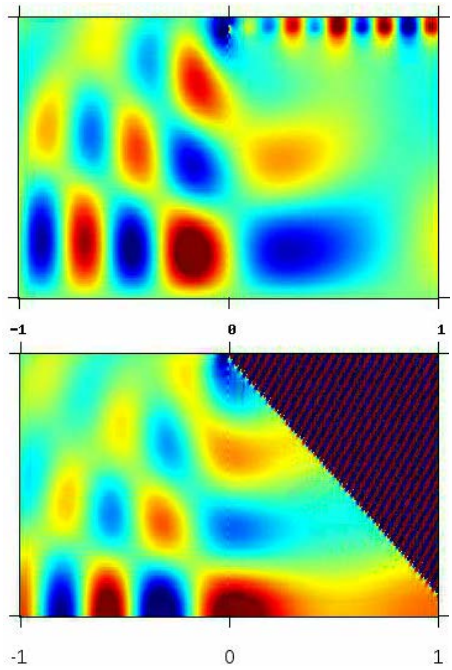

Fig. 4. Acoustic and vortical modes in (boundary layer) shear flow

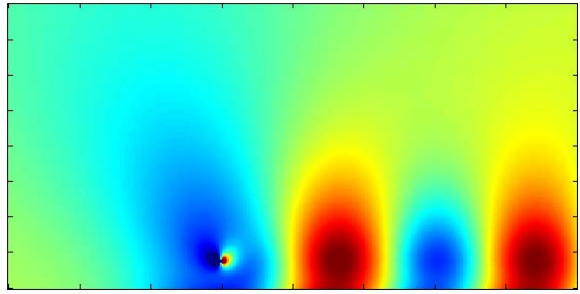

Fig. 5. Vortical modes due to a mass source in a mean shear flow

If these vortices, for example convected in the (sheared) boundary layer, pass a hard-soft transition of the wall, they generate in return sound[8].

Modes, being self-similar solutions that remain the same everywhere down the duct, exist strictly speaking only in exact parallel mean flow. Since this is only possible for inviscid flow, which is a modelling assumption, also

modes in mean flow have to be considered as a modelling assumption. It is therefore of interest to see if slowly varying Pridmore-Brown modes in a slowly varying medium can be formulated in the framework of the WKB technique. This is to a certain extent possible and we will give an example in 2D with linear shear flow [9]. However, the beautiful result of an exact adiabatic invariant, available for potential mean flow, is not obtained. This is possibly due to the absence of a conserved acoustic energy in vortical flow.

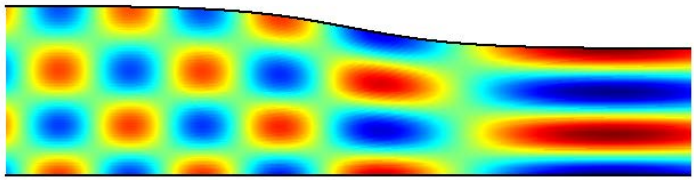

Fig. 6. Slowly varying Pridmore-Brown mode

References

1. S.W. Rienstra. Fundamentals of Duct Acoustics, Von Karman Institute Lecture Notes. 2015.
2. D. Pridmore-Brown. Sound Propagation in a Fluid Flowing Through an Attenuating Duct, Journal of Fluid Mechanics, 4 (4), 1958, 393–406.
3. M. Oppeneer, S.W. Rienstra and P. Sijtsma. Efficient Mode-Matching Based on Closed Form Integrals of Pridmore-Brown Modes, AIAA Journal, 54 (1), 2016, 266–279.
4. S.W. Rienstra, M. Darau, E.J. Brambley. The trailing vorticity field behind a line source in two-dimensional incompressible linear shear flow. Journal of Fluid Mechanics, volume 720, 2013, 618–636.
5. E.J. Brambley, S.W. Rienstra and M. Darau. The critical layer in linear-shear boundary layers over acoustic linings, Journal of Fluid Mechanics, 710, 2012, 545–568.
6. G.G. Vilenski and S.W. Rienstra. On Hydrodynamic and Acoustic Modes in a Ducted Shear Flow with Wall Lining, Journal of Fluid Mechanics, 583, 2007, 45–70.
7. S.W. Rienstra. A Classification of Duct Modes Based on Surface Waves, Wave Motion, 37, 2003, 119–135.
8. S.W. Rienstra and D.K. Singh. Hard wall - soft wall - vorticity scattering in shear flow. AIAA 2014-3350, 20th AIAA/CEAS Aeroacoustics Conference, 16-20 June 2014, Atlanta, Georgia, USA.
9. S.W. Rienstra, Sound Propagation in Slowly Varying 2D Duct with Shear Flow, AIAA-2016-2925, 22nd AIAA/CEAS Aeroacoustics Conference, Lyon, 2016.

REGULAR TALKS

NUMERICAL SIMULATION OF ROTOR AERODYNAMICS AND ACOUSTICS USING HIGHER-ACCURACY EDGE-BASED ALGORITHMS ON UNSTRUCTURED MESHES

I.V. Abalakin[1], V.A. Anikin[2], P.A. Bakhvalov[1], **V.G. Bobkov**[1], T.K. Kozubskaya[1]

[1]*Keldysh Institute of Applied Mathematics, Moscow, Russia, veld13@gmail.com*

[2]*Kamov Design Bureau, Luberetsky District, Moscow Region, Russia, v.anikin@kamov.ru*

The talk is devoted to the numerical simulation of aerodynamic and acoustic characteristics of helicopter rotors in hover using higher-accuracy lower-cost algorithms on unstructured meshes.

The helicopter rotor construction is being constantly developed and inevitably complicated. It is connected with the permanent necessity to optimize the shapes in order to improve aerodynamic characteristics of rotors and also to reduce acoustic noise produced by rotor blades. In this situation mathematical modeling and numerical simulation become one of the efficient tools since it allows easily change the rotor geometry and flight regimes and to perform serial predictions needed for the optimization and production.

The rotor blade shapes are composed of basic varying elements such as tips, twists and constitutive airfoils. To handle complicated changeable geometry of a blade numerically, an efficient way is to use unstructured meshes. To carry out the corresponding computations for reasonable time, high accuracy numerical schemes and efficient parallel algorithms for multi-CPU computer systems are needed.

In the talk we present a numerical technique for predicting rotor aerodynamics and acoustics. The numerical algorithm is generally applicable to all the family of models based on the Euler equations within DNS, RANS, LES and hybrid RANS-LES approaches for simulating compressible turbulent flows. However in the predictions considered here we use the Euler and Navier-Stokes equations taken in non-inertial reference framework.

A feature of the numerical technique presented is the usage of vertex-centered EBR scheme [1,2] for unstructured meshes which provides accuracy higher than most second order schemes in terms of error values and takes lower computational costs in comparison with very high order algorithms. The higher accuracy of the scheme is provided due to the edge-based reconstruction of variables involved in the calculation of fluxes arbitrary unstructured meshes. As a result, when operating on uniform grid-like meshes the scheme possess the ac-

curacy of the 5th order. For the time advancing we use the second order implicit scheme with BiGSStab method for solving linear algebraic equations. For the acoustic properties prediction in the far field the Ffowcs Williams-Hawkings [3] approach was used. The numerical techniques are implemented in the in-house code NOISEtte++ [4] for solving aerodynamics and aeroacoustics problems on unstructured meshes. The hybrid MPI-OpenMP parallel model of NOISEtte++ allows its efficient performance on tens thousands of CPU-cores.

We demonstrate an efficiency of the numerical tools on solving two model problems on rotor aerodynamics in hover: configuration "shrouded rotor" (Fig. 1) aerodynamics prediction and main rotor (Fig. 2) aerodynamic and acoustic characteristics prediction.

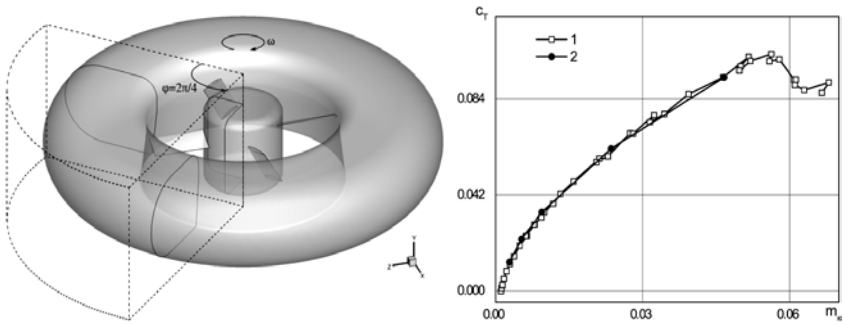

Fig. 1. Configuration “rotor in ring” (problem 1) with problem geometry (left) and the results on rotor polar curve: 1 – physical experiment, 2 – computation

The first problem considers the configuration “rotor in a ring”. The rotor installed in toroidal channel (“ring”) consists of four blades located in the same disc plane and a central body. The blades are based on one airfoil with the liner twist of -9°. We consider the case of the same pitch angle for all the blades. The problem configuration is shown in Fig. 1, left.

For the rotational speed 1166 rpm which corresponds to the linear tip speed of the blade 73.3 m/s we present the results for different pitch angles. The evaluated integral aerodynamic characteristics as trust, torsion and their coefficients are in a good agreement with the corresponding experimental data. In Fig. 1, right, we show the polar curve.

In the second problem we simulate the flow generated by the model main rotor. The rotor consists of four blades of complicated configuration based on five different airfoils. The blade geometry includes piecewise linear twist and swept tip. The problem configuration with the cross-section of tetrahedral mesh in use is shown in Fig. 2. The aerodynamics and acoustic properties are evaluated for the rotational speed 668 rpm which corresponds to the linear tip speed of the blade 136.6 m/s for set of blade pitch angle values. The evaluated integral

aerodynamic characteristics and their coefficients are in a good agreement with the corresponding experimental data (Fig. 2, left).

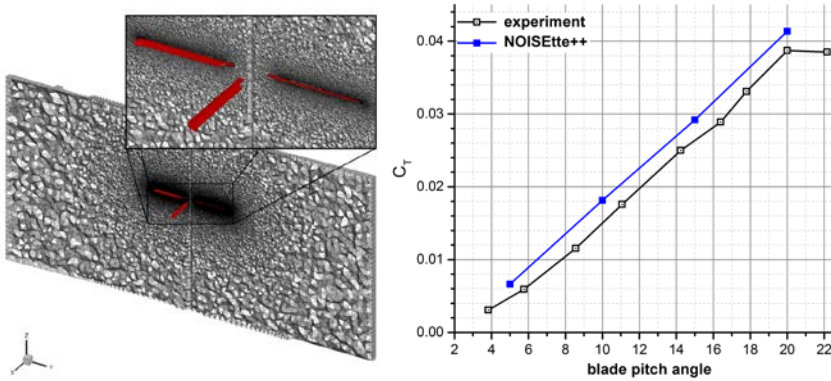

Fig. 2. Configuration “main rotor” (problem 2) with the mesh cross-section (left) and the torque coefficient against blade pitch angle (right)

The work is supported by the Russian Ministry of Science and Education (Project RFMEFI60414X0092).

References

1. Abalakin I., Bakhvalov P., Kozubskaya T. Edge-based reconstruction schemes for prediction of near _field flow region in complex aeroacoustics problems. International Journal of Aeroacoustics, v.13 (3-4), 2014, pp. 207–234.
2. Ilya Abalakin, Pavel Bakhvalov, Tatiana Kozubskaya. Edge-Based Reconstruction Schemes for Unstructured Tetrahedral Meshes. Int. J Num. Meth. in Fluids, v.81, Issue 6, 2015, pp.329–396.
3. J.E. Ffowcs Williams, D.L. Hawkings. Sound generated by turbulence and surfaces in arbitrary motion. Philosophical Transactions of the Royal Society, v.A264, №1151, 1969, pp.321–342.
4. Abalakin I.V., P.A. Bakhvalov, A.V. Gorobets, A.P. Duben, T.K. Kozubskaya. Parallel research code NOISEtte for large-scale CFD and CAA simulations. Vychislitelnye Metody i Programmirovanie (Numerical methods and Programming), v.13, 2012, pp. 110–125.

UNSTEADY FLUX CORRECTION METHOD FOR SOLVING AEROACOUSTIC PROBLEMS ON UNSTRUCTURED MESHES

P.A. Bakhvalov, T.K. Kozubskaya

Keldysh Institute of Applied Mathematics (Russian Academy of Sciences), Moscow

High accuracy of the numerical method is an mandatory property when solving aeroacoustic problems. On structured meshes finite-difference methods present an effective solution. They allow to reach a high order of accuracy at the cost of rather small computational efforts. For problems with discontinuities the finite-difference WENO scheme is developed. On unstructured meshes the schemes of very high order (3^{rd} and higher), such as Discontinuous Galerkin method and polynomial-based finite volume (k-exact) schemes are still very expensive. When solving the problems with discontinuities by these schemes, the usage of monotonizers strongly degrades the accuracy so that their advantage becomes not big, to compensate the costs. This fact inspires to look for alternative methods which produce the results of higher accuracy.

Among such alternative methods there is a family of vertex-centered schemes with edge-based reconstruction of flux variables. The initial step in their development consisted in providing the P1-Galerkin method with additional numerical dissipation. The resulting scheme is known as the linear scheme of T. Barth [1]. The EBR (Edge-Based Reconstruction) schemes [2]-[3] also belong of this family. The EBR schemes are of the second order of accuracy on unstructured meshes, however on uniform grid-like meshes they transform to the finite-difference schemes of very high (from 3^{rd} to 6^{th}) order. This property of being of very high order on uniform grid-like meshes provides significantly smaller values of numerical error on arbitrary unstructured meshes.

Another example of edge-based schemes was proposed in 2011. It is the Flux Correction method (FC) [4][5] which is of the third order on unstructured meshes for steady problems. At the same time, on unsteady cases the FC scheme either loses the conservation property and becomes very costly, to keep the third order, or degrades to the second order of accuracy.

We have developed a new modification of the FC method for solving unsteady problems and named it Unsteady Flux Correction scheme, UFC [6]. The UFC scheme is conservative and does not deteriorate steady solutions as compared to the FC method. In addition, it offers a property to evolve into the high-order (3^{rd}-4^{th} order) scheme on uniform grid-like meshes. For a better comparison, the properties of the edge-based schemes, including the new UFC method, are represented in Table 1.

Property \ Scheme	Linear scheme [1], EB scheme [9]	EBR[2], SEBR [3], LV6, NLV6 [7]	**UFC** [6]	FC, with unsteady term approximation:	
				pointwise	Nishikawa [8], Pincock [5]
Conservation	+	+	**+**	+	–
1-exactness	+	+	**+**	+	+
3rd order on uniform grid-like meshes	–	+	**+**	–	+
3rd order on arbitrary meshes for steady problems	–	–	**+**	+	+
3rd order on arbitrary meshes for unsteady problems	–	–	**–**	–	+
Low price in comparison with very high order schemes	+	+	**+**	+	–

Table 1. Comparison of edge-based schemes

As it is in the case of EBR schemes, the 3rd order of the UFC scheme on uniform grid-like meshes significantly improves the accuracy in terms of error values on arbitrary unstructured meshes. This property will be demonstrated on several linear test problems with analytical solutions. The UFC scheme will be also compared with some other schemes based on edge-oriented reconstruction of variables.

The study is supported by the Russian Foundation of Basic Research. The UFC scheme is being developed within Project 16-31-60072-mol-a-dk. The simulations using the EBR schemes have been carried out in the frames of Project 15-01-07911-a.

References

1. Barth T.J. A 3-D upwind Euler solver for unstructured meshes, AIAA Paper No. 91-1548.
2. I.V. Abalakin, T.K. Kozubskaya. Schema na osnove reberno-orientirovannoi kvaziodnomernoi rekonstruktsii peremennyh dlya resheniya zadach aerodinamiki i aeroakustiki na nestructurirovannyh setkah. Mathematical modeling, vol. 25, № 8, 2013, pp. 109–136. (In Russian).

3. I. Abalakin, P. Bakhvalov, T. Kozubskaya, Edge-based reconstruction schemes for unstructured tetrahedral meshes. International Journal for Numerical Methods in Fluids 81 (2016) 331–356.
4. A. Katz, V. Sankaran, An efficient correction method to obtain a formally third-order accurate flow solver for node-centered unstructured grids. J. Sci. Comput. 51 (2) (2012) 375–393.
5. B. Pincock, A. Katz, High-order flux correction for viscous flows on arbitrary unstructured grids. J. Sci. Comput. 61 (2) (2014) 454–476.
6. Bakhvalov P.A., Kozubskaya T.K. Modification of Flux Corrector method for accuracy improvement on unsteady problems. KIAM preprint series, 2015, № 69. 24 p. (In Russian).
7. Koobus B., Alauzet F., Dervieux A. Computational Fluid Dynamics, CRC Press, 2011, Ch. Numerical algorithms for unstructured meshes, pp. 131–204.
8. H. Nishikawa. Divergence formulation of source term. Journal of Computational Physics 231 (2012) 6393–6400.
9. Eliasson P., EDGE, a Navier-Stokes solver for unstructured grids, Tech. Rep. FOI-R–0298–SE, FOI Swedish defence research agency, Division of Aeronautics, FFA, SE-172 90 Stockholm, 2001.

ROLE OF EXPERIMENTAL DATA IMPEDANCE AND TRANSFER FUNCTIONS CONSTRUCTION AIRFRAME AND ENGINE IN THE COMPUTATIONAL EXPERIMENTS ASSESSMENT OF EXPECTED VIBROACOUSTICAL PERFORMANCE AIRCRAFTS OF NEW GENERATION

V.S. Baklanov[1], S.N. Panov[2]

[1]*PAO "Tupolev", Moscow, Russia, baklanov@tupolev.ru*

[2]*Oktava+, Moscow, Russia, snpanov@mail.ru*

The spectrum noise and vibration from the vibration impact of the power plant of new generation aircraft in connection with the transition on the engines high and extra high bypass ratio has changed significantly.

The main change is associated with a shift to lower frequencies caused by the decrease of the fan shaft speed engines high bypass.

Besides that, the experience of determining dynamic compliance engine housing (in the place of installation of attachment points) showed a significant change in dynamic compliance housing with increasing degree of bypass ratio engines (Fig. 1) [1].

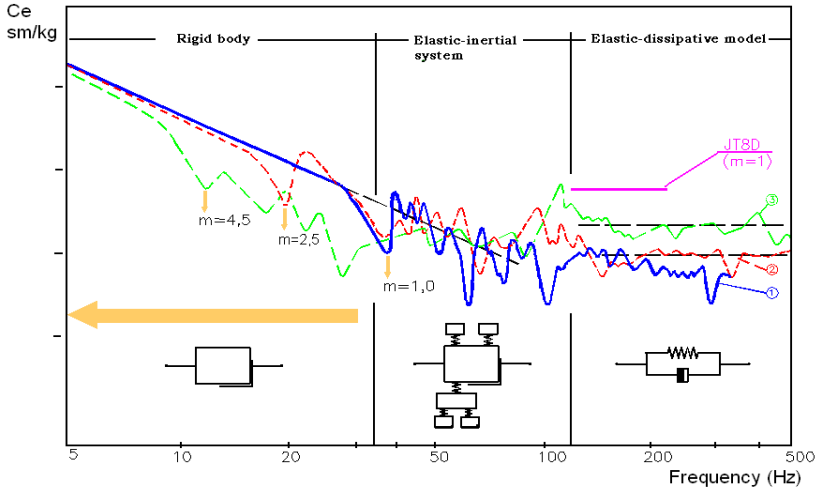

Fig. 1. Dynamic compliance module housing front mounting belt engine (for engines varying degrees bypass ratio - m)

Due to the marked, to assess the expected noise and vibrations in the cockpit and cabin of the new generation of aircraft is very important to apply

the method of impedances in the study of oscillations of a multi-coupling system "engine-mounting-airframe".

A necessary part of this study is to identify impedances (dynamic compliance) housings engines and airframe places supporting bonds (attachment points) and the transfer functions of the engine mounting points to the places of noise and vibration control.

An example of the transfer function of the structure of the main plane of the engine mounting place to the crew cabin is shown in Fig. 2 [1].

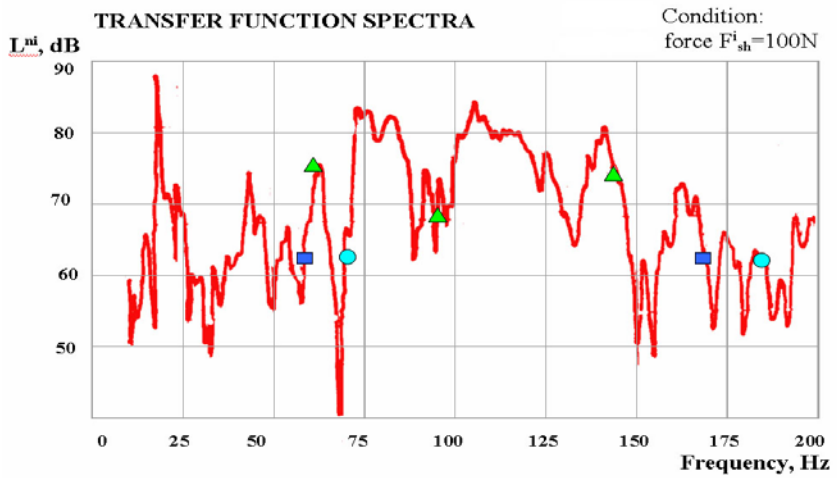

Fig. 2. The transfer function of the structure of main plane of one of the engine mounting points to the cockpit

Rotor frequency of cruise mode for three variants of engine applications to assess the expected structural noise from vibration impact of these engines are marked in the graph.

The report discusses the different approaches to the definition of these characteristics.

Application of Transfer Functions lead to development of Transfer path analysis (TPA) method, which suppose the creation of TPA model, where the system is divided into an active part , which include sources (for example, sources) and passive part (the airplane airframe with salon), where responses are measured. Loads are applied in the points of interface of active and passive parts (For example, in the points of engines mounts), and Transfer Functions (Frequency Response Functions –FRF) characterize the transfer paths from the loads (for example, vibration and noise) to receiver and presented the base characteristic of the system. Individual contribution of each transfer path to the

total response can be calculated by multiplying the loads by corresponding transfer functions.

The procedure of testing to built a conventional TPA model (load – response relationship based) need to determine operational loads and estimates the Frequency Response Functions under excitation usually in the laboratory conditions.

Application of TPA in simulation allow to execute “contribution analysis” during numerical simulation.

Measurement of the Transfer functions (FRF) for structural paths are executed by direct measurements or by reciprocal measurements using multichannel data acquisition systems with impact excitation by instrumented hammer or by the shaker (using random or burst random excitation, stepped sine and other excitation techniques) . For noise transfer paths the method of acoustic excitation using calibrated Volume Velocity Sources is applied. The separation of the sources (engine) and the structure (airframe) to the separate subsystems for elimination of decoupling is used for precise measurements the noise transfer paths.

Method of reciprocity (changing of source and receiver -excitation in the target points and measuring responses in the interface points) is based on keeping reciprocity for the most types of aircraft constructions. The method is especially effective for a limited access to some sources.

Today, there is a big demand for the methods of improving TPA to make it simpler and faster. For example, Operational Path Analysis—OPA, based on operational data use "response - response" relationship (vibrational responses in the points of loads application, measured by accelerometers, installed on the mounts; sound pressure near vibrating surfaces in the target points in the saloon). The method applies well with uncorrelated sources, time efficient, but has limitations connected with absence of information about physical loads, reflection all transfer paths contribution, separation of each causes big difficulties (for example, for airplane power plant, including several engines).

The task of Transfer Path analysis is to determine as structural as air paths from sources of excitation to the receivers, to provide a quantitative estimation of different sources contribution.

The work shows the example of conventional TPA, which provide reliable estimation of contribution, for example, vibrational influence of the new generation of engines (with new wide frequency content spectrum) on the vibroacoustical condition in the saloon of passenger aircraft.

References

1. V.K. Agafonov., V.S. Baklanov, V.M. Vul, V.I. Popkov and A.V. Popov. The Investigation of Dynamic and Vibroacoustic Characteristics of Aircraft and an Engine by Impedance Data Tests Methods.VII Aero-acoustic Conference.TsAGI, 1990. Moscow. pp.141–144.
2. V.S. Baklanov. Dynamic model of Engine-Mount-Airframe System of Trunk-Aircraft Basing on Results of Impedance Data Tests at Attachment Points. Ninth Int. Congress on Sound and Vibration. Orlando, Florida, USA. 2002.
3. What is transfer path analysis. Siemens PLM Software.

CREATING OF EXPERIMENTAL ACOUSTIC DATABASE FOR AN ISOLATED HELICOPTER`S MAIN ROTOR

G.N. Barakos[1], A.S. Batrakov[2], A.N. Bozhenko[2], L.I. Garipova[2], A.N. Kusuymov[2], S.A. Michailov[2], **V.V. Pakhov**[2], R.P. Stepanov[2]

[1]*University of Glasgow, Glasgow, UK, George.Barakos@glasgow.ac.uk*

[2]*KNRTU-KAI,Kazan, Russia, pahov.agd@kstu-kai.ru*

This paper presents results of experimental results performed in the acoustic facility in KNRTU-KAI (Kazan, Russia), which is a a modified low-speed closed-circuit opened test-section wind tunnel. An acoustic chamber was built around the test section for acoustic measurements. Schematic of the wind tunnel with the acoustic chamber shown in Fig. 1.

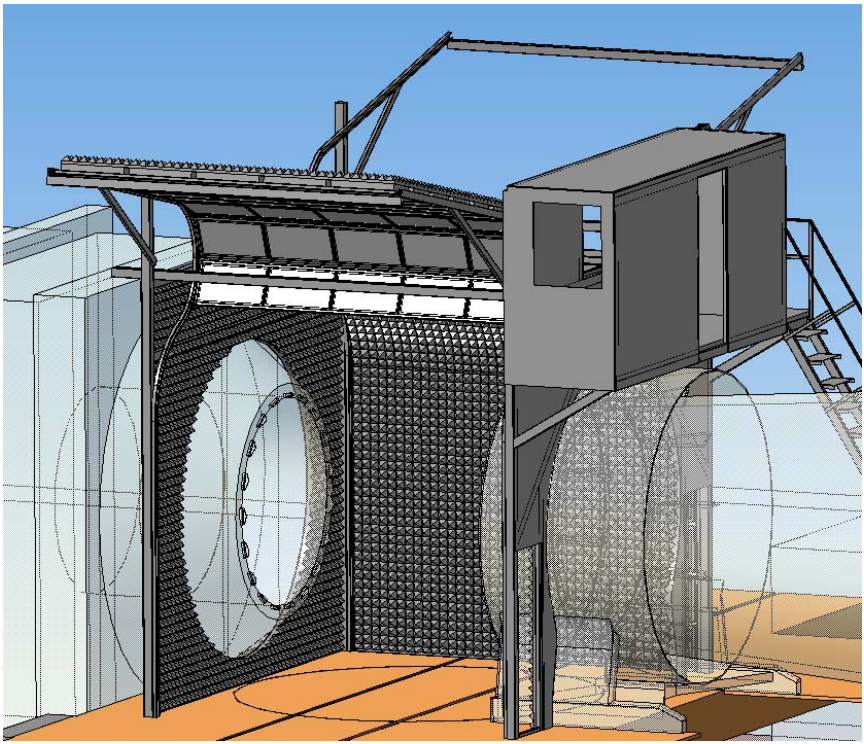

Fig. 1. Schematic of the modified wind tunnel

The acoustic chamber has retractable walls (see Fig. 1), which can be lifted or lowered. The retractable walls consist of Helmholtz`s resonators for absorbing acoustic pressure in low frequencies, and pyramid shape melamine foam material for absorbing acoustic noise of higher frequencies. Helmholtz resonators configuration was calculated in the design phase to satisfy measurement requirements for experiments in the tunnel.

The modification of the test section allows carrying out acoustic and aerodynamic experiments. Due to design constraints, Helmholtz resonators were placed only on walls and roof of the chamber.

In this work, helicopter`s isolated main rotor was investigated. To perform aforementioned tests, rotor rig of the T-1K wind tunnel was used. Its schematic is shown in Fig. 2.

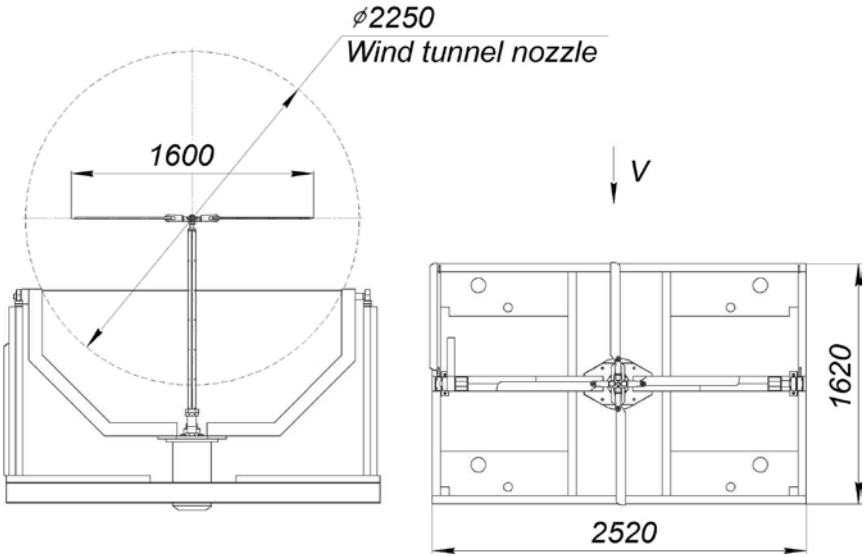

Fig. 2. Rotor rig used in the T-1K wind tunnel. Dimensions are millimeters

Rotor rig in Fig. 2 had the following specifications: up to 2500 rpm, collective pitch can vary from -15° to +15°, cyclic pitch can be applied, rotor`s angle of attack can vary from -30° to +30°. In this work, the rotor rig had angular speed of 900 rpm, collective pitch diapason took values from -2° to +8°, with a step of 2°, rotor`s angle of attack was set to 0°. All tests were performed in hover mode, i.e. free stream speed was equal to zero.

Proprietary measurement system has been used for acoustic measurements. The measurement system consisted of DBX RTA-M microphones, based on Panasonic WM-61A cartridges. Acquired signal was amplified by own-designed device and read by NI-PXI 4496 ADC card. This design allowed per-

forming measurements with up to 204 kS/s sampling rate with 24-bit analog-to-digital conversion.

For the described experiments, 9 out of 64 channels were used. Microphones were placed as shown in Fig. 3. A number of tests were performed using a linear array of microphones at relative distances from 1.2r to 2.1r from the axis of rotation of the rotor; the rotor had radius r = 820mm.

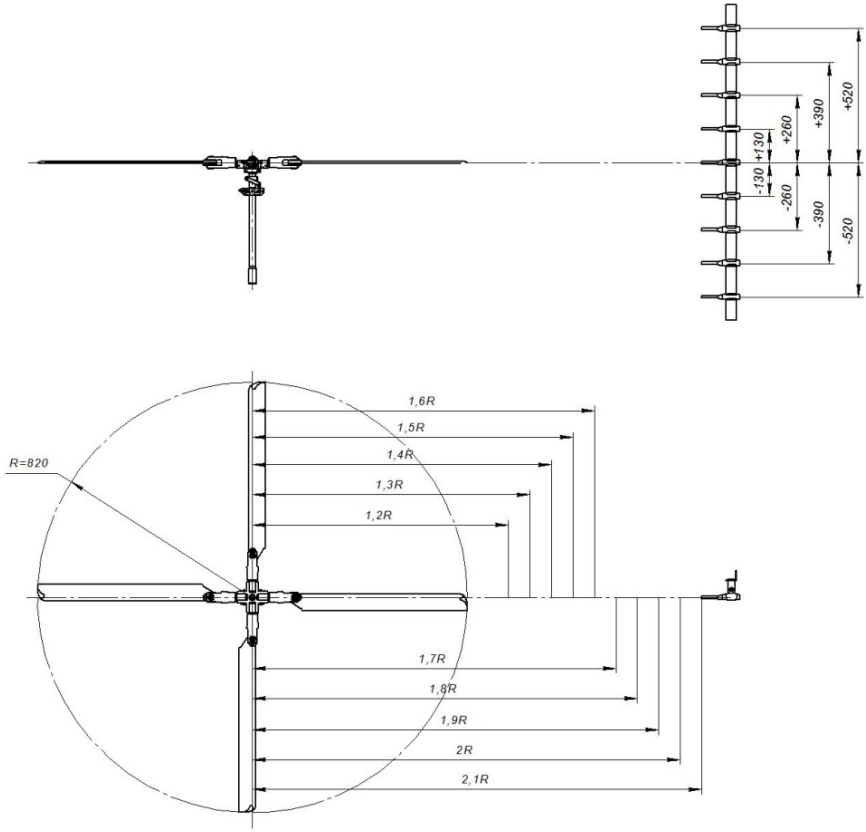

Fig. 3. Microphone positioning during the tests

Results of the tests are shown on Fig 4. Also this figure presents comparisons between experimental signal with CFD results (in temporal domain) for microphone at the plane of rotation. Numerical simulation of the flow around the rotor model for hover mode is based on RANS simulation with the k-ω turbulence model and was carried out in HMB CFD-code. The flow around isolated rotor in hover mode has periodical structure. On this reason computational

domain was constructed only for one blade (Fig. 5). The multiblock hexa-grid grid was created in ICEM CFD tool and contains about 4.4 $\cdot 10^6$ cells.

Pressure field around the rotor model was analyzed using Tecplot 360 tool. The near field sound generation at considered point is determined as fluctuations of static pressure due to the rotor rotation.

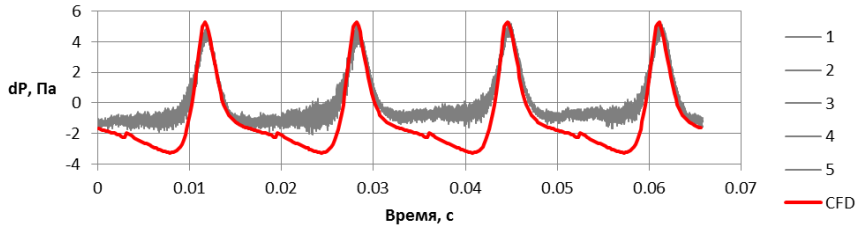

Fig. 4. Comparison of experimental results (1 to 5) with CFD results (red line)

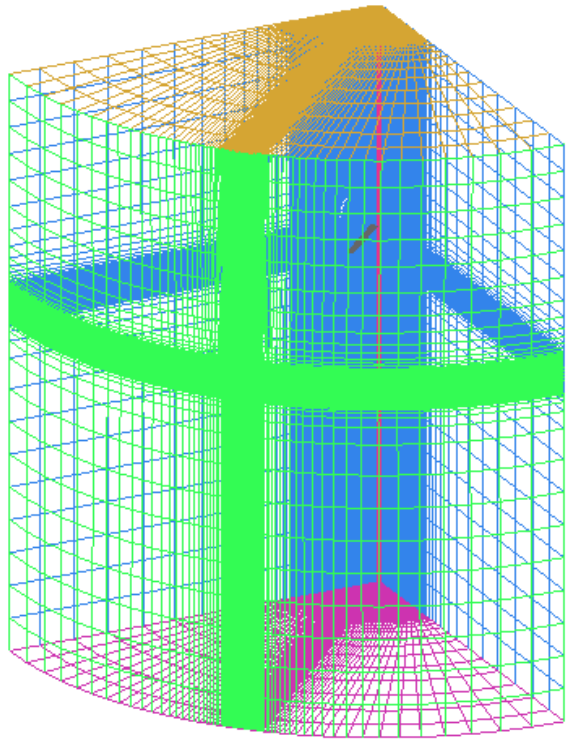

Fig. 5. Computational grid for one blade of rotor

ACOUSTIC FIELD AROUND A TRANSONIC CAVITY FLOW

George N. Barakos[1], **Gaëtan J.M. Loupy**[2]

[1]*Professor - CFD Laboratory, School of Engineering, University of Glasgow, G12 8QQ, United Kingdom, george.barakos@glasgow.ac.uk*

[2]*PhD Student - CFD Laboratory, School of Engineering, University of Glasgow, G12 8QQ, United Kingdom, g.loupy.1@research.gla.ac.uk*

Cavity flows are encountered in many aerospace applications. For military applications, the opening of the weapon bay has to emit as less noise as possible to maintain the aircraft stealth. The acoustics of the cavity is due to two contributions: broadband noise and narrow band tones. The tones called Rossiter modes [1] are caused by a feedback loop. The shear layer develops, and crossing the bay, impacts the aft wall producing acoustic waves. The reflected acoustic waves interact with the shear layer. Lawson [2,3] used CFD to show that tones and noise propagation depend on the geometry of the cavity, on the presence of doors and on the inflow conditions. The effect of the doors had been assessed for open position, and one door opening configurations showing a modification of the dominant tones and of the acoustic feedback mechanism that contributes to the overall noise [4]. However, the transient positions are yet not been investigated in the literature.

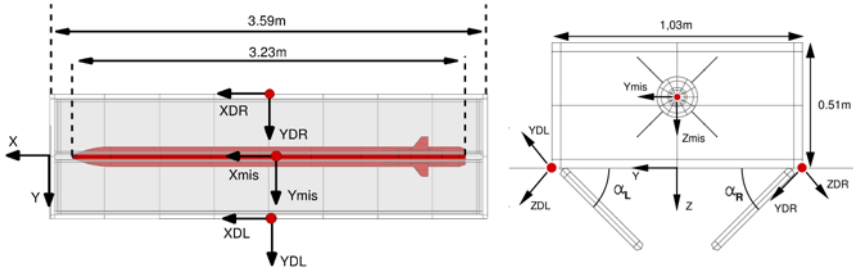

Fig. 1. Schematic view of the vented cavity with store. The red dots correspond to the moment axis

The effect of the door angle on the emitted noise is investigated numerically, using the k-ω Scale Adaptative Simulation (SAS) model validated for cavity flows with and without doors [5]. The flow over a square cavity of ratio L/D=7 at a Mach number of 0.85 is considered (Fig. 1). The doors are modelled as two solid flat plates with a thickness of 0.3% of the cavity depth. The simulation used a fix-finned store of 3,23m length placed at a carriage position inside the cavity. Having 5 points by waves, the mesh can resolve frequencies up to

4600Hz in the cavity and of 1000Hz at two cavity depths from the shear layer. This is deemed sufficient to resolve all the Rossiter modes.

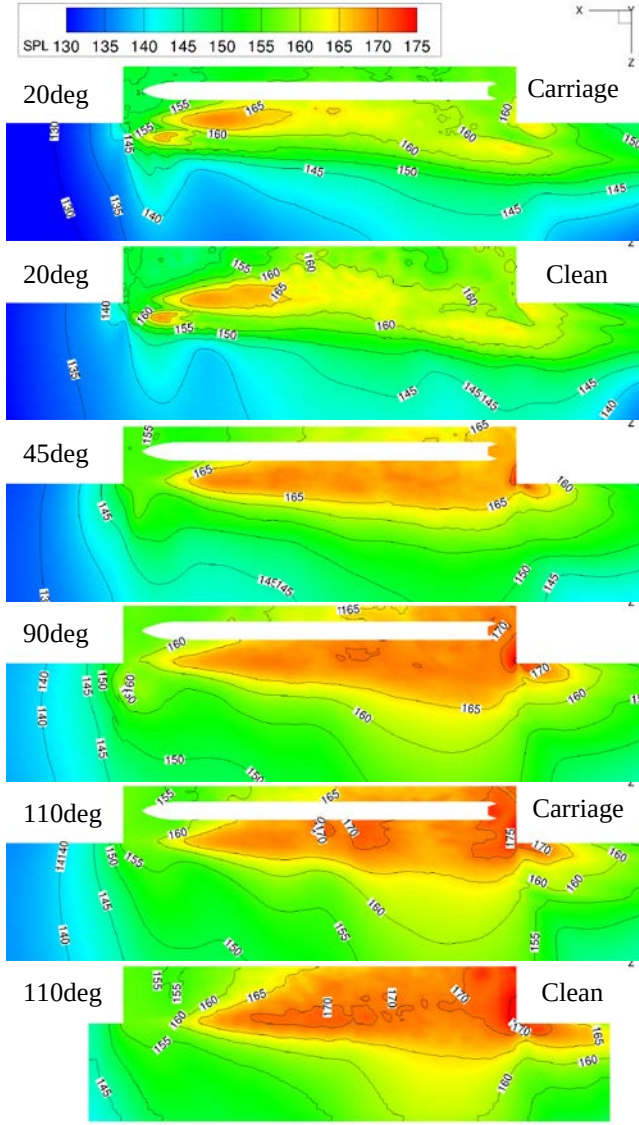

Fig. 2. OASPL(dB) at the cavity center plane for fix position. Comparison between clean and carriage case at 20 and 110 degrees

The doors are held at fixed positions of 20, 45, 90 and 110 degrees. Fig. 2 shows the contours of Overall Sound Pressure Level (OASPL) at the center plane of the cavity. The noise level is plotted at the ceiling, at the shear layer, and at one and two cavity depths from the shear layer (Fig. 3).

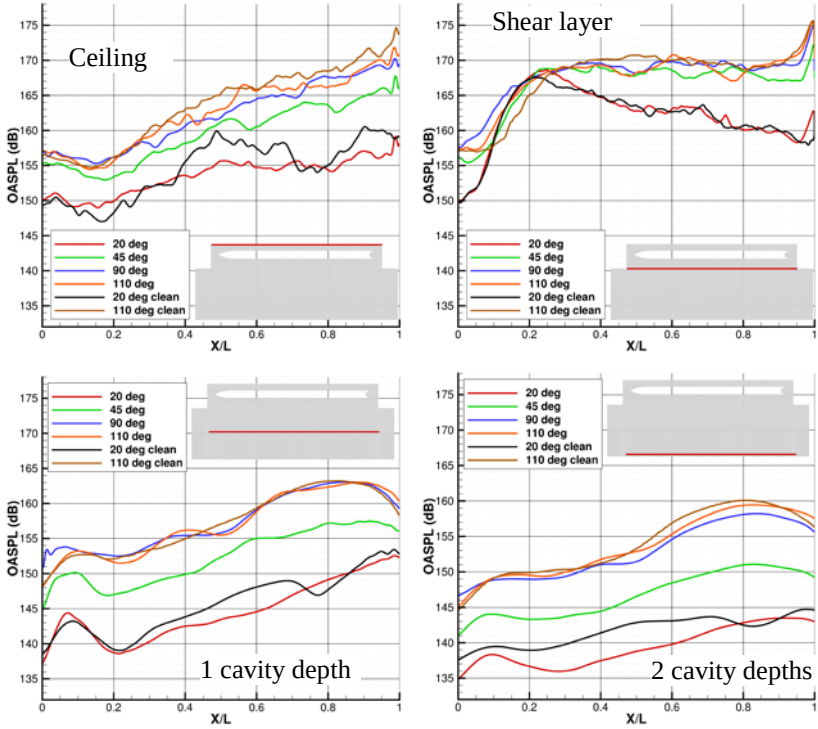

Fig. 3. OASPL level variation with the distance from the ceiling

The noise results show that the feedback loop is not established for the case with doors at 20 degrees and the noise inside the cavity and at the shear layer is lower than for larger door angles. This should be an effect of the doors that limits the space for the shear layer to move and to develop tones in the cavity. Consequently, the noise outside of the cavity is also lower than for the other cases.

The case at 45 degrees shows a similar noise field at the shear layer compared to the cases at 90 and 110 degrees showing its full establishment. However, inside the cavity, the doors at 45 degrees decrease the noise up to 5dB than for larger opening, showing that the feedback loop is yet limited in this configuration. The cases at 90 and 110 degrees show fairly identical results with the feedback loop fully established.

The store had little influence on the noise field at carriage position. The diameter of the store represents 15% of the cavity width, this does not change the topology of the flow and the tones [6].

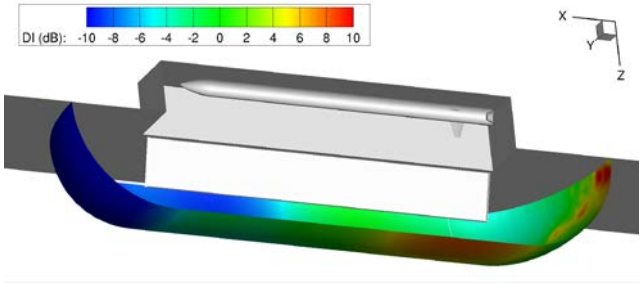

Fig. 4. Iso-surface to compute the noise directivity

The propagation of the noise is computed with the directivity. The source of the noise is considered to be the shear layer. The directivity is computed on a surface two cavity depths away from the shear layer equivalent to 1m (Fig. 4). The directivity factor Q is given by the ratio of the local noise intensity I and the mean noise intensity I_{av} of the iso-surface. Then the directivity is given by

$$DI = 10 \log_{10}(Q) \quad \text{with} \quad Q = I/I_{av}$$

Figure 5 shows the noise directivity along the center line and on the transversal plane at X/L=0.85 of the cavity for the cases with the store at carriage. The cases with doors at 90 and 110 degrees show similar noise directivity that could be explained by a similar distribution of the noise sources in the cavity.

The doors at 45 degrees show a lower directivity in the second half of the cavity and in the vertical direction. This noise intensity decrease is related to the partially established feedback loop that emits less noise from the rear of the cavity (Fig. 6). The noise at the rear of the cavity originates from the impact of the shear layer on the rear wall. This noise is stronger if the shear layer has the space to oscillate and to hit the wall with a large depth of penetration. On the velocity dilatation animation, the noise is seen to travel upstream from the aft wall with an angle of 45 degrees with respect to the cavity ceiling. It is this source of noise that creates the bump on the directivity plot on the second half of the cavity (Fig. 5).

The doors at 20 degrees have a lower directivity above the cavity than the other cases because of the partial establishment of the feedback-loop so that the most important directivity is seen at the wake after the cavity.

The noise coming from the shear layer is fully established from a door angle of 45 degrees and is produced by the turbulence inside the shear layer. The noise due to the feedback loop is fully established from a door angle of 90 degrees and is produced by the interaction of the shear layer with the upstream

acoustic waves coming from the rear wall. This noise is fully established if the shear layer has the space to oscillate in the vertical direction to reach a large depth of penetration.

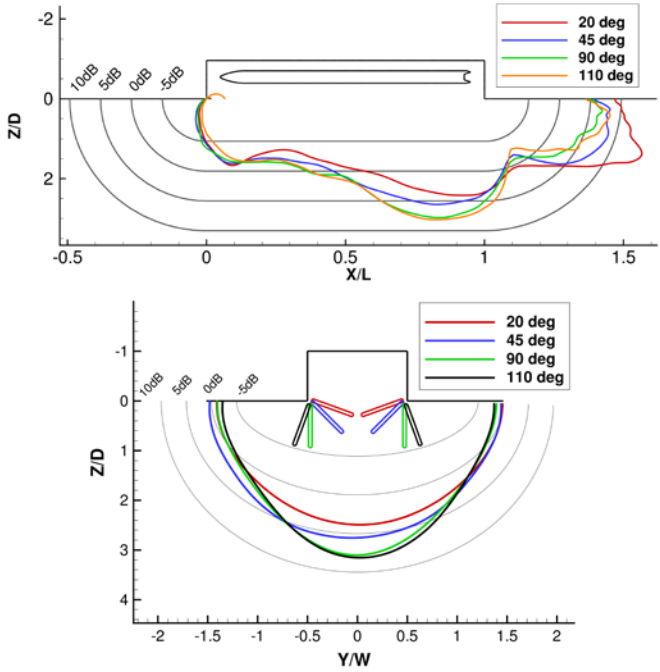

Fig. 5. Noise directivity 1 meter away from the shear layer at the centerline and at X/L=0.85. The computing surface is deformed along its normal

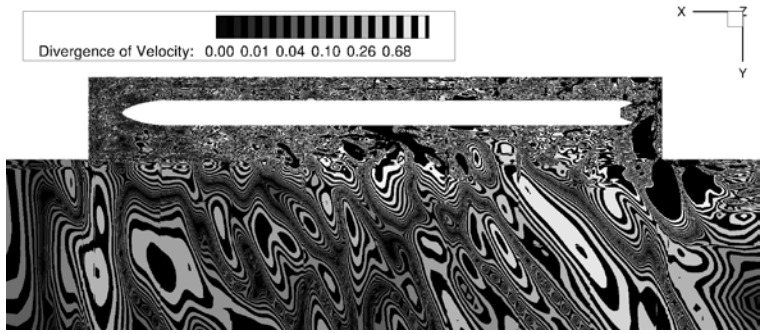

Fig. 6. Velocity dilatation on the middle plane of the cavity for door angle of 110 degrees. The red arrow shows the travel direction of the waves

The full paper assesses the effect of the door dynamics on the noise emission and propagation.

The financial support of MBDA Missile Systems is gratefully acknowledged. The use of the EPSRC funded ARCHIE-WeSt High Performance Computer (EPSRC grant no. EP/K0005 86/1) is also gratefully acknowledged.

References

1. J. Rossiter. “Wind Tunnel Experiments on the Flow Over Rectangular Cavities at Subsonic and Transonic Speeds,” Technical Report 64037, Royal Aircraft Establishment, October 1964.
2. S.J. Lawson and G.N. Barakos. Evaluation of DES for Weapons Bays in UCAVs. Aerospace Science and Technology, 14(6):397–414, 2010.
3. S.J. Lawson and G.N. Barakos. Computational Fluid dynamics analyses of Flow over weapons-bay geometries. Journal of Aircraft, 47(5):1605–1623, 2010.
4. M.B. Panickar, N.E. Murray, B.J. Jansen Jr., M.P. Joachim, R. Birkbeckand, C. Kannepalli and N. Sinha. Reduction of noise generated by a half-open weapon bay. Journal of Aircraft, 50(3):716–724, 2013.
5. G. Zografakis, S.V. Babu and G.N. Barakos. Evaluation of scale-adaptive simulations for transonic cavity flows. Notes on Numerical Fluid Mechanics and Multidisciplinary Design, 130:433–444, 2015.
6. C.J. Coley and A.J. Lofthouse. Correlation of weapon bay resonance and store unsteady force and moment loading. Nashville, TN, United states, 2012.

AIR FLOW EXPLORATION USING ACOUSTICAL MLS-SIGNAL

A.A. Belous[1], **A.I. Korolkov**[1], N.N. Ostrikov[2], A.V. Shanin[1]
[1]Moscow State University, Moscow, Russia, korolkov@physics.msu.ru
[2]Central Aerohydrodynamics Institute, Moscow, Russia, aeroacoustics@mktsagi.ru

Experiment based on the MLS technique is very useful in architectural acoustics [1, 2]. The experiment is performed as follows. The investigated area is explored with a quasi-noise signal, whose autocorrelation function is close to a delta function. After a correlation-based data processing one obtains an impulse response of the area for given positions of source and receiver.

MLS experiment can be useful in aeroacoustics because it allows direct observation of fields diffracted by obstacles having complex shape. For example, sometimes it is necessary to measure the coefficient o shielding of the engine and flow noise by an airfoil. This can be done using the MLS technique.

Besides, authors are not aware of any MLS experiments in presence of an air flow. The current work is aimed to field this gap and to find a pulse response corresponding to the acoustical path in presence of turbulent and laminar flows.

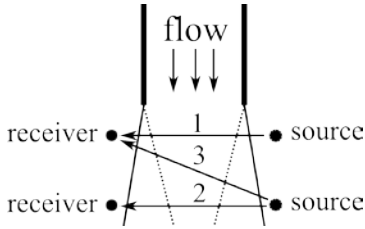

Fig. 1. Experimental setup

The experimental setup is shown in Fig. 1. Three acoustical paths have been explored. Two of them were perpendicular to the flow and the third one crossed it tangentially. The third path allows one to study the longitudinal Doppler effect and first two allows to study the transversal Doppler effect. The velocity of the flow were taken as 0, 20, 40, 60, 80 m/s. The amount of noise was significant at all nonzero velocities, but a considerable measurement time made us possible to recover pulse responses.

Typical results of the experiment are shown in Fig. 2. It is obvious that the flow perpendicular to the acoustical path (bottom) does not affect the signal and longitudinal part of the flow (top) causes drift and focusing.

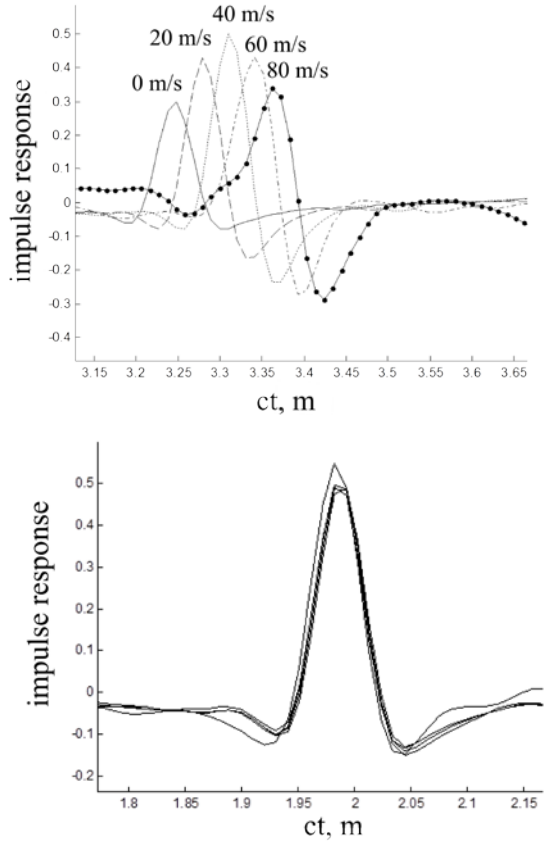

Fig. 2. Impulse responses for path 3 (top) and paths 1 and 2 (bottom)

References

1. V.Yu. Valyaev, A.V. Shanin. Method of the Maximum Length Sequences in a Diffraction Experiment. Acoust. Phys., v. 57, 2011, pp. 427–431.
2. V.Yu. Valyaev, A.V. Shanin. Acoustical estimation of parameters of porous road pavement. Acoust. Phys., v. 58, 2012, pp. 731–739.

AZIMUTHAL MODE MEASUREMENTS WITH ARRAY OF MICROPHONES IN LIMITED ANGULAR RANGE

I.V. Belyaev[1,2], Yu.V. Bersenev[2,3], R.V. Burdakov[2,3], V.V. Ershov[2], O.Yu. Kustov[2], V.V. Palchikovskiy[2], T.A. Viskova[2,3]

[1]*Central Aerohydrodynamic Institute, Moscow, Russia, aeroacoustics@tsagi.ru*

[2]*Perm National Research Polytechnic University, Perm, Russia, vvpal@perm.ru*

[3]*OJSC «Aviadvigatel», Perm, Russia, bersenev@avid.ru*

Azimuthal mode measurements are quite common in aeroacoustics and are performed for sound fields both inside ducts [1, 2] and in the free space [3, 4]. For these measurements, rotating rakes or circular stationary microphone arrays are primarily used. However, there are practical situations where the azimuthal modes have to be measured in the conditions that prevent locating microphones in a range of azimuthal angles. Therefore, the present work addresses the problem of the feasibility of azimuthal mode determination with a microphone array, which comprises microphones located in a limited angular range instead of the full circle (360º).

Azimuthal modes were determined from the measurements performed with a sparse circular microphone array installed inside the intake duct of a turbofan engine. The experiments were performed in the laboratory conditions in the anechoic chamber of Perm National Research Polytechnic University (Fig. 1) with azimuthal modes generated by a number of loudspeakers, and during static engine tests on the ground rig.

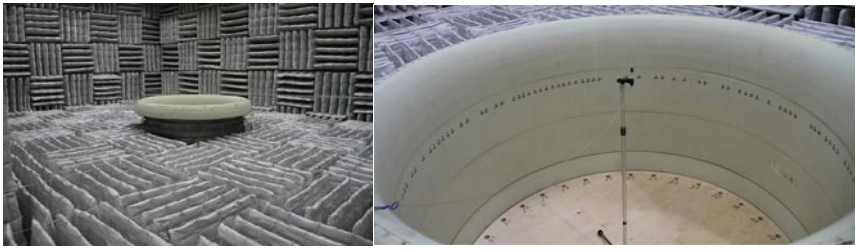

Fig. 1. A photo of the intake installed in the anechoic chamber of PNRPU (left) and a photo of microphone array in the duct (right)

The microphone array comprised 100 microphones located along the full circle, with their positions being optimized for increasing the dynamic range of the array [2]. To check the feasibility of the correct determination of azimuthal modes with an array that consists of microphones in a limited angular range, a limited number of microphones from the array were used in post-processing of the data. The results obtained with this limited microphone arrays were compared with the results of the full 100-microphone array.

As expected, the arrays with limited angular range of microphone positions have smaller dynamic range and therefore their measurements of azimuthal mode amplitudes tend to be contaminated by spurious contributions from the other modes. Nevertheless, the limited arrays still allow correctly determining the dominant mode order, provided their angular range is not too small. It could be envisaged that increase of the number of microphones in a limited array would compensate for the decrease in the dynamic range due to angular position limitations. However, the study demonstrates that such an increase in microphone number does not significant improve the azimuthal mode amplitude measurements and may even deteriorate the results. It seems to suggest that there is the optimal number of microphones for a limited array, which depends upon its angular range and the number of modes to be measured.

It should be noted that the positions of the microphones in the limited arrays were not optimized from the viewpoint of their dynamic range; instead, available microphones from the full array were used. It can be expected that optimization of microphone positions in the limited angular range will somewhat increase the dynamic range of the arrays and will lead to better comparison of the mode amplitudes.

Although the study was performed for induct modes, the results are applicable to azimuthal measurements in the free space as well.

The work has been performed with the financial support of the Russian Foundation for Basic Research under grant RFBR 16-41-590250 p_a.

References

1. D.L. Sutliff. Turbofan duct mode measurements using a continuously rotating microphone rake, Int. J. Aeroacoustics, 2007, V. 6, pp. 147–170.
2. E.R. Rademaker, P. Sijtsma, B.J. Tester. Mode detection with an optimized array in a model turbofan engine intake at varying shaft speeds, AIAA Paper 2001-2181.
3. V.F. Kopiev, M.Yu. Zaitsev, R.K. Karavosov. Experimental Investigation of Azimuthal Structure of Dipole Noise for Rigid Cylinder Inserted in Turbulent Jet, AIAA Paper 2004-2927.
4. G.A. Faranosov, I.V. Belyaev, V.F. Kopiev, M.Yu. Zaytsev, A.A. Aleksentsev, Yu.V. Bersenev, V.A. Chursin, T.A. Fadeeva. Adaptation of the azimuthal decomposition technique to turbulent jet noise of an aircraft engine in the ground tests, AIAA Paper 2015-2995.

LOCATING NOISE SOURCES OF SUBSONIC JET USING RANS/ILES-METHOD

L. Benderskiy, S. Krasheninnikov
FGUP «CIAM named after P.I. Baranov», Moscow, leosun.ben@gmail.com

One of the important tasks of jet calculating is the definition of jet noise and the influence of various factors on noise. Large eddy simulation (LES) is one of tools which can give detail picture of flow. However, at present, it is estimated [1], the simulation of jet flow with flow in the nozzle with help LES method require about 40×10^9 computational cells. The using various combined simulation methods (example high resolution RANS/ILES-method [2]) reduces these requirements and provides a good agreement with experiments [2-4] for the jet calculations with high Re number. Comparisons of calculations with experimental data by flow characteristics and jet noise was carried out in [2-4]. The good agreement with jet nose in far field suggests the possibility of a correct description of noise generation mechanisms in these calculations. The purpose of this work to describe the formation of noise sources in the subsonic jet based on data obtained from jet calculation using RANS/ILES-method [2].

The object of study is the cold subsonic jet from the conical SMC000 [5] nozzle previously calculated in [4]. The parameters correspond to the Mach number of 0.985 at the nozzle exit and the acoustic Mach is equal 0.9. The nozzle pressure ratio (NPR) is 1.86. The total temperature at the nozzle inlet is 300K and equal temperature of ambient air. The Re number by parameters at nozzle exit is equal 1.2×10^6. The mesh contains 3.1×10^6 cells. The time step is 1×10^{-4} s. Fig. 1 shows the comparison of calculated jet noise and experimental data. The distance of microphones is R/D=50 (D=2 m - diameter of the nozzle exit). The noise calculation was carried out by FWH method in combination with forward time stepping technology [6] and with averaging by out cups [7].

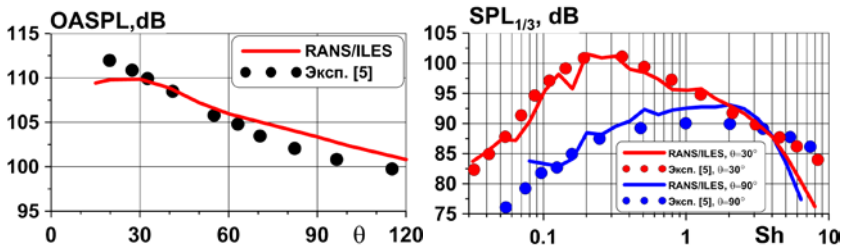

Fig. 1. Overall sound pressure level of jet (left picture) and one-third octave spectrum of jet noise for microphones at 30° and 90°

In calculation result fields of pressure and velocity vector in the longitudinal plane of the jet flow were saved for approximately 5000 time steps. An

analysis of the calculation results showed that there are zones of high pressure and low pressure relative to the environment pressure in mixing layer at instantaneous fields (Fig. 2a). Their size increases with the distance from the nozzle exit. While on average, there is only underpressure in the mixing layer (Fig. 2b).

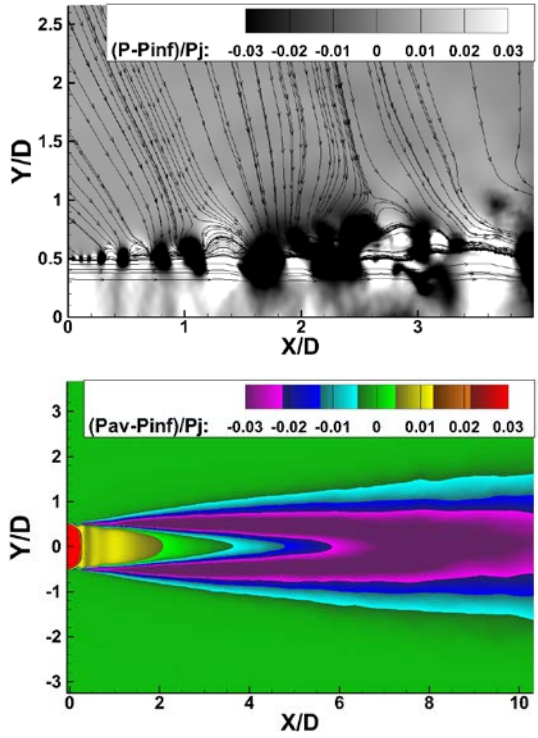

Fig. 2. Pressure field in the longitudinal plane
(a) instantaneous field (b) average field

The study of noise source location was conducted with the help of phase analysis. There are references to this type of analysis, but with obtain a stationary phase distribution. For example, in [8] this analysis was used to describe the feedback loop while generating discrete tone in a supersonic jet impingement on a perpendicular wall. In this paper, a study of changes over time of noise emission phase at different frequencies was carried out. To conduct this analysis at each point of a longitudinal section for each time step it was performed a fast Fourier transform of static pressure for interval of the 1024 time steps. The result of this analysis for frequency 156.25Hz (Sh≈1) is shown in Fig. 3. This figure shows that the position of noise emission correspond longitudinal coordi-

nate X/D≈1.8. Similar calculations were made for the vertical velocity fields and other radiation frequency.

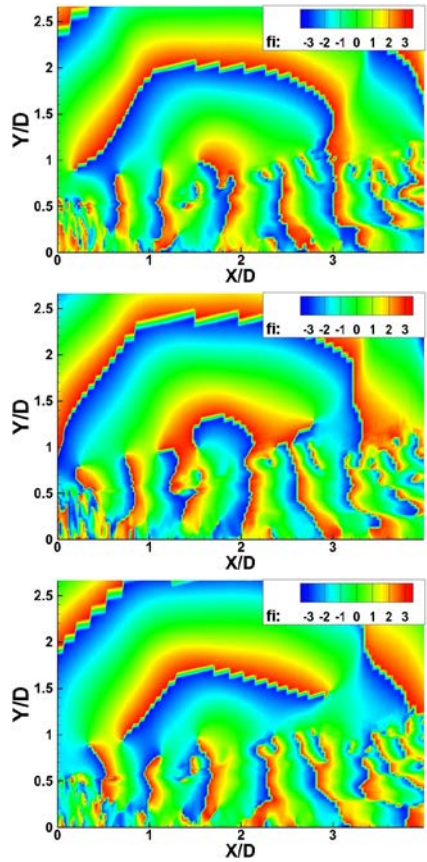

Fig. 3. Fields of phase for radiation frequency 156.25Hz (St≈1) with time step ≈0.0024 second

This work was supported by RFBR (grant number 14-01-00325_a).

References

1. Uzun A., Hussaini M.Y. Simulation of Noise Generation in the Near-Nozzle Region of a Chevron Nozzle Jet. AIAA J., 2009, Vol. 47, № 8, P.1793–1810.

2. Lyubimov, D.A. Development and application of a high-resolution technique for Jet flow computation using large eddy simulation. High Temperature, 2012, Vol. 50, №3, P. 420–436.
3. Bendersky, L. A., Lyubimov, D. A. High-resolution RANS/ILES method for complex turbulent jets. TsAGI Science Journal, 2014, Vol. 45, № 3-4, P. 215–236.
4. Benderskiy L.A., Lyubimov D.A. Investigation of flow parameters and noise of subsonic and supersonic jets using RANS/ILES high resolution method. 29-th Congr. Int. Counc. Aeronaut. Sci., St. Petersburg, Russ., Sept. 7-12., 2014, № 2014_0373.
5. Bridges J., Brown C. Parametric Testing of Chevrons on Single Flow Hot Jets. AIAA P., 2004, № 2004-2824.
6. Ozyoruk Y., Long L. A New Efficient Algorithm for Computational Aeroacoustics on Parallel Processors. JCP, 1995, Vol. 125, P. 135–149.
7. M.L. Shur, P.R. Spalart, M.Kh. Strelets. Noise prediction for increasingly complex jets. Part I: Methods and tests. International Journal of Aeroacoustics, 2005, Vol. 4, № 3&4, P. 213–246.
8. A. Dauptain, L.Y.M. Gicquel, S. Moreau. Large Eddy Simulation of Supersonic Impinging Jets. AIAA Journal, 2012, Vol. 50, № 7, P. 1560–1574.

ABOUT ACCURACY OF EXPERIMENTAL DATA FOR VALIDATION OF NUMERICAL METHODS

S.M. Bosnyakov[1,2], A.F. Chevagin[1], A.R. Gorbushin[1], I.A. Kursakov[1], S.V. Matyash[1], S.V. Mikhailov[1]

[1]*Central Aerohydrodynamic Institute named after prof. N.E. Zhukovsky (TsAGI), Zhukovsky, Russia, bosnyakov@tsagi.ru*

[2]*Moscow Institute of Physics and Technology (state university), Dolgoprudhy, Russia*

The wind tunnel (WT) is a main tool to obtain high-quality experimental data. It has the elements that significantly influence on the test results, for example, supporting devices, duct before the model, deflectable walls of test section, pre-chamber, nozzle, etc. Neglecting these devices leads to the fact that comparison of the numerical and experimental data gives incorrect results. In practice, WT of various types are applied. In each case, an approach that takes into account the specific features of the experimental equipment and experimental methodologies for this equipment [1] is necessary. The main attention is attended to transonic WT of T-128 type with perforated walls and to subsonic WT of T-104 type of with an opened test section.

It is known that the computational codes, which realize the 3D approaches, work at full capacity of available computers [2]. It results in the fact that, as a rule, the numerical methodology is closely connected with the capabilities of the computer system for maximal optimization of its resources. Now there are modern clusters with hundreds or thousands of processors. An essential factor is the multiple reduction of such system cost. It permits to organize the validation of computational methodologies at a fundamentally new level.

This report presents estimations that characterize the demands of various firms-developers for aviation equipment to the accuracy of experimental and calculated data. The influence of various factors on the error values is discussed. In particular, it is shown that even such "inessential" phenomena as changes of strain-gauge balance temperature or neglecting the height of mounting the gauges for measuring the flow parameters in the WT test section can lead to significant errors that influence on the results of the numerical method validation.

The problem of differences between the experimental data obtained in different WT is discussed. For example, the numerical methodology based on corrected comparison with the experiment results is developed in order to eliminate different errors. The main attention is paid on a problem of Reynolds number simulation in the tests of small size models. Negative consequences of excessive growth of pressure in WT pre-chamber because of changing the air thermodynamic properties are demonstrated.

The data showing that, in many cases, there are errors, which can not be taken into account when during the experimental result processing, are presented. In particular, the model tail sting and a cavity between the "core" and the model are considered. It is shown that this cavity under certain conditions results in errors that are comparable with the order of the studied variables.

The results of [3] are discussed and the thesis is shown that the difference between the numerical and experimental data, which is noted in this work, is resulted not from the physical aspects of the problem but due to implementation the experimental data at stall regime, which have been obtained in WT with solid walls.

Examples of experimental data application for turbulence model adjustment are presented. They permit to extend the scope of computational approaches in the zones of separated flow. It is shown how the sensor inertia influences on the accuracy of non-stationary parameters determination. The application of devices with a narrow range (vacuum-gauge, for example) for measurements in selected zones to increase the accuracy and quality of theory-experiment comparison is substantiated.

The procedure of evaluating the accuracy of calculation methods proposed by Cassidian is described. Approaches to determine the effectiveness of numerical codes with different architecture computers are discussed. The definitions of "confidence interval" and "effective performance" are given. The examples of calculation are discussed.

The work was supported by Russian Ministry of Education and Science within the Federal Target Program “Studies and Designs on Priority Directions of the Russian Science-Technology Complex Development in 2014-2020”. Agreement No. 14.628.21.0005, 18 November 2015.

References

1. S.A. Glazkov, A.R. Gorbushin, A.I. Ivanov, A.V. Semenov. Recent experience in improving the accuracy of wall interference corrections in TsAGI T-128 wind tunnel. Progress in Aerospace Sciences, Pergamon Press, v.37, No.3, 2001.
2. V. Neyland, S. Bosniakov, S. Glazkov, A. Ivanov, S. Matyash, S. Mikhailov, V. Vlasenko. Conception of electronic wind tunnel and first results of its implementation. Progress in Aerospace Sciences, v.37, №2, 2001, pp.121-145.
3. URL: "http://hiliftpw.larc.nasa.gov/index-workshop1.html"

PARALLEL IMPLEMENTATION OF DG METHOD HIGH ORDER OF ACCURACY AND SOLUTION OF CLASSICAL TESTING PROBLEMS

S.M. Bosnyakov, **S.V. Mikhaylov**, V.Yu. Podaruev, A.I. Troshin
TsAGI, Zhukovsky, sergey.mikhaylov@tsagi.ru

The paper provides a brief description developed in TsAGI code based on the Discontinuous Galerkin method with high order of accuracy basis functions. Reconstruction of the functions carried out for the conservative variables. This makes it possible to simplify the formulation of the scheme for unsteady flows. Gradients of parameters to calculate the diffusion fluxes are calculated using the method of Bassi-Rebay-2 [1]. Scheme requires precise integration of cell volume and surface. For this purpose, Gauss quadrature rules are used, that are written for the standard cube. Coordinate transformations are done by serendipity elements. For K=2 and K=3, calculations are performed taking into account the curvature of the surface. Number of quadrature points at the cell and on the face are shown in the table.

N	DG, K=0	DG, K=1	DG, K=2	DG, K=3
N_V	1	25	38	62
N_S	1	4	10	18
$6\,N_S+N_V$	7	49	98	170

A comparison with the finite volume method is performed. We consider the methods of Godunov, linear reconstruction, WENO with linear weights. For the integration parameters on the face uses alone quadrature point. Reconstruction of the functions carried out for the nonconservative variables.

Testing of the developed method was carried out on the calculations of the set of tests, that are used to determine the order of accuracy of the schemes. The first test is subsonic flow around a circular cylinder in an ideal gas. The calculations were performed on a series of nested grids dimension from 16 x 4 up to 128 x 32 cells. The first size determines the number of cells along the cylinder, the second - along the radius. Radius of cylinder r_0 =0.5, border radius r_J =20. Radius of grid lines selected so that the cells near the cylinder should have the same size in all directions. On the surface of the cylinder and at planes perpendicular to the cylinder sets a symmetry boundary condition. On the outer boundary, parameters of the far field are used. Calculations were carried out at the next set of parameters of gas: p_{inf} = 100000Pa, T_{inf} = 293K, u_{inf} = 50m/s ($M \sim 0.15$).

The order of accuracy for different schemes was estimated by calculating the entropy error, which is defined as $e_{entropy} = S/S_{inf} - 1$. Calculation results are

presented below as the dependence on the entropy errors of L2 norm from *NDOF* (product of mesh size to the number of basis functions). In the case of finite volume method, *NDOF* coincides with the number of cells. It is evident that the order of accuracy of the method of finite volume does not exceed 2. DG demonstrates a predictable $O(h^{k+1})$ order of convergence of a smooth solution.

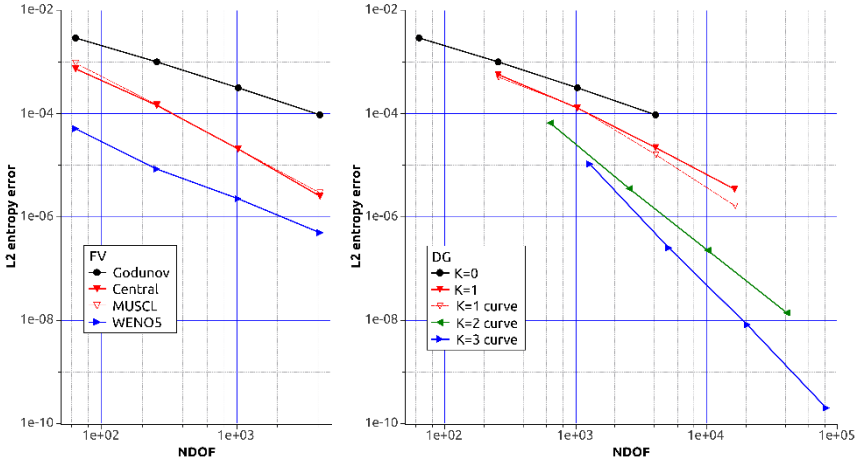

Fig. 1.

Other tests to determine the accuracy of numerical schemes are: 2D evolution of isentropic vortex, 3D convection of the disturbance of pressure in the form of Gaussian "hats", the decay of the Taylor-Green vortex.

This work was supported by the Ministry of Education and Science of the Russian Federation (grant from the November 18, 2015 №14.628.21.005).

References

1. F. Bassi, S. Rebay. A high-order accurate discontinuous finite element method for the numerical solution of the compressible Navier–Stokes equations. J. Comput. Phys., vol. 131, № 1, p. 267–279, 1997.

TILDA : Towards Industrial LES/DNS in Aeronautics – PAVING THE WAY OF FUTURE ACCURATE CFD

Vincent Couaillier[1], Charles Hirsch[2], Werner Haase[3]
[1]*ONERA, The French Aerospace Lab, Palaiseau, France, vincent.couaillier@onera.fr*
[2]*NUMECA, Brussels, Belgium, charles.hirsch@numeca.be*
[3]*Aeronautics Consultant, Neubiberg, Germany, whac@haa.se*

The ability to simulate aerodynamic flows using CFD methods has progressed rapidly over the last decades and has given rise to a change in design processes in aeronautics already. But more improvement is necessary to overcome the (still) existing lack in confidence in CFD usage, based on turbulence modelling. The TILDA project will offer methods combining advanced and efficient high-order numerical schemes (HOMs) with innovative approaches for LES and DNS in order to solve all relevant flow features on tens of thousands of processors in order to get close to a full LES/DNS solution for 1 billion DOF's not exceeding turn-around times of a few days.

The TILDA project will provide both an improved physical knowledge and more accurate predictions of non-linear, unsteady flows which will directly contribute to an enhanced reliability. The main highly innovative objectives, targeting at industrial needs read:

- Advance methods to accelerate HOM for unsteady turbulence simulations on unstructured grids.
- Advance methods to accelerate LES and future DNS methodology by multi-level, adaptive, fractal and similar approaches on unstructured grids.
- Use existent large scale HPC networks to enable industrial applications of LES/DNS close(r) to daily practice. Compact high-order methods offer a very high ratio between computational work per DOF combined to a low data dependency stencil, making these methods extremely well adapted for shared-memory parallel processors.
- Provide grid generation methods for HOM on unstructured grids with emphasis on valid curvilinear meshes for complex geometries.
- Provide suitable I/O and interactive co- and post-processing tools for large datasets.
- Demonstration of multi-disciplinary capabilities of HOM for LES in the area of aeroacoustics.

The presentation will address some notable results after one year of the project.

NUMERICAL SIMULATION OF TURBULENT FLOW OVER A CAVITY FOR FUNDAMENTAL AND APPLIED PURPOSES

B.N. Dankov[1], A.P. Duben[2], **T.K. Kozubskaya**[2], N.S. Zhdanova[2]
[1]Central Research Institute of Machine Building (TsNIIMash), Korolev, Moscow region, Russia
[2]Keldysh Institute of Applied Mathematics RAS, Moscow, Russia, Alexey.Duben@gmail.com

Nowadays computational experiment has become one of the approaches for solving both fundamental and applied problems related to complex turbulent flows. It happens owing to the gradual development of supercomputers, mathematical models and numerical methods. Therewith the scale resolving approaches (DNS, LES of hybrid RANS-LES) have been developed well enough, to provide correct predictions of turbulent flows and associated acoustical fields. In contrast with the RANS methods, they allow to obtain unsteady characteristics like turbulent and acoustic pulsations which are of crucial importance for revealing the flow physics and evaluating the technical parameters needed for engineering.

Besides the traditional ways of numerical data processing and visualization, an interesting information can be provided by spectral and correlation analysis. This type of analyses is implementable since, unlike full-scale physical experiments, the numerical simulation has practically no limitations in spatial and temporal resolution of unsteady output data.

At another point, the development of efficient numerical methods on unstructured meshes and modern computational techniques (like, for instance, immersed boundary conditions (IBC)) open the door for treating complex geometries and therefore solving applied problems with real configurations.

There is no doubt that, in order to take full advantage of a computational experiment, a rigorous validation of the numerical algorithms and the corresponding codes on similar cases with reliable experimental or reference data available is required. Only this way can guarantee the correctness of numerical results both for applied and fundamental problems. This requirement is crucial especially if dealing with complex turbulent flows simulated using scale-resolving approaches.

Transonic turbulent flows over cavities are considered in the paper. The research code NOISEtte [1] is used for computational experiments. NOISEtte is being developed for solving aerodynamic and aeroacoustics problems on unstructured meshes. The numerical algorithms are built on the higher-accuracy quasi-1D edge-based reconstruction (EBR) scheme [2]. The most recent enhanced DDES formulation [3] accelerating RANS-to-LES transition in shear layers is chosen as a scale-resolving approach for turbulent flow modeling.

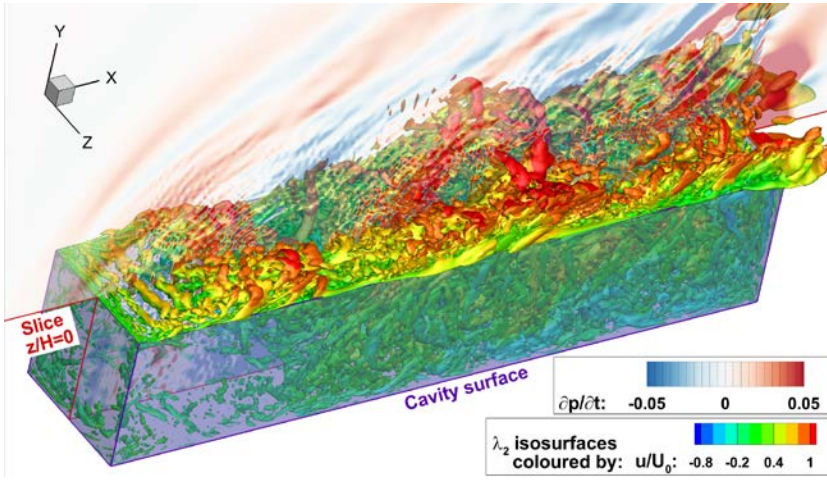

Fig. 1. Visualization of the flow over M219 cavity

The transonic turbulent flow over the M219 cavity [4] is considered as a case for validation. The M219 cavity has a parallelepiped geometry with the parameters: $L_x \times L_y \times L_z = 5H \times H \times H$ (H is cavity depth), $\mathrm{Re}_H = 1.37 \cdot 10^6$, M_∞ = 0.85. The flow visualization is presented in Fig. 1. This case is widely used to verify computational algorithms which implement scale-resolving methods. The results of validation based on the comparative analysis against the corresponding experimental data [4] speak for the good accuracy and correctness of the simulations. The validation data will be presented in detail.

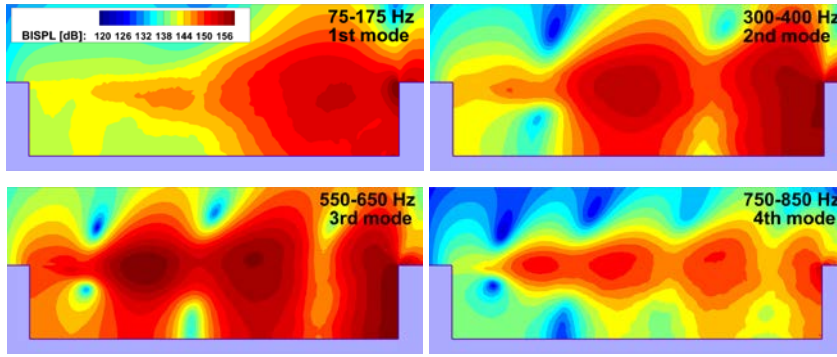

Fig. 2. Fields of band integrated sound pressure levels (BISPL) extracted from the results of simulation of M219 cavity case

The validity of the numerical results obtained on M219 cavity case offers scope for a further deeper investigation of the inside-cavity processes. We do it

basing on the large amount of unsteady flow data accumulated during the simulation. The data on the central cross-section and the cavity surfaces are postprocessed using the methods of spectral and correlation analysis. The study provides a comprehensive information for understanding of the flow physics and associated noise generation mechanisms which are specific for the cavity configuration under consideration. For example, the fields of band integrated sound pressure levels covering the corresponding Rossiter modes are presented in Fig. 2. The patterns of averaged pressure fields resemble standing waves which are generated inside the cavity. Note that the spectral and correlation analysis of unsteady flow fields can be useful not only for fundamental but for applied purposes.

The transonic turbulent flow ($M = 0.85$, $\mathrm{Re}_H = 7 \cdot 10^6$) over the cavity of more complex configuration is considered as an example of related industry-oriented problem. The cavity geometry involves a wedge face on the aft edge and has the following parameters: $L_x \times L_y \times L_z = 7.59H \times H \times 1.82H$.

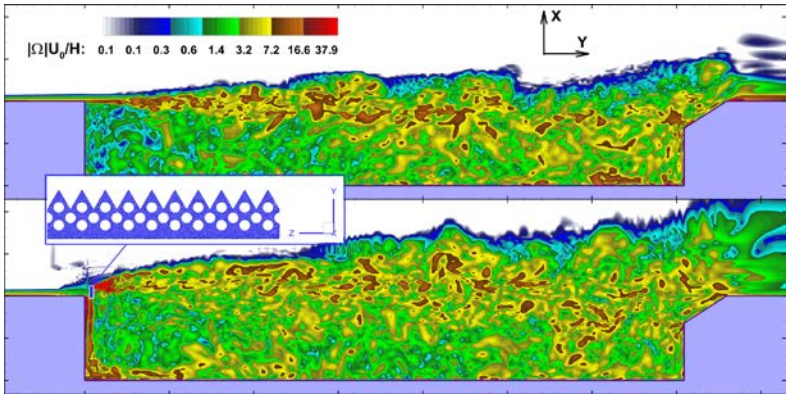

Fig. 3. Visualization of turbulent flow over the cavity without (left) and with deflector (right) in the central cross-section

The predictions of turbulent flow over the cavity with and without the deflector installed at the leading edge are carried out. The IBC method is used for the description of the deflector. The visualization of both flows (without and with the deflector) in the central cross-section is given in Fig. 3. A comparative study of the numerical results will be presented in detail. Generally, it shows the deflector impact on the structure of turbulent flow inside the cavity and its potential to reduce the acoustic loads on the cavity walls.

The work is supported by the Russian Science Foundation (projects № 14-11-00060 – development of scale-resolving methods on unstructured meshes, and № 16-11-10350 – development of immersed boundary conditions for solid-body description in a turbulent flow).

References

1. I.V. Abalakin, P.A. Bakhvalov, A.V. Gorobets, A.P. Duben, T.K. Kozubskaya. Parallel research code NOISEtte for large-scale computations of aerodynamics and aeroacoustics problems. Vych. Metody i program., vol. 13, 2012, pp. 110–125.
2. I.V. Abalakin, P.A. Bakhvalov, T.K. Kozubskaya. Edge-based reconstruction schemes for unstructured tetrahedral meshes. Int. J. Numer. Meth. Fl., 2016, **81** (6), pp. 331–356.
3. M. Shur., P. Spalart, M. Strelets, A. Travin. An Enhanced Version of DES with Rapid Transition from RANS to LES in Separated Flows. Flow, turbulence and combustion, 2015, **95** (4), pp. 709–737.
4. de Henshaw M.J.C. M219 cavity case: Verification and validation data for computational unsteady aerodynamics. Tech. Rep. RTO-TR-26, AC/323(AVT)TP/19. QinetiQ, UK, 2002, p. 453–472.

AVIATION NONCOMPACT NOISE SOURCES SHIELDING IN PRESENCE OF THE MEAN FLOW: EXPERIMENTAL AND THEORETICAL INVESTIGATIONS

Stanislav L. Denisov, Nikolay N. Ostrikov
Aerohydrodynamic Institute (TsAGI), Moscow, Russia, aeroacoustics@mktsagi.ru

The shielding effect was first estimated for aviation noise in the 1970s [1, 2] and showed extremely high efficiency of the engine noise shielding. As a result, shielding effect is considered as a realizable tool for satisfying of the new requirements for the external noise level reduction; the investigations of shielding effect were enhanced.

In our previous papers [3, 4, 5], theoretical and experimental investigation was carried out for clearing influence of sources noncompactness on shielding efficiency *without the mean flow effect.* Experiments showed what noise reduction by means of acoustical shielding is a difficult task which depending from the relative position of the source (engine) and screen (airframe). Different aviation noise sources (jet noise, rotor or fan noise) have different mechanisms of noise shielding. In particular, shielded tone and broadband noise generated by propellers (rotors or fans) have different properties. It was shown that this fact especially connected with them noncompact nature, and the investigations showed that the noncompactness is very important property of sound source for shielding effect if source disposal closely to the screen.

Analysis of the different diffraction theories showed what Geometrical Theory of Diffraction (GTD) are more appropriate methods in comparison with Fresnel/Kirchhoff methods for shielding effect calculation if noncompact sources are under consideration. We found that the GTD has rather simple form for explaining the main features of diffraction pattern revealed in our experiments.

The GTD shows the importance of phase characteristics in near field for shielding effect description. It means that the mean flow effect is to be taken into consideration for correct describing the diffraction (especially for the inhomogeneous flow) because the flow appearance changes the phase distribution of incident acoustic field that alters the diffraction pattern.

A lot of successful investigations were carried out with the purpose to take into account the flow effect on diffraction [6-10]. In the present work, we take into account these results to investigate the mean flow effect on shielding efficiency for *noncompact* noise sources.

In the experimental part of the present work the following results are presented: jet noise acoustic shielding effect (single and dual stream nozzles) in presence of co-flow, rotor noise shielding effect in the presence of mean flow. TsAGI's small scale propeller rig was modified after the previous work [4] and

the screen of smaller size is used for the present investigations, therefore we obtain new result for rotor noise shielding efficiency already for the case of mean flow absence. Comparing the results of both test campaigns, we clarify the difference between the shielding efficiency for tone and broadband noise in the presence of mean flow.

In the theoretical part of the present work, we consider inviscid formulation of the diffraction problem in the presence of mean flow and simple geometry of flat screen is used such as infinite strip which doesn't disturb the mean flow. GTD is applied for extracting main feature of shielding effect for model noncompact sources of tone and broadband noise.

It is shown that the comparison of shielding and unshielding field at different Mach number deals simultaneously with two factors: the variations of the diffracted field and the variations of free source due to Mach number effect. The calculations confirm the experimental results that mean flow effect on shielding efficiency exhibits ambiguity feature: the mean flow velocity increasing leads to increasing shielding efficiency also in some cases, but the opposite behavior is observed for other cases.

Calculations show that the behavior of the shielding efficiency depends directly on the variations of unshielded field at co-flow Mach number growth. It is show that the shielding efficiency of tone noise component exhibits a great sensitivity to the variations of Mach number in shadow zone, while broadband noise component is weak depended on it. This fact connects especially with the noncompact nature of the source. Moreover, the mean flow effect exhibits weaker for broadband noise shielded by swept strip.

Calculations show that the effects of noise amplification in light zone and asymmetry of shielded field for the scattering of rotating modes (it were explained in details in [4]) are maintained at co-flow appearance also.

In the whole, the present investigations show that the mean flow effect on shielding efficiency has multifactors character in principle. For predicting it in practice, it is necessary to know in details the source noise characteristics as function of Mach number. Moreover, the source noise characteristics can depend on the mutual position source and screen. For example, propellers, fans, rotors noise is determined by flow nonuniformity arisen at close position sources and screens. Thus, the diffraction problem is rather difficult at co-flow presence.

Performed experiments showed what noise reduction by means of acoustical shielding is a difficult task which depending from the mean flow velocity, the relative position of the source and screen. The experiments show that mean flow effect on shielding efficiency exhibits ambiguity feature and depends from geometrical parameters of the shield. An important feature is that the shielded tone and broadband noise generated by propellers (rotors or fans) have different properties. This fact especially connected with them noncompact nature. The

investigations show that the noncompactness is very important property of sound source for shielding effect if source disposal closely to the screen, especially in the presence of the mean flow.

References

1. U. Von Glahn, D. Groesbeck, and M. Reshotko. Geometry Considerations for Jet Noise Shielding with CTOL Engine-Over-The-Wing Concept. AIAA Paper 74-568, June 1974.
2. U. Von Glahn, D. Groesbeck, and J. Wagner. Wing Shielding of High-Velocity Jet and Shock – Associated Noise with Cold and Hot Flow Jets. AIAA Paper 76-547, July 1976.
3. S.L. Denisov, M.Yu. Zaitsev, V.F. Kopiev, N.N. Ostrikov. Theoretical and Experimental Investigations of the Aircraft Noise Shielding by means of Airframe Structures. Third International Workshop "Computational Experiment in Aeroacoustics", Svetlogorsk, Russia, September 24-27, 2014.
4. N.N. Ostrikov, S.L. Denisov. Airframe Shielding of Noncompact Aviation Noise Sources: Theory and Experiment. AIAA Paper 2015-2691, June 2015.
5. S.L. Denisov, N.N. Ostrikov. Comparison of the Methods for Noncompact Aviation Noise Sources Shielding Calculation. The 22nd International Congress on sound and Vibration (ICSV), Florence, Italy, 12-16 July, 2015.
6. D.G. Crighton, F.G. Leppington. "Scattering of aerodynamic noise by a semi-infinite compliant plate". J. Fluid Mechanics, vol. 43, part 4, 1970, pp. 721–736.
7. S.M. Candel. Diffraction of a Plane Wave by a Half Plane in a Subsonic and Supersonic Medium. J. Acoustic Society of America, vol. 54, No 4, 1973, pp.1008–1016.
8. R.K. Amiet. High Frequency Thin-Airfoil Theory for Subsonic Flow. AIAA Journal, vol. 14, No 8, 1976, pp. 1076–1082.
9. S.W. Rienstra. Sound diffraction at a trailing edge. J. Fluid Mechanics, vol.108, 1981, pp. 443–460.
10. R.K. Amiet. Unified Aeroacoustics Analysis for High Speed Turboprop Aerodynamics and Noise. Volume II - Development of Theory for Wing Shielding. NASA Contractor Report 185192, May 1991.

APPLICATION OF STRUCTURED AND UNSTRUCTURED NUMERICAL ALGORITHMS BASED ON ENHANCED DDES FORMULATION ACCELERATING THE RANS-TO-LES TRANSITION IN SHEAR LAYERS FOR SIMULATION OF TURBULENT JET NOISE

A.P. Duben[1], T.K. Kozubskaya[1], M.L. Shur[2], M.Kh. Strelets[2]
[1]*KIAM RAS, Moscow, Russia, Alexey.Duben@gmail.com*
[2]*SPbPU, Saint-Petersburg, Russia*

The gradual development and enhancement of the hybrid RANS-LES approach DES (Detached Eddy Simulation) have significantly expanded the frames of its application. The most recent DES formulation [1] has strongly advanced in solving one of the fundamental problems of the original method which is the so-called "grey area" problem resulting in the delay of "numerical" transition from the steady RANS to unsteady LES solution in shear layers. The acceleration of RANS-to-LES transition and the developed turbulence generation in [1] is achieved by the modification of LES subgrid scale. It provides an automatic identification of the initial regions of shear layers and the corresponding reduction of subgrid viscosity in these areas. At the same time, the new (Shear-Layer Adapted) subgrid scale Δ_{SLA} naturally switches to the classical (for LES branch of DES) definition $\Delta = \Delta_{max} = \max\{\Delta_x, \Delta_y, \Delta_z\}$ in the region of developed turbulent flow. As a result, the method has been extended to the simulation of a wide range of problems where the delay of developed 3D turbulence generation in shear layers causes unacceptably poor accuracy in the prediction of most important ("principal") properties. Jets are a typical demonstrative example of such flows which is considered in the paper.

The simulations of immersed unheated subsonic round jet ($M_{jet} = 0.9$, $Re = 1.1 \cdot 10^6$) which is widely used for testing numerical methods for aeroacoustics have been carried out using two essentially different numerical algorithms: "structured" and "unstructured". The first one exploits regular meshes and the finite volume numerical methods which are implemented in the research CFD code NTS (Numerical Turbulence Simulation) [2]. The unstructured algorithm is built basing on the higher-accuracy numerical techniques implemented in the research code NOISEtte [3]. The common feature of both methodologies is the usage of hybrid central-difference – upwind numerical scheme based on MUSCL approach and the Roe Riemann solver for the approximation of convective fluxes. Note that the new subgrid scale definition in the recent modification [1] of DES has been formulated for structured cell-centered schemes. Here it is generalized for arbitrary unstructured meshes and vertex-centered method.

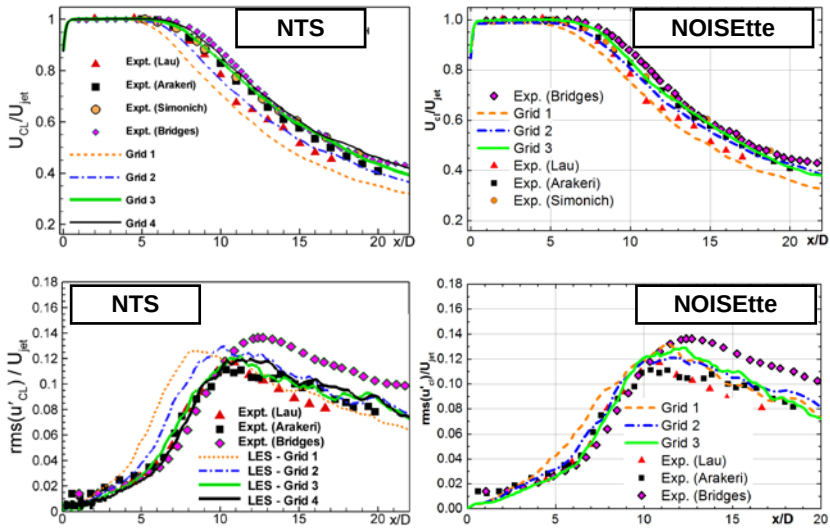

Fig. 1. Comparison of streamwise velocity component (left) and its root mean square deviation (right) profiles along the centerline obtained from the computations using the structured (NTS) and unstructured (NOISEtte) approaches

The computations are carried out on the sequence of refining meshes which contain from 1.5 M up to 21 M cells (or vertices) using both algorithms. The evaluation of the results of simulations includes the comparison of the near field aerodynamic and turbulence characteristics and the far field noise with the corresponding experimental data. Some comparisons are shown in Figs. 1 and 2. An obvious common trend is that the mesh refinement leads to the convergence and better agreement with the experiment of the results obtained using both structured and unstructured algorithms. A slight discrepancy between these algorithms (the reasons are still unclear) is observed on the far field noise spectrums (see Fig. 2).

Generally, the results obtained using both structured and unstructured algorithms are well correlated. This fact and the convergence of results confirms a correctness of the considered formulation of new subgrid scale [1] for unstructured meshes. Furthermore, the results prove that the developed methodology of solving the Navier-Stokes equations with the use of higher-order numerical schemes on unstructured meshes provides the accuracy well compared with that obtained by low-dissipative numerical algorithms for structured meshes.

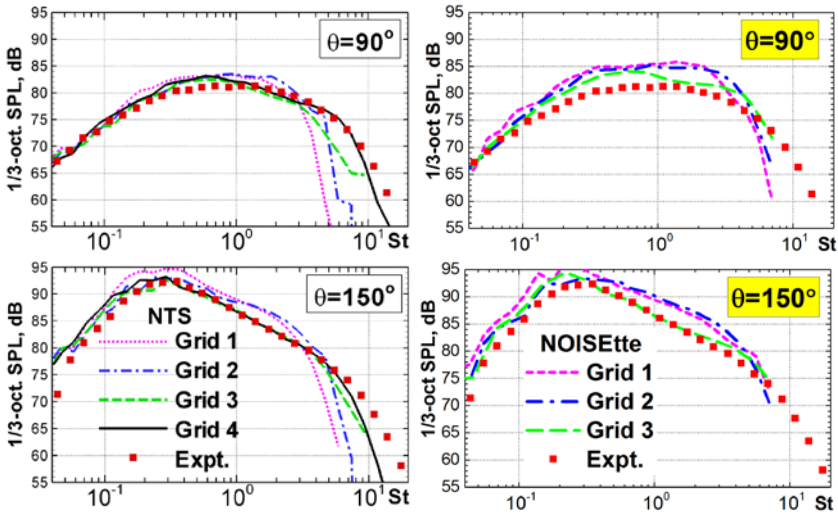

Fig. 2. Comparison of 1/3-octave noise spectrums at far field points obtained using integral Ffowcs-Williams-Hawking method and the data provided by structured (NTS), left, and unstructured (NOISEtte), right, approaches

The research is supported by Russian Science Foundation (Project № 14-11-00060).

References

1. M. Shur., P. Spalart, M. Strelets, A. Travin. An Enhanced Version of DES with Rapid Transition from RANS to LES in Separated Flows. Flow, turbulence and combustion, 2015, **95** (4), pp. 709–737.
2. M. Shur, M. Strelets, A. Travin. High-Order Implicit Multi-Block Navier-Stokes Code: Ten-Years Experience of Application to RANS/DES/LES/DNS of Turbulent Flows. Invited lecture. 7th Symposium on Overset Composite Grids and Solution Technology, October 5-7, 2004, Huntington Beach, USA.
3. I.V. Abalakin, P.A. Bakhvalov, A.V. Gorobets, A.P. Duben, T.K. Kozubskaya. Parallel research code NOISEtte for large-scale computations of aerodynamics and aeroacoustics problems. Vych. Metody i program., vol. 13, 2012, pp. 110–125.
4. Abalakin I., Bakhvalov P., Kozubskaya T. Edge-based reconstruction schemes for unstructured tetrahedral meshes. Int. J. Numer. Meth. Fl., 2016, **81** (6), pp. 331–356.

ON A POSTERIORI SUBCELL FINITE VOLUME LIMITERS FOR THE DISCONTINUOUS GALERKIN METHOD AND APPLICATIONS TO NONLINEAR HYPERBOLIC SYSTEMS

Michael Dumbser

University of Trento, Department of Civil, Environmental and Mechanical Engineering, Via Mesiano 77, I-38123 Trento, Italy

In our talk we present a new robust, accurate and very simple a posteriori subcell finite volume limiter technique for the Discontinuous Galerkin (DG) finite element method for nonlinear systems of hyperbolic partial differential equations in multiple space dimensions that works well for arbitrary high order of accuracy in space and time and that does not destroy the natural subcell resolution properties of the DG method. High order time discretization is achieved via a fully-discrete one-step ADER approach that uses a local space-time discontinuous Galerkin predictor method to evolve the data locally in time within each cell. The new limiting strategy is based on a novel *a posteriori* verification of the validity of a discrete candidate solution against physical and numerical detection criteria. In particular, we employ a relaxed discrete maximum principle, the positivity of the numerical solution and the absence of floating point errors as detection criteria. For those troubled cells that need limiting, our new approach recomputes the discrete solution by starting again from a valid solution at the old time level, but using a more robust finite volume scheme on a refined subgrid of $N_s=2N+1$ subcells, where N is the polynomial approximation degree of the DG scheme. The new method can be interpreted as an element-local check-pointing and restarting of the solver, but using a more robust scheme on a finer mesh after the restart. The performance of the new method is shown on a large set of different nonlinear systems of hyperbolic partial differential equations using uniform and space-time adaptive Cartesian grids (AMR), as well as on unstructured meshes in two and three space dimensions. In particular, we will also show applications to a new unified first order hyperbolic theory of continuum mechanics proposed by **G**odunov, **P**eshkov & **R**omenski (GPR model).

The presented research was financed by the European Research Council (ERC) with the research project STiMulUs, ERC Grant agreement no. 278267 and by the European Union's Horizon 2020 Research and Innovation Programme under the project ExaHyPE, Grant agreement number No.671698 (call FETHPC-1-2014).

References

1. M. Dumbser, O. Zanotti, A. Hidalgo and D.S. Balsara. ADER-WENO Finite Volume Schemes with Space-Time Adaptive Mesh Refinement. Journal of Computational Physics, **248**:257–286, 2013.
2. O. Zanotti, F. Fambri, M. Dumbser and A. Hidalgo. Space-Time Adaptive ADER Discontinuous Galerkin Finite Element Schemes with a Posteriori Subcell Finite Volume Limiting. Computers and Fluids, **118**:204–224, 2015.
3. O. Zanotti, F. Fambri and M. Dumbser. Solving the relativistic magnetohydrodynamics equations with ADER discontinuous Galerkin methods, a posteriori subcell limiting and adaptive mesh refinement. Monthly Notices of the Royal Astronomical Society (MNRAS), **452**:3010–3029, 2015.
4. M. Dumbser and R. Loubère. A simple robust and accurate *a posteriori* subcell finite volume limiter for the discontinuous Galerkin method on unstructured meshes. Journal of Computational Physics, **319**:163–199, 2016.
5. S.K. Godunov and E. Romenski. Nonstationary equations of nonlinear elasticity theory in Eulerian coordinates. J. Appl. Mech. Tech. Phys., **13**:868–884, 1972.
6. S.K. Godunov and E. Romenski. Thermodynamics, conservation laws and symmetric forms of differential equations in mechanics of continuous media. Comput. Fluid Dyn. Rev., **95**:19–31, 1995.
7. S.K. Godunov, E.I. Romenski. "Elements of Continuum Mechanics and Conservation Laws," Kluwer Academic/Plenum Publishers, 2003.
8. I. Peshkov and E. Romenski. A hyperbolic model for viscous Newtonian flows. Continuum Mechanics and Thermodynamics, **28**:85–104, 2016.
9. M. Dumbser, I. Peshkov, E. Romenski and O. Zanotti. High order ADER schemes for a unified first order hyperbolic formulation of continuum mechanics: viscous heat-conducting fluids and elastic solids. Journal of Computational Physics**, 314**:824–862, 2016.
10. W. Boscheri, M. Dumbser and R. Loubère. Cell centered direct Arbitrary-Lagrangian-Eulerian ADER-WENO finite volume schemes for nonlinear hyperelasticity. Computers and Fluids, **134–135**:111–129, 2016.

APPLICATION OF REGULARISED GASDYNAMIC EQUATIONS FOR NUMERICAL SIMALATION OF TURBULENT FLOWS WITH MODERATE REYNOLDS NUMBERS

T.G. Elizarova[1], I.A. Shirokov[2]

[1]*Keldysh Institute of Applied Mathematics RAS, Moscow, telizar@mail.ru*

[2]*CompMath. and Cybern Faculty, MSU, Moscow, ivanshirokov@inbox.ru*

We report our results of numerical modeling of laminar and turbulent subsonic viscous compressible gas flow based on quasi-gas dynamic (QGD) equations. The free-flows are examined for Taylor-Green vortex decay, the boundary layer flows are investigated basing on Couette flow. Comparison with DNS and LES reference data demonstrates that QGD numerical algorithm provides a uniform and adequate simulation of both laminar and turbulent evolution of the Taylor-Green vortex for Reynolds numbers from 100 up to 5000. Comparison with experimental data shows that QGD algorithm describes boundary-layer velocity profile including velocity pulsations. Compared with standard high-order accurate DNS simulations QGD algorithm demands a smaller number of spatial grid.

We underline, that QGD-based algorithm describes laminar and turbulent flows uniformly. It means that in numerical simulations the transition from laminar to turbulent flows are obtained by changing only the Reynolds number, without introducing turbulent viscosity and heat conductivity coefficients. QGD algorithm does not include near-wall functions for boundary layer simulations.

The quasi-gas dynamic (QGD) system can be interpreted as the Navier-Stokes equation system averaged or smoothed, over some small time or space interval. The smoothing gives rise to strongly non-linear additional dissipation terms, proportional to a small parameter τ that has the dimension of a time. These τ-terms are the second-order space derivatives in factor of τ and bring an additional entropy production that proves their dissipative character. Additional terms appear not only in the momentum and energy equations, but also in the continuity equation that models the turbulent mass-diffusion, which is inherent to turbulent mixing. In the boundary layer approach (Prandtl equations) the additional QGD dissipative terms vanish. These features of the QGD equations open nice perspectives for the simulation of turbulent flows together with laminar-turbulent transition. The variants of the QGD system have been developed previously for supersonic flow simulations and have been published firstly more than three decades ago. Modern variants of the system can be seen in, e.g. [1]–[3] and in the later papers in the subject.

We examine the QGD system in calculations of laminar and turbulent flows in Nitrogen at a temperature of normal conditions. The different values of Reynolds number Re are achieved by variations of gas density and pressure.

As an example of the laminar-turbulent transition in a free-flow we examined the Taylor-Green vortex decay. Our numerical results are compared with DNS and LES reference data for laminar flows with Re=100 and 280 and for the turbulent vortex decay regimes for Re=1600 and 5000. In these calculations Mach number is taken equal to 0.1.

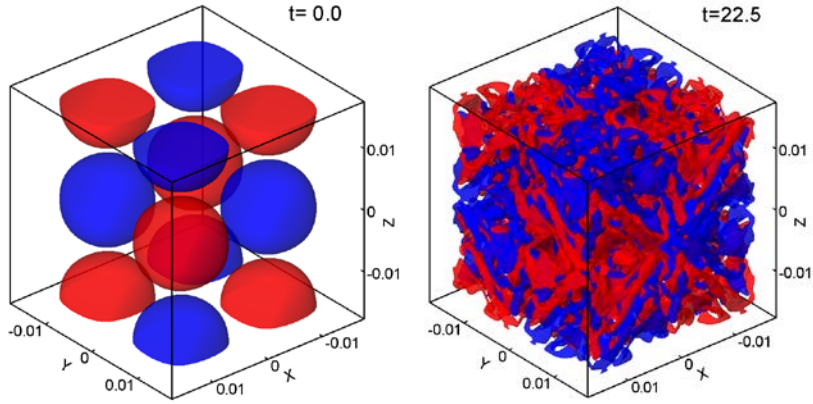

Fig. 1. Taylor-Green vortex decay; iso-surfaces of z-component of vorticity for Re=1600

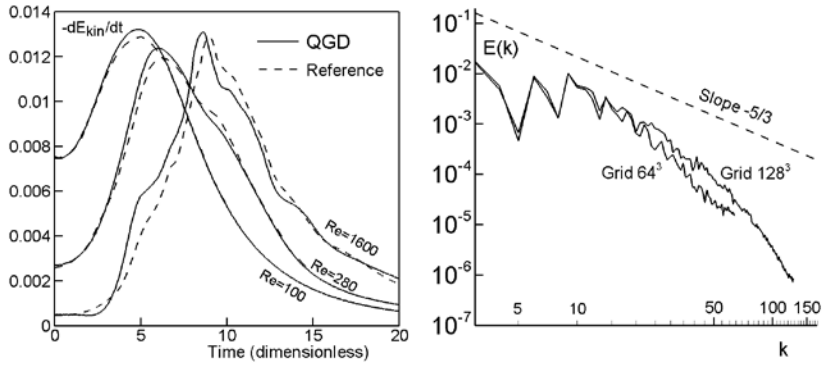

Fig. 2. Taylor-Green flow: dissipation rates of kinetic energy (left) and energy spectrum for Re = 1600 (right)

Figs. 1–2 show our results in Taylor-Green vortex decay simulations according with [4]. Fig. 1 presents the vorticity contours for Re = 1600 for the

initial time and the finale time t = 22.5 for 128x128x128 computational grid points.

Fig. 2 (left) shows the evolutions of the dissipation rate of kinetic energy for Re = 100, 280 and 1600 in comparison with the reference data from [4]. Good agreement with the reference for laminar and turbulent flow regimes is clearly seen.

The spectrum of kinetic energy for Re=1600 was examined for computational grids with 128^3 and 64^3 points. The slope of the spectra approximates correctly the Kolmogorov-Obukhov law that shows an inertial range behavior of the flow for both grids. Increasing the number of grid points makes the curve more smooth and more close to the line with -5/3 slope, Fig. 2 (right). Additional computational results can be found in [5].

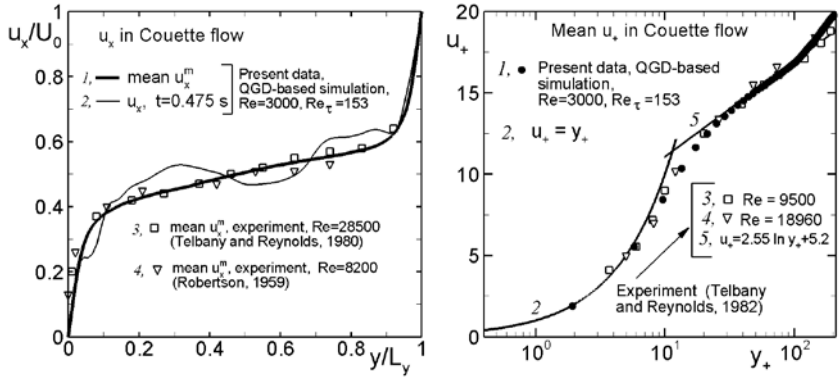

Fig. 3. Mean streamwise velocity distribution in Couette flow in comparison with experimental data

The QGD-based results of the Couette flow in Nitrogen are shown in Figs. 3 and 4. Here the computation domain is L_x=0.16m, L_y=L_z=0.08m, space step h=0.001m, with the number of computational points 162x82x82. The upper and down walls are adiabatic with no-slip velocity conditions, for other boundaries the periodic boundary conditions are imposed. Reynolds numbers were taken as Re = 300, 3000 and 4200 for Mach number equal to 0.5. By disturbing the initial laminar velocity profile we obtain the nonstationary turbulent flow patterns for Re = 3000 (dynamic Reynolds number 153) and 4200 (dynamic Re number 198), and a stationary laminar flow for Re=300.

Fig. 3 (left) presents the computed mean and instantaneous velocity profiles for Re=3000. Fig 3 (right) shows the streamwise profile in dimensionless variables in comparison with experimental data [6]. The computational points in boundary layer for QGD algorithm are marked by black circles. The number of

space points in QGD calculations is smaller than estimated and commonly used for DNS calculations.

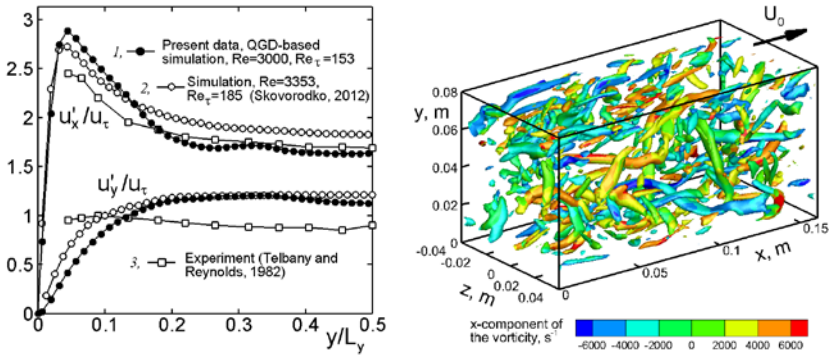

Fig. 4. Couette flow: distributions of averaged (rms) velocity fluctuations (left) and iso-surface of the Q-criterion and contour lines of the x-component of vorticity (right)

Fig. 4 (left) depicts the distributions of the velocity fluctuations compared with known computed and experimental data. Fig 4 (right) shows the coherent structures for Re=3000. Visualization of the vortices is obtained by iso-surfaces of Q-criterion colored by the x-component of the vorticity. Developed coherent vortices are usual for turbulent gas-dynamic flows.

The calculations were carried out on highly-parallel computer installed in K-100. Our code is portable between multiprocessor systems that support the C language and MPI standard.

The work is supported by grant RFFI 16-01-00048_a.

References

1. Chetverushkin B.N. Kinetic schemes and quasi-gas dynamic system of equations. CIMNE, Barselona, 2008.
2. Sheretov Yu.V. Continuum Dynamics under Spatiotemporal Averaging, RKhD, Moscow-Izhevsk (in Russian), 2009.
3. Elizarova T.G. Quasi-Gas Dynamic Equations, Springer, Dordrecht, 2009.
4. Brachet M., Meiron D., Orszag S., Nickel B., Morf R., Frisch U. Small-scale structure of the Taylor-Green vortex. J. Fluid Mech., 1983, vol. 130, pp. 411–452.
5. Shirokov I.A., Elizarova T.G. Simulation of laminar–turbulent transition in compressible Taylor–Green flow basing on quasi-gas dynamic equations. J. of Turbulence, 15, Issue 10 (2014), pp. 707–730.
6. El Telbany M.M.M., Reynolds A.J. The structure of turbulent plane Couette flow. J. of Fluids Engineering. 104 (1982), pp. 367–372.

A TWO-LEVEL APPROACH FOR DESIGN OPTIMIZATION OF ACOUSTIC LINERS

Nicolas R. Gauger[1], Emre Özkaya[1], Junis Abdel Hay[1]
[1]*Kaiserslautern University of Technology, Chair for Scientific Computing, 67663 Kaiserslautern, Germany, nicolas.gauger@scicomp.uni-kl.de*

We present a novel two-level approach for design optimization of acoustic liner panels that are commonly used to damp engine noise in turbofan engines. The method combines an adjoint based gradient search algorithm with a global search method applied on a surrogate model. In this way, we effectively exploit the benefits of both approaches to achieve a good compromise between computational effort and degree of freedom used in optimization.

In the first level, a global search is performed with few design parameters employing a Gaussian process surrogate model. In the second level, taking the global optimal solution as the initial setting for the refined design vector, an adjoint based gradient search procedure is started. The unsteady discrete adjoint solver, which is an essential ingredient of the optimization framework, has been developed using Algorithmic Differentiation (AD) techniques. The AD generates a robust discrete adjoint solver, which solves the unsteady adjoint Linearized Euler Equations (LEE) backward in time.

The capability of the two-level approach is demonstrated by finding the optimal liner parameters of a turbofan engine by-pass duct.

AIRFOIL-GUST INTERACTIONS IN TRANSONIC FLOW

James Gill[1], **Xin Zhang**[2]
[1]*University of Southampton, United Kingdom, j.gill@soton.ac.uk*
[2]*Hong Kong University of Science and Technology, Hong Kong SAR, aexzhang@ust.hk*

The noise produced by interactions between an airfoil and oncoming vortical disturbances is a significant broadband noise source in turbofan and contra-rotating open rotor engines (CRORs). Turbulence that is generated upstream will interact with the leading edge of the outlet guide vane in turbofans, or with the rear rotor in CRORs. The significance of leading edge noise has led to various studies to understand the mechanisms by which it is caused. Studies to improve understanding of leading edge noise often consider simplified situations, such as isolated blade interactions and simplified blade geometries. Amiet [1], for example, developed an analytical method to predict the far-field leading edge noise from a flat plate. This theory often forms the basis of current industrial prediction models of broadband leading edge noise [2]**.**

The majority of studies that have measured or predicted leading edge noise have considered low free stream speeds. To the author's knowledge, the highest speeds to date were considered by Paruchuri *et al.* [3], who studied isolated turbulence airfoil interactions computationally at Mach numbers of up to M=0.6. It was shown that noise reductions caused by changes in airfoil thickness will scale with increasing Mach number. However, this relationship will break down at sufficiently high speeds when new physics, such as shock waves, will appear.

The current work describes a computational aeroacoustic (CAA) study to understand the effect of locally supersonic flow regions on the interactions between an airfoil and oncoming vortical gusts. The supersonic flow region adds complexity to the modelling process, as treatments must be made to provide numerical stability in complex flow regions while maintaining sufficient accuracy to study acoustics. Furthermore, additional noise sources can be added by the presence of the supersonic region which may make it difficult to study the leading edge noise.

Problem Description

This work considers interactions between oncoming vortical gusts with a vortical wavelength of λ=0.5 m, and a NACA 0006 airfoil placed at an angle of attack of 6 degrees in a M=0.5 flow. This case is chosen to be representative of a real situation that might occur on a CROR engine, for example. Single frequency vortical gusts have been chosen to allow for identifying and highlight-

ing major physics in the study. A schematic of the configuration is shown in Fig. 1.

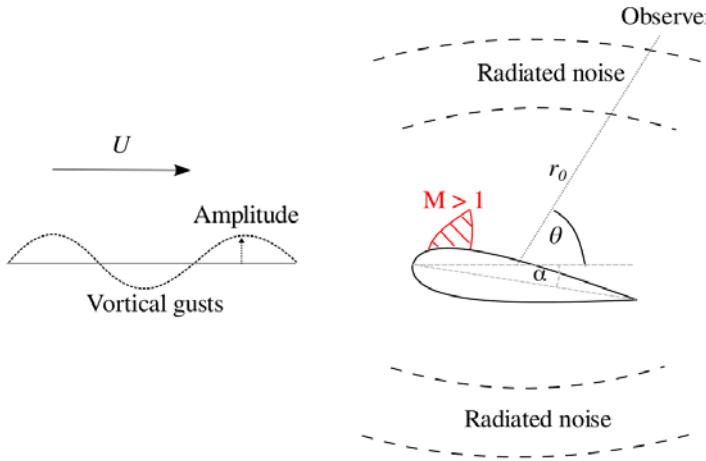

Fig. 1. Schematic of the airfoil-gust configuration: U is the freestream speed, r_0 is the observer radius, θ is the observer angle and α is the airfoil angle of attack

Numerical Method

An established computational aeroacoustics (CAA) code has been chosen to perform the simulations. This code has been previously used to study problems such as duct mode radiation [4], high lift device noise [5], and the leading edge noise of isolated airfoils [6]. It is used to solve the Euler equations using high-order schemes with low-dispersion and low-dissipation properties **[7]**. A local artificial dissipation method has been implemented to allow numerical stability near shocks. The general simulation consists of two parts. A steady state simulation is first performed to establish a steady mean flow surrounding the airfoil. Then, vortical gusts are introduced and interacted with the isolated airfoil. The vortical gusts are described by $v(x,t) = v_{gust}\cos(k_x(x-Ut))$, where U is the free stream speed, v_{gust} is the gust amplitude (set to $0.01U$), k_x is the transverse vortical gust wavenumber, and t is time.

Leading Edge Noise Predictions in Transonic Flow

Figure 2 shows contours of steady pressure and velocity magnitude around the NACA 0006 airfoil. The majority of the flow field is subsonic, but there is a small region of supersonic flow near the leading edge on the suction-side.

The acoustic flow field, created by the interactions between the vortical gusts and the airfoil, is shown in Fig. 3. The acoustic radiation pattern is clearly seen, with radiation peaks in both upstream and downstream directions. The pattern is not symmetric about the free stream axis due to the angle of attack. Peaks in the pressure can be seen in the wake region behind the airfoil. These are caused by deformations of the vortical gusts and are not representative of leading edge noise.

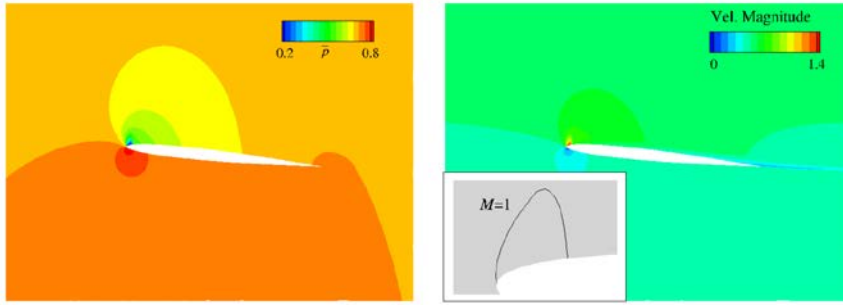

Fig. 2. Steady pressure and velocity magnitude contours around a NACA 0006 airfoil at M=0.5 and $\alpha = 6°$; magnified area shows the line of M=1

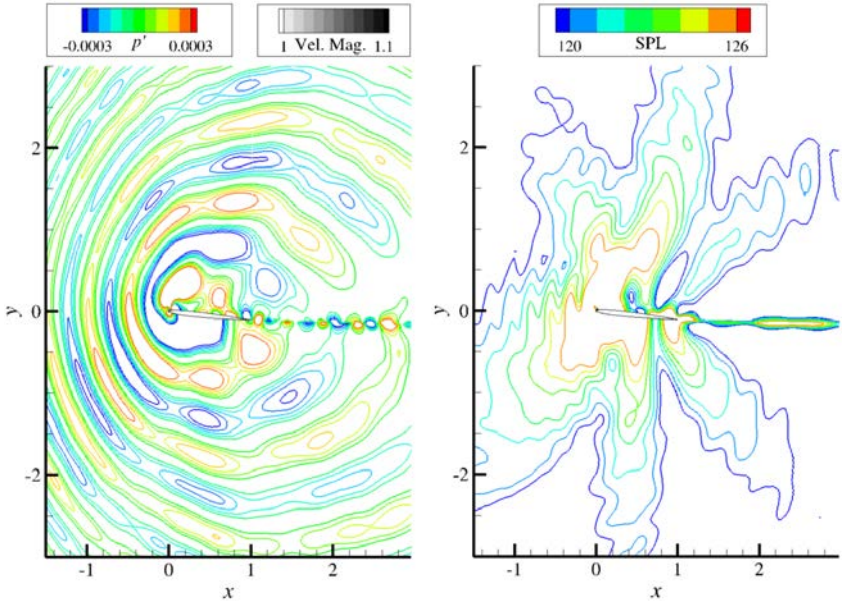

Fig. 3. Contours of instantaneous acoustic pressure and SPL

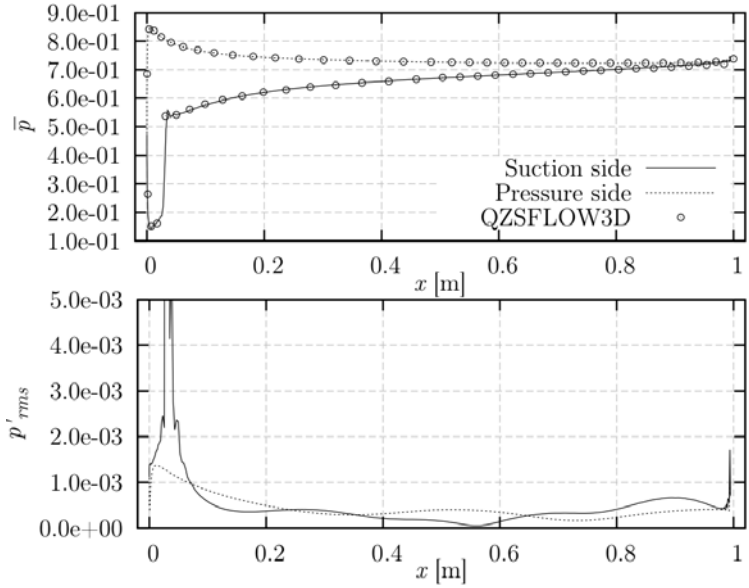

Fig. 4. Variation of non-dimensional mean pressure (top) and pressure fluctuations (bottom) along the airfoil chord

Figure 4 shows the mean pressure, and pressure fluctuations, along the surface of the airfoil. The mean pressure prediction has been compared with results from the QZSFLOW3D code [8] and a good match is seen. The presence of the supersonic region near the leading edge can be seen in the jump in steady pressure on the suction-side of the airfoil at about x = 0.04 m. This causes a corresponding spike in p_{rms}. This spike appears to coincide with the location of strongest leading edge noise generation. It is not yet clear whether this spike represents an additional noise source, or shows changes in the acoustic wave amplitude due to shock oscillations.

This abstract has presented a method to allow the study of leading edge noise for transonic airfoil configurations. In the final paper, acoustic predictions of the NACA 0006 airfoil will be compared with predictions from a NACA 0018 airfoil, and with cases at slower free stream Mach numbers, in order to show the differences caused by the presence of the shockwave.

References

1. R.K. Amiet. Acoustic radiation from an airfoil in a turbulent stream. J. Sound Vib., Vol. 41, No. 4, 1975, pp. 407–420.
2. T. Node-Langlois, F. Wlassow, V. Languille, Y. Colin, B. Caruelle, J. Gill, X. Chen, X. Zhang, A.B. Parry. “Prediction of Contra-Rotating Open Rotor

Broadband Noise in Isolated and Installed Configurations", 20th AIAA/CEAS Aeroacoustics Conference, Atlanta Georgia, No. 2014-2610, 2014.
3. C. Paruchuri, J. Gill, S. Narayanan, P. Joseph, C. Vanderwel, X. Zhang, B. Ganapathisubramani, "Aerofoil Geometry Effects on Turbulence Interaction Noise", 21st AIAA/CEAS Aeroacoustics Conference, Dallas Texas, No. 2015-2830, 2015.
4. X. Zhang, X. Chen, P.A. Nelson. Computation of spinning modal radiation from an unflanged duct", AIAA J., Vol. 42, No. 6, 2004, pp. 1795–1801.
5. X. Wang, Z. Hu, X. Zhang. Aeroacoustic effects of high-lift wing flat track and cut-out system", Int. J. of Aeroacoustics, Vol. 12, No. 3, 2013, pp.283–308.
6. J. Gill, X. Zhang, P. Joseph. Symmetric airfoil geometry effects on leading edge noise", J. Acoust. Soc. Am., Vol. 134, No. 4, 2013, pp. 2669–2680.
7. J.W. Kim. Optimised boundary compact finite difference schemes for computational aeroacoustics. J. Comp. Phys., Vol. 225, 2007, pp.995–1019.
8. Z. Qian, C.H. Lee. A class of large time step Godunov schemes for hyperbolic conservation laws and applications. J. Comp. Phys., Vol. 230, No. 19, 2011, pp. 7418–7440.

SOUND FIELD OF POINT SOURCE IN THE LAYER WITH CONSTANT GRADIENT OF SOUND VELOCITY

A.V. Gladilin, **M.A. Mironov**
Andreyev Acoustics Institute, Moscow, mironov_ma@mail.ru

In a medium with linearly changing speed of sound $c(z) = c_0 \cdot z / z_0$ along the axis *z*, plane wave propagating in the direction of decreasing sound speed has propagation time to the cross section $z = 0$ equal to infinity [1]. The wave can not reach this cross section and, as a consequence, is not reflected from it. Therefore, the finite thickness layer of the medium is an effective absorber of plane waves incident normally to it. In [1] this type of media is called "black hole" by analogy with the corresponding cosmological objects. In [1,2,3] the possibility of constructing gradient media with sound speed tending to zero was considered.

In this paper the solution to the 3-D problem of **point source field** in a medium with constant gradient of the speed of sound is given. It turns out that this problem has an exact analytical solution in the form of simple power functions. For the first time the appropriate formula was given in [4]. The work [4], a classic one in hydroacoustics, is devoted to the analysis of the sound field of a point source in a layered ocean in the shadow zone. In the real ocean the speed of sound varies very little and, of course, is not approaching zero in any layer section. Therefore, formulas, obtained in [4], were not analyzed there from the point of view of the theory of "black hole". The construction of artificial media, considered in [1], provides the velocity reduction by means of spring-like impedance of wave guide's wall. In [2,3] velocity reduction supplies with increase of the medium equivalent density. A generalization of [4] to the case when the medium has not only the variable speed of sound, but variable density as well, is given in [5].

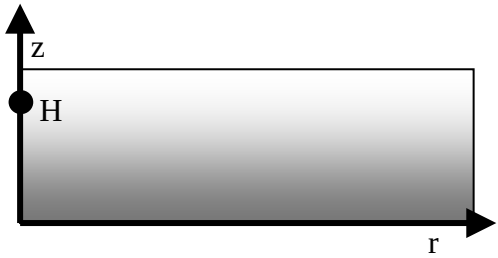

Fig. 1. Point source in semi space with constant gradient of sound speed at the height *H*

The problem is formulated in the following way. In the half-space at height *H*, a point source of volume velocity $V(t) = V_0 \cdot \delta(\vec{r} - \vec{r}_0) \cdot e^{-i \cdot \omega \cdot t}$, $\vec{r} = (r, z), \vec{r}_0 = (0, H)$ is placed (Fig. 1). The speed of sound in the medium depends on the coordinate *z* linearly: $c(z) = c_0 \cdot z / z_0$. The density of the me-

dium changes according to the power law: $\rho(z) = \rho_0 (z / z_0)^{\alpha}$. The exponent α can be arbitrary. In respect to the constructions, considered in [4, 5], it is equal to $\alpha = -2$. Pressure field satisfies the Helmholtz equation with a point source in the right side

$$\frac{\omega^2}{c(z)^2} p + \rho(z) \cdot div \frac{\nabla p}{\rho(z)} = i\omega V_0 \delta(\vec{r} - \vec{r}_0) .$$

After Fourier-Bessel transformation on radial coordinate *r*, the equation for the spectrum $p(\xi, z)$ (ξ is horizontal wave number) assumes the form:

$$\frac{d^2 p}{dz^2} - \frac{dp}{dz} \cdot \frac{d(\ln \rho(z))}{dz} + (k(z)^2 - \xi^2) p = \frac{i\omega\rho \cdot V_0}{(2\pi)^2} \delta(z - H) e^{-i(\vec{\xi} \cdot \vec{r})},$$

where $k(z)^2 = \omega^2 / c(z)^2$. It is assumed, that at the lower boundary $z = 0$ the condition of absence of the reflected wave should be realized. This happens when $\omega^2 z_0^{\,2} / c_0^{\,2} > 1/4$ (see also [1]). In the source cross section $z = H$ pressure field is supposed continuous, and the vertical velocity has a jump. After taking into account the boundary conditions the following expression for the field $p(z, r)$ should be obtained [5]:

$$p(z,r) \sim -\frac{1}{2\pi} \cdot \left(\frac{z^{1+\alpha}}{z^{1-\alpha}} \right)^{1/2} \int_0^{\infty} J_0(\xi \cdot r) I_m(\xi \cdot z_-) K_m(\xi \cdot z_+) \xi d\xi,$$

where $m = \left[\frac{(\alpha+1)^2}{4} - k_0^{\,2} z_0^{\,2} \right]^{1/2}$, $\mathrm{Re}\, m > 0$, $z_- = \min(z, H)$, $z_+ = \max(z, H)$.

At $\alpha = -2$ the expression for *m* is transferred to the corresponding formula from [4].

It turns out that the integral in the right side may be expressed through elementary functions and the field expression can be rewritten in the following form [5]:

$$p(z,r) = \frac{(z^{1+\alpha} \cdot H^{1-\alpha})^{1/2}}{-2\pi \cdot R \cdot R_1} \left(\frac{R_1 - R}{R_1 + R} \right)^m ,$$

$R = [r^2 + (H - z)^2]^{1/2}$, $R_1 = [r^2 + (H + z)^2]^{1/2}$, R_1 is the distance from the source to the point of reception, R_2 the distance from the mirror image source relative to the plane $z = 0$ to the point of reception. This formula is the main result of the report.

Ray interpretation of this expression is as follows (see Fig. 2). All the rays outgoing from the source to the lower hemisphere, continuously reduce the an-

gle of incidence and at the approach to the plane $z = 0$ fall on it normally. As a result one-dimensional situation, considered in [1], is realized. All the rays outgoing from the source to the upper hemisphere, gradually turn down, cross the plane of the source location $z = H$ and approach the plane $z = 0$, normally to it as well.

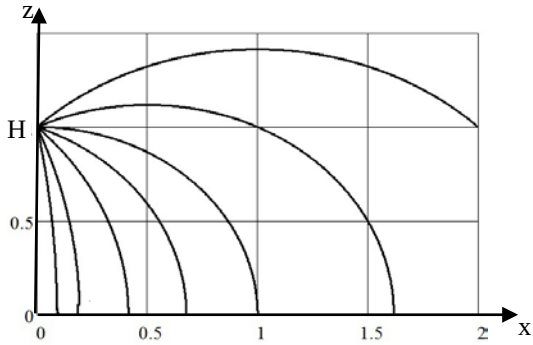

Fig. 2. 3-D rays in 1-D "black hole" medium

References

1. M.A. Mironov and V.V. Pislyakov. One-dimensional Waves in retarding Structures with Propagation Velocity Tending to Zero. Acoustical Physics 48(3) May 2002, pp. 347–352.
2. M.A. Mironov. "Gradient sound absorber". Seminar "Aviation acoustics". Dubna, 23 – 27 May 2006. (in Russian).
3. A.A.E. Ouahabi, V.V. Krylov, D.J. O'Boy. Quasi-flat acoustic absorber enhanced by metamaterials. Proceedings of Meetings on Acoustics, V. 22, 040002 (2014).
4. C.L. Pekeris. Theory of Propagation of Sound in a Half-Space of Variable Sound Velocity under Condition of Formation of a Shadow Zone. J. Acoust. Soc. of Am., v.18, 1946, pp. 295–315.
5. Brekhovskikh L.M., Godin O.F. Acoustics of Layered Media I, II Berlin: Springer-Verlag, 1990, 1992.

EXPERIMENTAL STUDY OF THE FLOW IN A DUAL-STREAM SUPERSONIC JET

D.A. Gubanov, **V.I. Zapryagaev**, N.P. Kiselev, S.G. Kundasev, A.A. Pivovarov

ITAM SB RAS, Novosibirsk, zapr@itam.nsc.ru

The instrumentation, the design of a model dual-stream jet nozzle, and the results of an experimental study of the jet flow structure are reported. The experimental data include flow-field visualization and PIV data, data that were obtained by probing the flow with a Pitot microtube, and the distribution of pressure over the inner nozzle contour of the nozzle. Measured data on the magnitude and spectral composition of mass-flow rate pulsations obtained using a hot-wire anemometer are reported.

The work is carried out within a project being executed by the Belotserkovskii Scientific-Educational Center for Computer Modeling and Security Technologies**.** The experimental data have served the basis for organizing a test case at TsAGI (Central Aerodynamic Institute) intended for verification of numerical data on the gas-dynamic structure of a model high-speed two-contour jet.

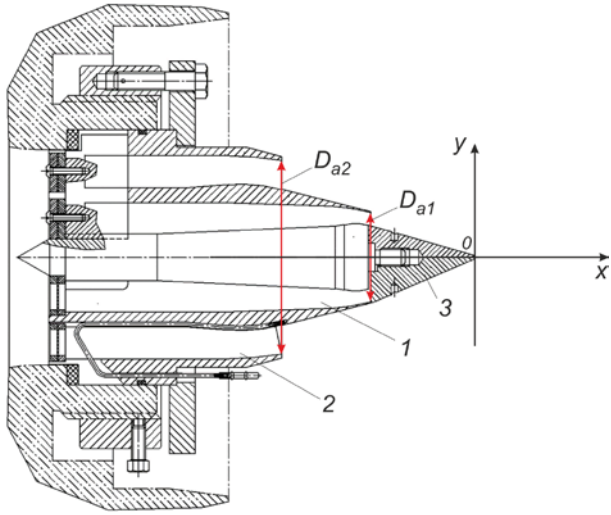

Fig. 1. The dual-stream jet nozzle: *1* – inner nozzle contour, *2* – outer nozzle-contour, *3* – central body, D_{a1} –inner-contour diameter, D_{a2} – outer-contour diameter

The experimental facility and the experimental procedure were described in [1]; in the same publication, data on the flow structure of an underexpanded jet exhausted out of a convergent nozzle into ambient space were reported. The experimental study of a jet exhausted into ambient space out of a convergent model dual-stream jet nozzle (Fig. 1) was performed on the jet module of the T-326 intermittent blowdown hypersonic wind tunnel, ITAM SB RAS. The geometric Mach number at nozzle exit was Ma= 1.0. The experiments were performed with cold air at fixed stagnation pressure values in the contours, Npr1 = 1.72 and Npr2 = 2.25, where Npr= $P_{01(2)}$/Pc, $P_{01(2)}$ is the pressure supplied to the inner/outer nozzle contour ; Pc is the Eiffel-chamber pressure; and subscripts 1 and 2 refer to the internal and outer nozzle contours. The required reduction of pressure in the inner nozzle contour was achieved using a grid installed at the entrance to that contour.

Schlieren visualization photographs of the high-speed two-contour jet are shown in Fig. 2. The averaged flow pattern is shown in Fig. 2,a, and an instantaneous flow pattern, in Fig. 2,b. Out of the inner nozzle contour (contour 1), a high-speed annular jet with Npr1 = 1.72 is exhausted; this jet moves past the central-body cone. An indistinct wake protruding along the axis is seen behind the cone. In the outer nozzle contour, a weakly underexpanded supersonic contour is formed at the exit, with compression shocks, a shock-wavy structure of the external boundary, and a cellular structure of the jet flow being observed.

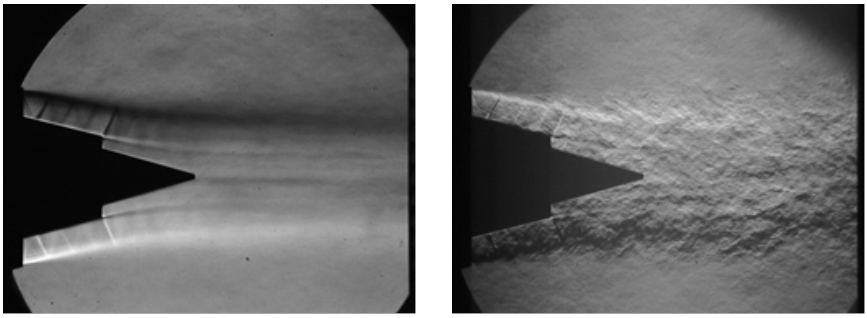

a b

Fig. 2. Schlieren photograph of the jet exhausted out of the dual-stream jet nozzle, a – exposure time 10^{-2} sec, b – exposure time $3 \cdot 10^{-6}$ sec

The jet exhausted out of the inner nozzle contour exhibit no barrel structure. The mixing layer of the supersonic and subsonic jet flows forms at the nozzle lip of the inner nozzle contour; it is distinctly registered in the photograph (Fig. 2,a). At short exposures, notable density fluctuations due to flow turbulization are registered.

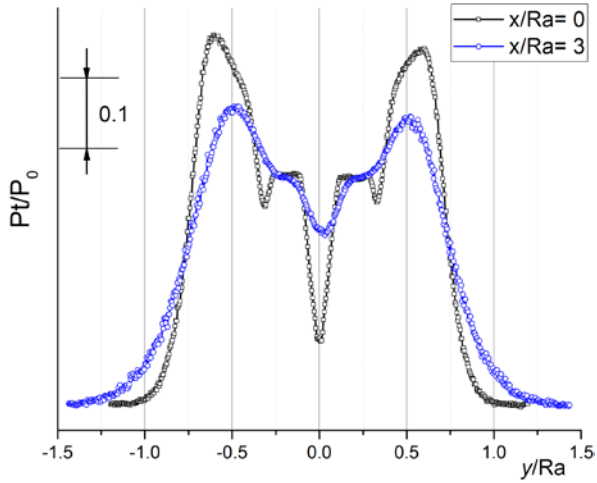

Fig. 3. The distributions of pressure over diameter measured with the help of a Pitot tube in several cross-sections of the jet flow

Pressure tap measurements were used to measure the distributions of pressure in the two-contour jet. Figure 3 shows relative pressure profiles measured with a Pitot tube in two cross-sections, x/Ra= 0 and 3 (here, Ra is the radius of the outer nozzle contour at the exit (item *2* in Fig. 1). The data at x/Ra = 0 were obtained in the vicinity of the cone forebody (item *3* in Fig. 1), and the data at x/Ra = 3, at the largest distance from it. At the axis, a pressure minimum due to the deceleration of the flow behind the cone is observed. Various levels of Pitot pressure for the outer and inner flows due to the supersonic regime of the outer jet and due to the subsonic regime of the inner jet are registered. Two neighboring minima at y/Ra = ± 0.3 (x/Ra = 0) correspond to the mixing layer in the region of interactions of the two flows. On moving over the distance x/Ra = 3, the maximum pressure in the jet decreases, and the pressure at the axis increases in value, and the internal and external mixing layers grow in size.

Using a hot-wire anemometer, measurements of the magnitude and spectral compositions of mass-flow rate pulsations were performed. Typical distributions of integral characteristics of mass-flow rate pulsations in three cross-sections of the jet are shown in Fig. 4.

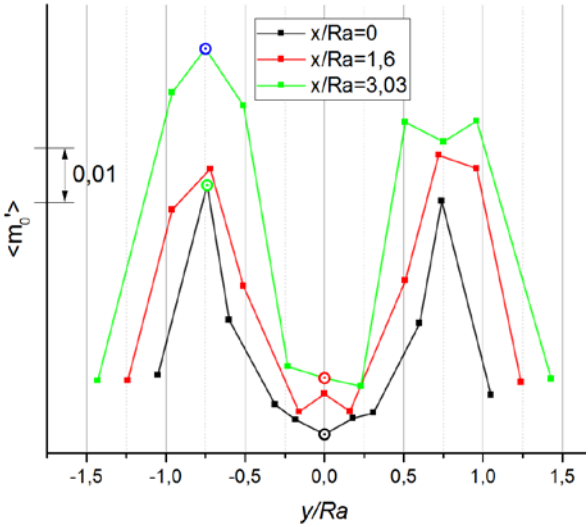

Fig. 4. The magnitude of relative mass-flow pulsations versus the relative radius, Npr1 = 1.72, Npr2 = 2.25

The profiles of the integral level of normalized mass-flow rate pulsations over diameter in the range from 20 Hz to 150 kHz are shown in Fig. 4. Evidently, in the wake behind the cone (central body, item *3* in Fig. 1) the pulsations are minimal. Some asymmetry is observed; this asymmetry can be attributed to different turbulence levels in the upper and lower parts of the jet which arise as a result of partial blockage of the flow with the hot-wire probe pylon. A maximum of relative mass-flow rate pulsations is registered in the mixing layer of the outer-contour jet; it reaches 20% at the outer edge of the jet. The pulsation level at the axis increases with the distance from the central cone.

References

1. V.I. Zapryagaev, N.P. Kiselev, and A.A. Pivovarov. The gas-dynamic structure of an axisymmetric supersonic underexpanded jet. Fluid Dynamics, 2015, Vol. 50, No. 1, pp. 87–97.

A DISPERSION IMPROVED CABARET SCHEME FOR LINEAR ACOUSTIC PROPAGATION PROBLEMS

S.A. Karabasov and A. Chintagunta
Queen Mary University of London, Mile End Rd, London, E1 4NS, UK,
s.karabasov@qmul.ac.uk

The CABARET scheme has a variety of uses in Computational Fluid Dynamics (CFD) for solving convection dominant flow problems. Since its introduction by Goloviznin and Samarskii [1] in 1998, CABARET was extended to non-linear aeroacoustics modelling by Karabasov and Golovinzin [2,3] and used for solving the Navier-Stokes equations in three dimensions by Faranosov et al. [4]. Semiletov and Karabasov [5] and Markesteijn et al. [6,7] implemented efficient asynchronous time stepping algorithms to make the original explicit single-step CABARET scheme as efficient as the implicit dual-time stepping schemes conventionally used in CFD for problems involving thin boundary and shear layers typical of high Reynolds number flows.

An important property of the CABARET scheme as compared to other second-order schemes of its class is low dissipation (the low dissipation refers to the flux correction algorithm and its relaxed version since the linear CABARET scheme is non-dissipative) as well as low numerical dispersion for relatively high Courant numbers, $0.3 < CFL < 1$. For small Courant numbers, the CABARET scheme still has a notable dispersion error for coarse grid resolutions which correspond to the number of grid cells per acoustic wavelength less than 15-20. This dispersion error is quite persistent in three dimensions where $CFL \sim 0.1$-0.3 becomes a typical local Courant number for linear flow regions where the grid cell size is much larger in comparison with the aerodynamic part of the grid.

In the seminal work of Goloviznin in Samarskii [1], among other things, there was a modification of the original three-time-level CABARET scheme suggested which included a third-order spatial derivative (by extending the one cell spatial stencil to include two more cell faces) with an adjustable parameter. The parameter was determined from the Von Neumann dispersion analysis so that the dispersion error could be greatly minimised for all Courant numbers.

In the present work, we have implemented the dispersion improved CABARET in a convenient two-time-layer staggered-variable form, equipped it with a low-dissipative relaxed flux correction algorithm from Karabasov and Goloviznin [3], and extended to 2D gas dynamics. Numerical examples are provided for 1D linear advection in comparison with the standard CABARET scheme and several other popular advection schemes including the 4^{th} order DRP scheme of Tam and Webb [8] combined with the 4^{th} order Runge-Kutta time scheme. To illustrate the feasibility of the dispersion improved CABARET

for computational aeroacoustics, further results are provided for a problem of normal and oblique (cut-on) acoustic wave propagation in a 2D duct for a range of grid resolutions and flow conditions.

References

1. V.M. Goloviznin, A.A. Samarskii. Some characteristics of finite difference scheme “Cabaret”. Computational methods and algorithms, 1998, Vol. 10, No. 1, pp. 101–116.
2. S.A. Karabasov and V.M. Goloviznin. New efficient high-resolution method for nonlinear problems in aeroacoustics. AIAA Journal, 2007, vol. 45 (12), 2861–2871. 10.2514/1.29796
3. S.A. Karabasov and V.M. Goloviznin. Compact Accurately Boundary-Adjusting high-REsolution Technique for fluid dynamics. J. Comput. Phys., 2009, vol. 228 (19), 7426–7451. 10.1016/j.jcp.2009.06.037
4. G.A. Faranosov, V.M. Goloviznin, S.A. Karabasov, V.G. Kondakov, V.F. Kopiev and M.A. Zaitsev. CABARET method on unstructured hexahedral grids for jet noise computation. Computers and Fluids, 2013, vol. 88, 165–179. 10.1016/j.compfluid.2013.08.011
5. V.A. Semiletov and S.A. Karabasov. CABARET scheme for computational aero acoustics: Extension to asynchronous time stepping and 3D flow modelling. International Journal of Aeroacoustics, 2014, vol. 13, (3-4) 321–336. 10.1260/1475-472X.13.3-4.321
6. A.P. Markesteijn, V.A. Semiletov, S.A. Karabasov. CABARET GPU Solver for Fast-Turn-Around Flow and Noise Calculations. 21st AIAA/CEAS Aeroacoustics Conference, June 2015, DOI: 10.2514/6.2015-2223
7. A.P. Markesteijn, V.A. Semiletov, S.A. Karabasov. GPU CABARET Solutions for the SILOET Jet Noise Experiment: Flow and Noise Modelling. 22nd AIAA/CEAS Aeroacoustics Conference, Lyon, France, DOI: 10.2514/6.2016-2967
8. C.K.W. Tam and J.C. Webb. Dispersion-relation-preserving finite difference schemes for computational acoustics. J. Comput. Phys., v.107, 1993, pp.262–281.

COMMUNITY NOISE ASSESSMENT FOR AIRCRAFT WITH CROR ENGINES BASED ON NUMERICAL SIMULATIONS

V.F. Kopiev[1], M.L. Shur[2], A.I. Travin[2], **I.V. Belyaev**[1], B.S. Zamtfort[1], Yu.V. Medvedev[1]

[1]*Central Aerohydrodynamic Institute, Moscow, Russia, vkopiev@mktsagi.ru*

[2]*St.Petersburg Polytechnic University, St. Petersburg, Russia, mshur@cfd.spbstu.ru*

Counter-rotating open rotors (CROR) have a potential for fuel savings of up to 20% compared with modern turbofans [1]. However, their higher aerodynamic efficiency is accompanied by higher noise levels. This constitutes a major hindrance to a wide practical use of aircraft engines of this type and makes necessary optimization of the CROR parameters aimed at lowering the level of the emitted noise while preserving good aerodynamic performance.

Noise spectra and directivities for open rotors are quite complex which significantly complicates an analysis of the effect of the CROR geometry modifications on their acoustic characteristics (e.g., suppression of some tonal components can be accompanied by an increase of the amplitude of some other tones). For this reason it makes sense to perform corresponding optimization studies using for the noise assessment the EPNdB metric, since it is this metric that is employed for aircraft certification on community noise. Exactly such an approach is used in the present work aimed at numerical investigation of the effect of geometrical parameters of the open rotors on community noise for a realistic aircraft equipped with CROR engines and at estimation of feasibility of meeting the ICAO requirements on community noise by this aircraft.

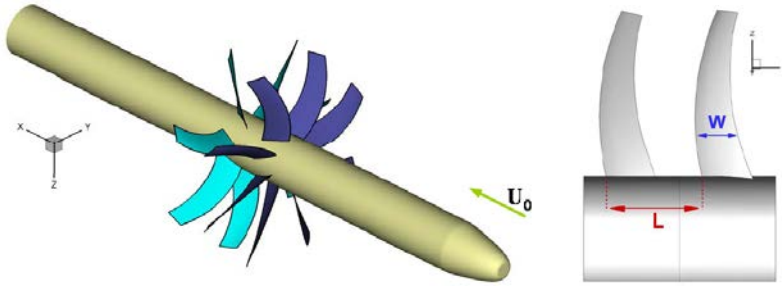

Fig. 1. Geometry of the open rotor in the reference configuration

A generic geometry of the considered open rotor (Fig. 1) was the same as that used in earlier study [2]. A baseline configuration has (8 + 7) blades on the front and the rear rotors of the counter-rotating pair, respectively, and the two rotors have the same diameter $D_1 = D_2 = 4$m and the same speed of rotation. In

the course of the computations, the following geometrical characteristics of the rotor were varied (see right frame in Fig. 1): the number of blades on both rotors, N_1 and N_2; the separation distance between the rotors L; the chord width W of the blades; and the diameter of the rear rotor D_2. In total, 9 configurations were considered, each of which differs from the baseline configuration in only one geometrical parameter. Other than that, in all the cases it was assumed that the front and rear rotor rotate at the same speed, which value was adjusted to provide the total thrust equal to the total thrust of the baseline configuration.

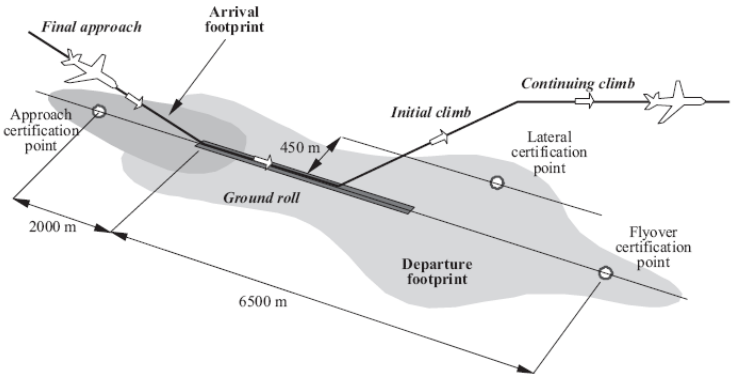

Fig. 2. Community reference points for noise certification and typical noise footprints on arrival and departure. Adapted from [5]

Computations of the acoustic characteristics of the described CROR installed on the aircraft were carried out in two stages.

In the first stage, the far field noise spectra of an isolated CROR were computed based on turbulence-resolving simulation of the flow over the CROR combined with the permeable Ffowcs Williams and Hawkings (FW-H) surface-integral method for the noise prediction. The simulations were carried out with the use of a hybrid RANS/LES approach of DES type, namely, DDES method [3] coupled with recently proposed definition of subgrid length scale [4] ensuring a rapid transition to developed 3D turbulence in the separated shear layers.

In the second stage of the computations, the far field acoustic data obtained in the first stage were transformed to 1/3-octave noise matrices and then used for assessment of community noise. For this purpose, a real passenger aircraft with two turbofan engines (MTOW = 108 tons) and its real flight trajectories were considered, with the noise matrices of turbofan engines being replaced with the calculated noise matrices for the CROR engines at the same thrust. Community noise at the flyover certification point was then calculated for all the considered configurations with the use of commercial software SOPRANO and in-house software BASTON, and the results were compared with those for the baseline case.

This allowed assessing the effect of different geometrical parameters on community noise. Particularly, the effect was found to be quite significant for varying the number of blades (reduction by more than 5 EPNdB compared to the baseline case) and unexpectedly small for decreasing the rear rotor diameter (reduction by only 0.2 – 1.1 EPNdB). The latter seems to be explained by an increase of CROR rotation speed needed for sustaining the same thrust as in the baseline case, which compensates the noise decrease due to weaker interaction of the rear rotor blades with the tip vortices shed from the front rotor.

For the quietest of the considered configurations (8 + 9 blades), two additional numerical simulations were performed, in which the thrust values corresponded to the takeoff and approach regimes. This allowed an assessment of the community noise of the aircraft with CROR engines in three certification points (Fig. 2). As a result, it was found that the noise meets the requirements of Chapter 4 with a small margin (0.4 EPNdB).

It should be noted that in practice the flight trajectories of the aircraft with CROR engines may differ from the flight trajectories of the turbofan aircraft used in this work. On the other hand, even the quietest of the considered CROR configuration is likely to be suboptimal, since the number of considered configurations is quite limited and the optimization procedure pursued in this study does not address simultaneous effects of different geometrical parameters. Therefore, further reduction of community noise can be expected for an optimal CROR configuration. Thus, in general, the present work demonstrates that an aircraft with open rotor engines is likely to be capable of meeting the ICAO norms on community noise of Chapter 4.

The authors from St. Petersburg Polytechnic University are grateful to Russian Science Foundation (grant 14-11-00060) for financial support of development of enhanced version of DDES [4].

References

1. Peake N., Parry A.B. Modern Challenges Facing Turbomachinery Aeroacoustics. Annu. Rev. Fluid Mech. 2012. V.44. P.227–248.
2. Spalart P.R., Travin A.K., Shur M.L., Strelets M.Kh. Initial Noise Predictions for Open Rotors Using First Principles. AIAA Paper 2010-3793.
3. Spalart P.R., Deck S., Shur M., Squires K., Strelets M., Travin A. A new version of Detached-Eddy simulation, resistant to ambiguous grid densities. Theor. Comput. Fluid Dyn. 2006. V.20. P.181–195.
4. Shur M., Spalart P.R., Strelets M., Travin A. An Enhanced Version of DES with Rapid Transition from RANS to LES in Separated Flows. Flow, Turbulence and Combustion. 2015. V.95.
5. Filippone A. Aircraft noise prediction. Prog. Aerosp. Sci. 2014. V.68. P.27–63.

LARGE SCALE MOTION IN A DUAL-STREAM JET

Felix Kramer, **Ulf Michel**, Charles Mockett
CFD Software E+F GmbH, Berlin, Germany, ulf.michel@cfd-berlin.com

It has been suggested since 1963 (Mollo-Christensen [1]) that large scales play an important role in the emission of jet noise. Michalke developed a theory that took special account of large scales [2,3,4] by introducing a wave model for the sources and decomposing the turbulence into azimuthal components. He demonstrated that the low-order components have much higher radiation efficiency. The dominance of low-order components in the noise far field was experimentally verified by Maestrello 1977 [5]. Armstrong, Michalke and Fuchs [6] demonstrated that even the near field inside the jet was dominated by low-order components. Using Michalke's wave model the directivity of jet noise can be explained as consequence of this large scale motion [7,8].

These theoretical and experimental findings of the past can now be compared with the results of computational experiments. The unsteady flow field of a dual-stream jet with a short-cowl nozzle is analysed in the following. The simulation was performed with a time step corresponding to a sampling Strouhal number $f_s D_e/U_e = 1035$ and every 32nd time step was stored for later source analysis. $D_e = 0.183$ m is the diameter of a circle that has the same area as the sum of the exit areas of the two nozzles. $U_e = [A_p(U_p-U_0)+A_s(U_s-U_0)]/(A_p+A_s)+U_0 = 236$ m/s is calculated with the nominal speeds U_p and U_s in the primary and secondary nozzles and the speed $U_0 = 90$ m/s of the flight stream. The simulation was run over 186 convective time units D_e/U_e.

All flow data that are possibly relevant for the noise sources were stored on disk but only the pressure fluctuations are analysed in the following. The one-third octave spectra of the pressure fluctuations in various positions x/D_e downstream of the secondary nozzle are shown in Fig. 1. The radial positions with the largest peak levels of the spectra are chosen. These positions are close to the largest radial gradient of the mean axial velocity in the jet. The pressures are normalized with the ambient pressure p_0. It can be seen how the peak frequencies get smaller with increasing axial distance from the nozzle. This is a well-known result for jet turbulence.

New results, made possible by the computational experiment, are the cross spectra and coherence spectra for the pressures for azimuthally displaced "probe" positions. Results for $x/D_e=3$ are shown in Fig. 2, the cross spectra on the left side and the coherence spectra on the right side. The range around the peak Strouhal number $St=0.7$ decays only slowly with increasing azimuthal probe separation $\Delta\varphi$, while the rest of the spectra at higher and lower Strouhal numbers decays rapidly. The range around the peak frequency is dominated by a large scale motion in the jet. The coherence is seen to increase again for very

high Strouhal numbers, but one has to consider that the pressure levels are more than 50 dB lower in this range. This range is likely dominated by the radiated sound field, an assumption to be checked by analysing the radial and axial components of the phase speeds.

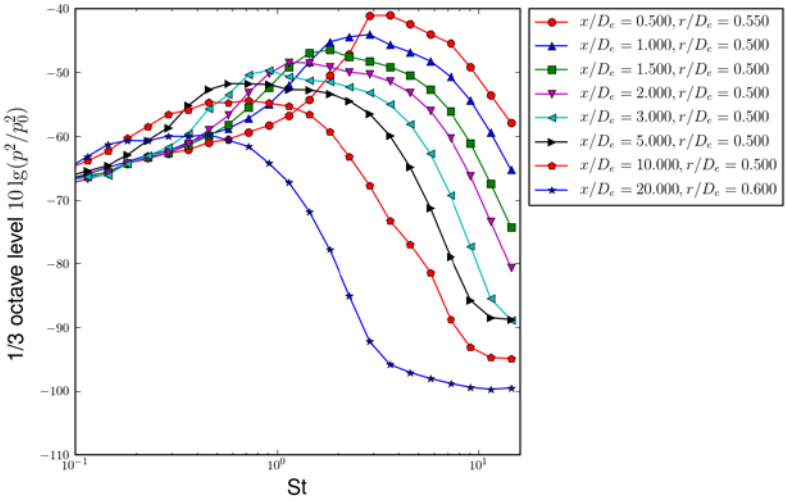

Fig. 1. One-third octave pressure spectra inside jet for various distances x/D_e from the nozzle for the radial position with highest one-third octave level (p_0 is ambient pressure)

The peak at St=0.7 for x/D_e =3 is analysed in more detail in Fig. 3. The decay of the cross spectrum with increasing probe separation $\Delta\varphi$ is shown in the left figure. The imaginary part should vanish for non-swirling jets since the time averaged turbulent quantities are axisymmetric. The non-zero values in this simulation are a consequence of the residual statistical error from the finite averaging time. The real part of the cross-spectrum is decomposed into azimuthal Fourier components on the right side. It can be seen that the pressure field is dominated by the Fourier component numbers m=0 and m=1, which contribute about 37% and 30%, respectively, to the mean square pressure fluctuation level. Since these components have a high radiation efficiency, the sound field originating from this axial location is dominated by these two azimuthal components.

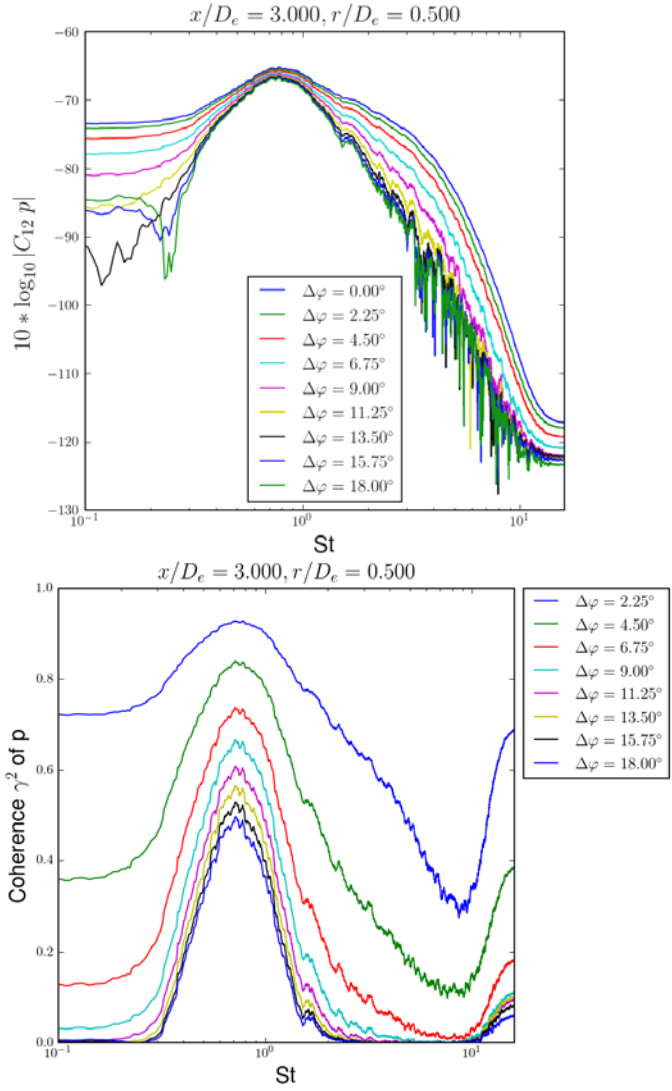

Fig. 2. Cross spectra and coherence spectra of circumferentially displaced probe positions for x/D_e=3

Figure 4 shows an analysis of the cross spectrum for the higher Strouhal number *St*=4.0. Here, the cross spectrum decays rapidly with increasing probe separation Δφ resulting in an almost uniform distribution of the azimuthal component levels. It can be seen in Fig. 1 that the one-third octave pressure level for

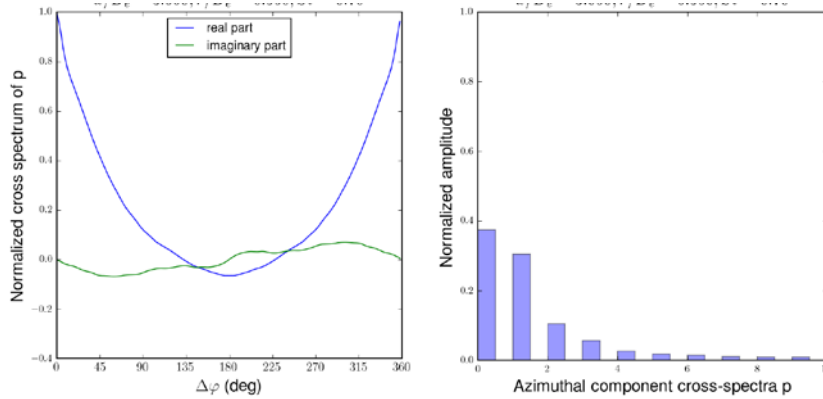

Fig. 3. Decay of normalized cross-spectrum with increasing azimuthal separation angle for St=0.70 at x/D_e=3.0 and r/D_e=0.5 (left). Decomposition of peak at St=0.7 into azimuthal Fourier components m (right)

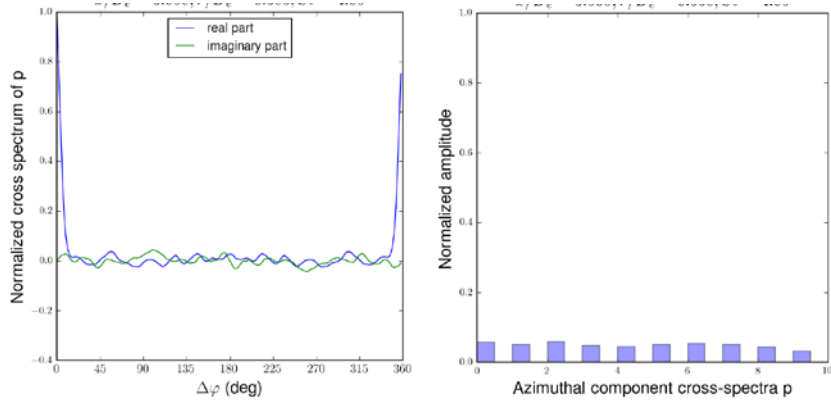

Fig. 4. Decay of normalized cross-spectrum with increasing azimuthal separation angle for St=4.0 at x/D_e=3.0 and r/D_e=0.5 (left). Decomposition of cross spectrum at St=4.0 into azimuthal Fourier components m (right)

St=4.0 is only 5 dB lower than the peak at St=0.7, but since the higher frequency is accompanied by much less efficient azimuthal components the radiated sound from this axial position is much smaller. Since the Fourier amplitudes of the efficient m=0 and m=1 components are roughly a factor of 10 (10 dB) smaller than those for St=0.7, it can be concluded that the far-field contributions of these component numbers are similarly reduced. Even though the peak level in the source field is only 5 dB lower at St=4.0 than at St=0.7 the radiated noise is likely 15 dB lower. We may conclude that the axial position x/D_e=3.0 contributes primarily to the sound radiation at a Strouhal number St=0.7.

The high azimuthal coherence of the pressure fluctuations in a relatively narrow frequency band is likely caused by the growth of instability waves in the jet's shear layer. These instability waves were studied by Michalke and Hermann [9] for a jet in a flight stream. They are dominated by low order azimuthal modes and their most unstable frequencies depend for given jet and flight speeds primarily on the shear layer thickness. The thin shear layers close to the nozzles are most unstable for high frequencies and the thick shear layers further downstream for low frequencies. It was shown by Michalke [2,3] that the mode numbers *m* of the instability waves are directly related to the order *m* of the Fourier decomposition of the cross spectrum. We conclude that the dominance of low order azimuthal components of the pressure fluctuations in a relatively narrow frequency band is caused by instability waves in the jet and that the wave-like motion in the jet shear layer dominates the jet noise emission.

The final paper will include results for other axial and radial positions and an analysis of the axial and radial components of the phase velocities of the disturbances.

The work was performed in the EU-funded project "JERONIMO" (ACP2-GA-2012-314692-JERONIMO).

References

1. E. Mollo-Christensen, M.A. Kolpin, J.R. Martucelli (1964): Experiments in jet flows and jet noise far-field spectra and directivity pattern. J. Fluid Mech. 18, 285–301.
2. A. Michalke (1970): A Wave Model for Sound Generation in Circular Jets. Tech. Rep. Deutsche Luft- und Raumfahrt. Forschungsbericht 70–57, Deutsche Luft- und Raumfahrt, November 1970, available at elib.dlr.de
3. A. Michalke (1972): An expansion scheme for the noise from circular jets. Z.Flugwiss. 6, 229–237.
4. A. Michalke (1977): On the effects of spatial source coherence on the radiation of jet noise. J. Sound Vib. 55, 377–394.
5. L. Maestrello (1977): Statistical properties of the sound and source fields of an axisymmetric jet. AIAA-1977-1267.
6. R.R. Armstrong, A. Michalke, H.V. Fuchs (1977): Coherent Structures in Jet Turbulence and Noise. AIAA Journal 15, 1011–1017.
7. U. Michel (2007): Influence of Source Interference on the Directivity of Jet Noise. AIAA-2007-3648.
8. U. Michel (2009): The role of source interference in jet noise. AIAA-2009-3377.
9. A. Michalke, G. Hermann (1982): On the inviscid instability of a circular jet with external flow. J. Fluid Mech. 114, 343–359.

DIRECT NUMERICAL SIMULATION OF TRANSITION TO TURBULENCE IN SUPERSONIC BOUNDARY LAYERS

A.N. Kudryavtsev[1,2], D.V. Khotyanovsky[1,2]
[1]*Khristianovich Institute of Theoretical and Applied Mechanics, RAS, Siberian Branch, Novosibirsk, alex@itam.nsc.ru, khotyanovsky@itam.nsc.ru*
[2]*Novosibirsk State University, Novosibirsk, Russia*

The development of instability and transition to turbulence in supersonic flat plate boundary layers at free stream Mach numbers M = 2 and 6 is simulated numerically. A 5th order WENO scheme is used to approximate the convective terms of the Navier-Stokes equations. The diffusive terms are calculated with central differences of 4th order on a compact stencil. The simulations are performed in a computational domain whose inflow boundary is located at some distance downstream of the plate leading edge (Fig. 1).

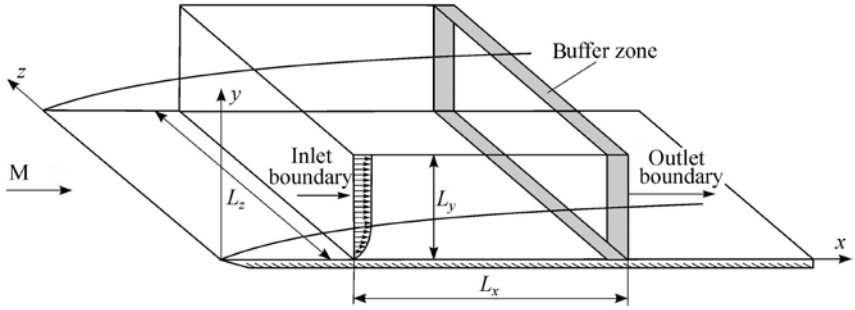

Fig. 1. Schematic of computational domain

At first, the steady basic flow is computed using the profiles of gasdynamic quantities obtained from the self-similar solution of boundary layer equations as inflow boundary conditions. After that, a superposition of eigenfunctions of the linear stability problem is added to the basic flow at the inflow boundary and the development of flow instability is simulated. The periodic boundary conditions are imposed on the lateral boundaries of the computational domain. Near the outflow boundary there is a special buffer zone where the flow relaminarization occurs as a result of action of source terms introduced into the equations of motion. The simulations are conducted at the wall temperature equal to the adiabatic temperature.

At moderate supersonic Mach numbers the most unstable disturbances are obliquely (with respect to the free stream direction) propagating vortical disturbances of the so-called first mode. Two different scenarios of transition to turbulence at such velocities were considered in literature. The first one is based on resonant three-wave interaction of the most unstable oblique wave with its

two subharmonics whose propagation angles can be determined from the phase synchronism conditions. Such an asymmetric subharmonic resonance was observed experimentally. The second scenario, oblique breakdown, is nonlinear interaction of two oblique waves with the angles $\pm\chi$ which form a resonant triad along with a steady vortical disturbance.

In our computations at M = 2 the second mechanism is simulated. It has a smaller threshold amplitude for the onset of nonlinear wave interaction and should lead to faster transition. In Fig. 2 the development of two disturbances with the amplitude of 0.5% from the free stream velocity and propagating at the angles ±55° is shown.

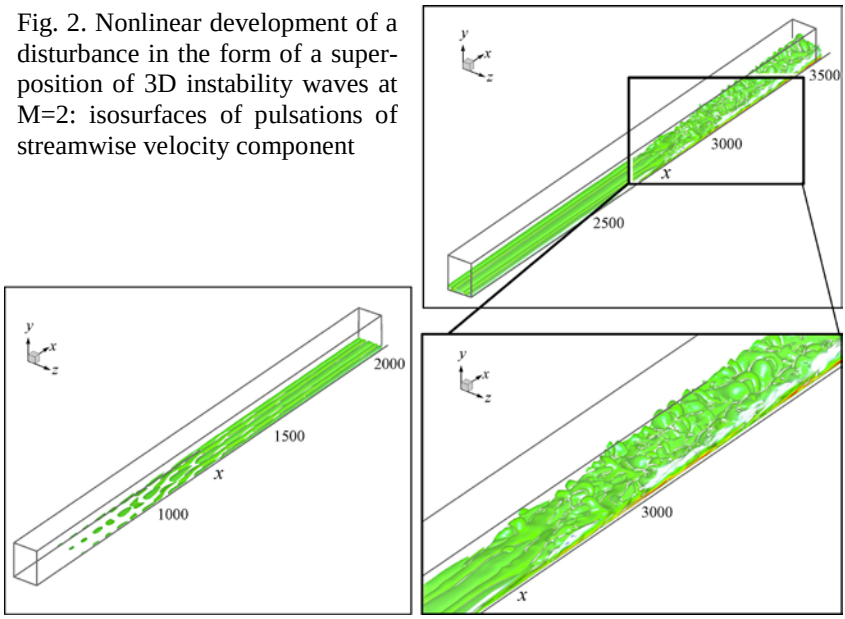

Fig. 2. Nonlinear development of a disturbance in the form of a superposition of 3D instability waves at M=2: isosurfaces of pulsations of streamwise velocity component

When the instability is developing, at first emergence of a secondary flow in the form of longitudinal vortex structures is observed. After that the secondary flow itself becomes unstable and a rapid, explosive growth of 3D fluctuations starts which leads finally to laminar-turbulent transition. At the initial stage the profiles of mean flow velocity are very close to the laminar boundary layer solutions. In the process of instability development they noticeably change their shape and, at some moment, the inflection point appears. After the transition the profiles have a typical turbulent, more filled shape. At the transition point the surface friction coefficient sharply grows.

In Fig. 3 the variation of root-mean-square amplitude of mass flow rate pulsations along the plate in the simulation and in the experiment [1] is shown.

It is evident that in both the cases the onset of transition is located not far from the point where the Reynolds number defined with the boundary layer thickness $Re_\delta \approx 1200$.

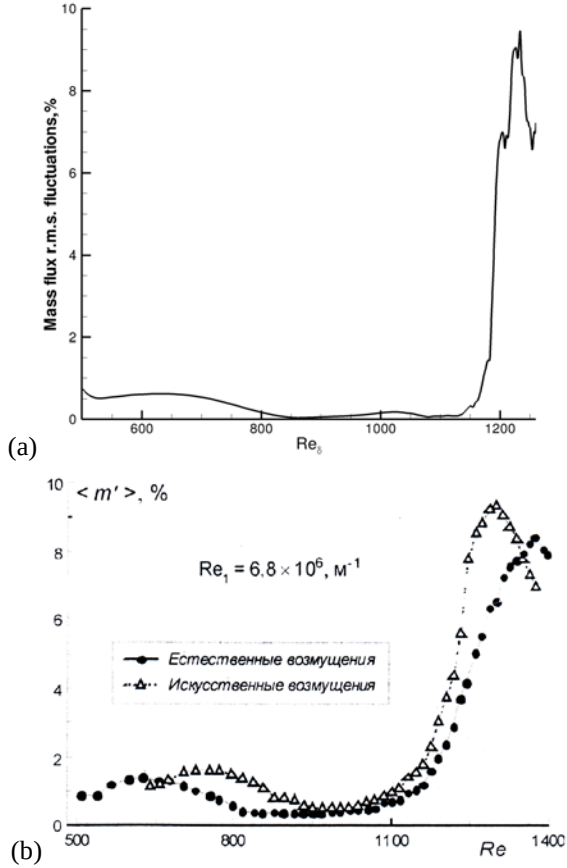

Fig. 3. Variation of rms amplitude of mass flow rate pulsations along the plate at M=2 in the simulation (a) and in the experiment (b)

At the free stream Mach number M = 6, in accordance with results of the linear stability theory, the most unstable disturbances are 2D disturbances of the so-called second mode which is of mixed, acoustical-vortical, nature. However, when propagating downstream, such disturbances with a given frequency rather quickly becomes stable as a result of the boundary layer thickness growth. At the same time, the first mode disturbances, among which, as earlier, oblique waves are most unstable, although their growth rate is an order of magnitude lower, remain unstable significantly farther downstream.

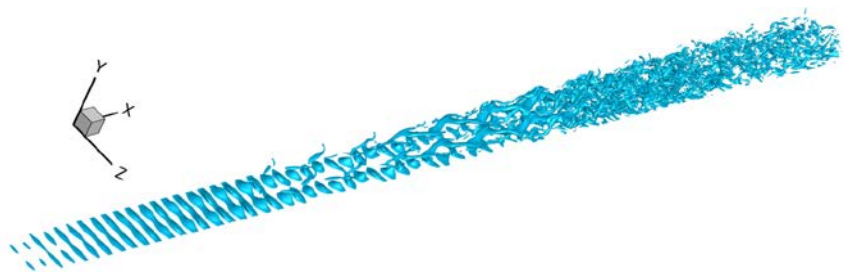

Fig. 4. Development of a disturbance in the form of a superposition of waves of the first and second modes at M = 6: isosurface of Q-criterion

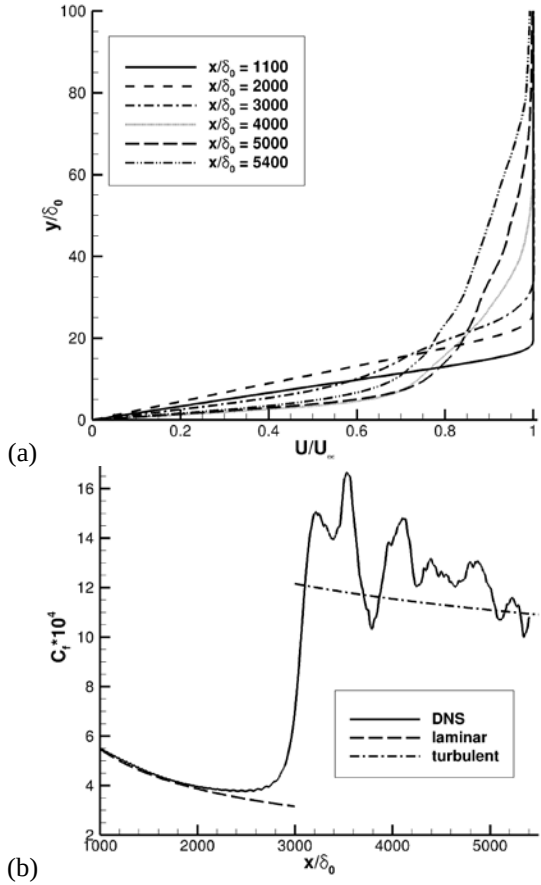

Fig. 5. Variations of the mean flow velocity profiles (a) and the friction coefficient (b) in simulations at M = 6

In Fig. 4 the development of a disturbance in the form a 2D wave of the second mode and two waves of the first mode propagating obliquely at the angles ±57°. The initial amplitudes of the waves are equal to 0.5%. At the initial stages the 2D disturbances of the second mode dominate. As 3D fluctuations grow, formation of hairpin vortex structures bursting out of the boundary layer is observed. The transition occurs approximately at $x/\delta_0 = 3000$ that corresponds to $\mathrm{Re}_\delta \approx 1750$. The variations of the mean flow velocity profiles and the friction coefficient along the plate are shown in Fig. 5.

The work was supported by Russian Foundation for Basic Research, Grants No. 14-07-00065 and No. 16-01-00743.

References

1. Yermolaev Yu.G., Kosinov A.D., Semenov N.V. Characteristics of weakly nonlinear interaction of instability waves in supersonic boundary layer. Vestnik NGU. Ser.: Physics. Vol. 3, No. 3 (2008), pp. 3–13.

PROPAGATION OF ACOUSTIC WAVES THROUGH MIXING LAYER OF SUBSONIC AND SUPERSONIC FLOWS

V.A. Lebiga[1,2], D.S. Mironov[1], A.Yu. Pak[1], V.N. Zinoviev[1]
[1]*ITAM SB RAS, Novosibirsk, lebiga@itam.nsc.ru*
[2]*Novosibirsk State Technical University, Novosibirsk*

Experimental investigation of acoustic wave propagation through plane mixing layer was performed with the help of hot-wire. The mixing layer was obtained by two flows with rated Mach numbers 0.5 and 2.0.

Acoustic disturbances were generated in subsonic flow by a slopping hole on the test section wall with adjustable depth *h*, Fig. 1, which serves as a source of sound. This whistle provided sound with frequencies $f = 5…9$ kHz, however artificial acoustic fluctuations of 6.8 kHz have been used in most described below experiments.

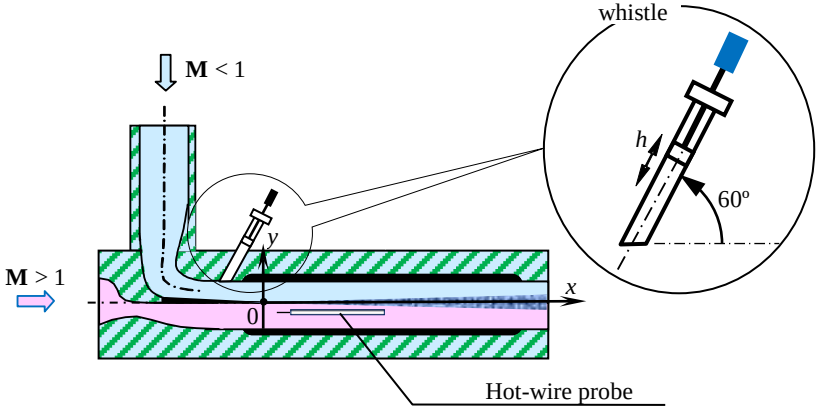

Fig. 1. Test configuration

Measurements were performed by constant current anemometer CCA-6 with the help of 5-micron hot-wire probe which can be moved in transverse direction. Profiles of mean velocity and fluctuations were obtained at eight cross-sections of the mixing layer along x-axis. It was found that intensity of artificially generated acoustic disturbances is essentially higher than the level of background fluctuations in subsonic flow. Hot-wire output signal was recorded at several overheat ratios of the probe and later was used to plot fluctuation diagrams and conducting analysis of fluctuations by spectral techniques. In order to define the most informative method of getting data about structure of acoustic disturbances propagating through the mixing layer different spectral techniques were utilized.

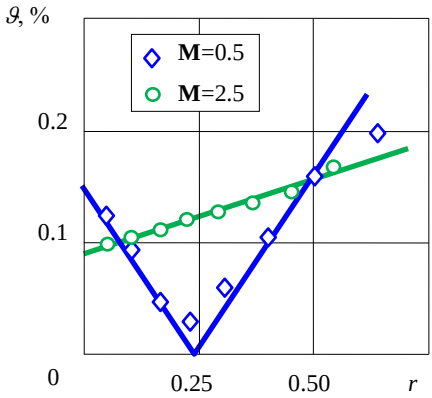

M	0.5	2.5
<*p*>,%	0.39	0.38
cos χ	0.49	–0.85
χ	61°	148°
$\chi_м$	-	114°
c/*u*	-	0.53

Fig. 2. Fluctuation diagrams for artificial disturbances

Examples of fluctuation diagrams for artificial disturbances measured in sub- and supersonic parts of flow are shown in Fig. 2. View of fluctuation diagrams corresponds to acoustic disturbances, namely: V-shape for subsonic flows and linear for supersonic flow velocity, [1].

Parameters of diagrams allow obtaining not only intensity of artificial generated pressure fluctuations <*p*>, but also direction of acoustic wave propagation, i.e. χ – angle between the normal to the front of the acoustic wave and mean flow velocity vector. Values of these angles both for subsonic and supersonic flows are presented in the table at Fig. 2. From fluctuation diagram for supersonic flow it was found that sources of acoustic disturbances are moving in mixing layer with averaged speed *c* which is 0.53 of velocity in the supersonic part of flow.

Integral and fluctuation characteristics of flow outside and inside the mixing layer were obtained: profiles of mean parameters, distribution of fluctuations intensities, and statistical characteristic – skewness K_3 and kurtosis K_4 coefficients in several sections along mixing layer.

Different techniques were used for analysis of fluctuations outside and inside of mixing layer: Fast Fourier Transform (FFT), Wavelet Transform (WT) and Empirical Mode Decomposition (EMD) which is a part of comparatively new mathematical technique – Hilbert-Huang Transform (HHT) proposed by Norden Huang [2].

Results of different methods are presented in Fig. 3 (FFT), Fig. 4 (WT), and Fig. 5 (EMD - HHT), where shown data correspond in each figure to (*a*) – subsonic flow; (*b*) – inside the mixing layer; (*c*) – supersonic flow.

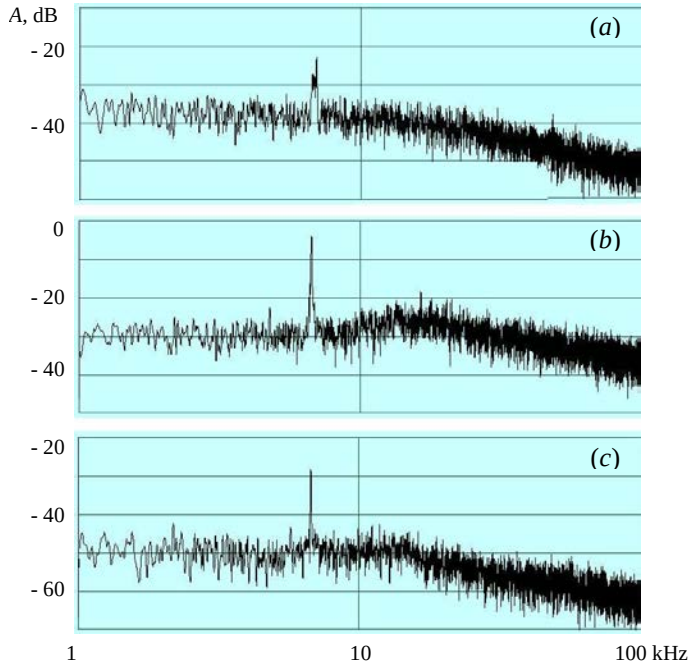

Fig. 3. Fourier spectra of flow fluctuations

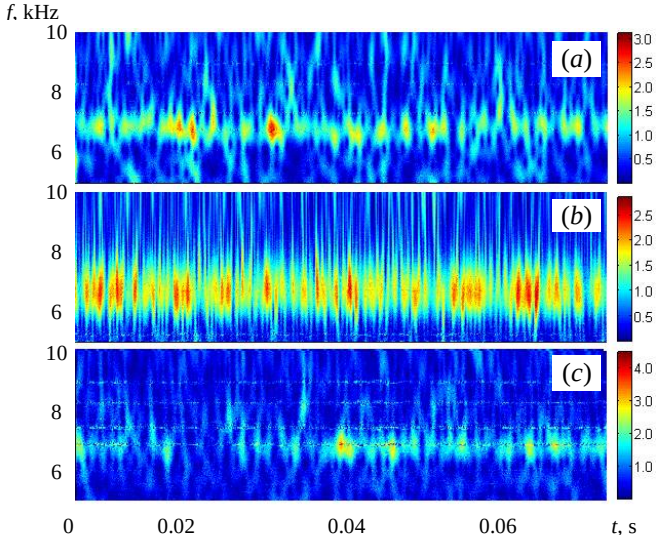

Fig. 4. Wavelet spectra

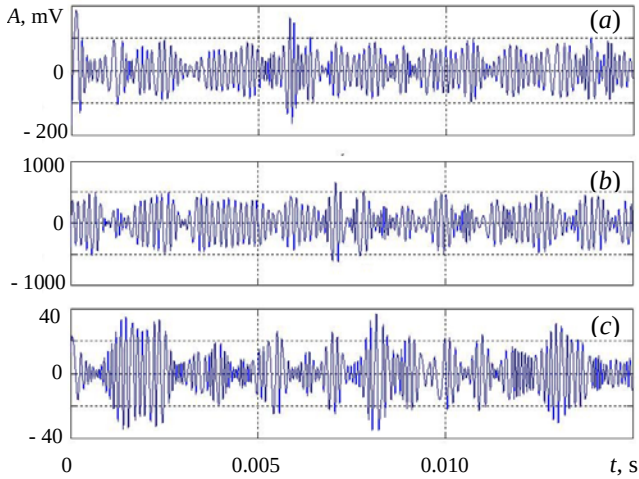

Fig. 5. Empirical mode of artificial acoustic fluctuations

From experimental data it follows that frequency and amplitude of artificial acoustic fluctuations generated in subsonic flow are not stable. This fact can be clearly seen from wavelet spectra in Fig. 4 and from empirical mode decomposition, Fig. 5. Artificial disturbances induce high intensity fluctuations in mixing layer, see data (*b*) in Figs. 3–5. Fluctuations as vortex structures, can be observed by optical visualization, are carried downstream in mixing layer and generate moving Mach waves in supersonic flow.

Method of fluctuation diagrams and different techniques of data analysis of hot-wire output allows one to obtain detailed information about mixing layer structure and propagation of acoustic disturbances through mixing layer.

This work has been partly supported by RFBR Grant No. 15-08-05738.

References

1. V.A. Lebiga, V.N. Zinoviev, A.Yu. Pak. Hot-wire measurements of acoustic waves propagating in compressible flows. Thermophysics and Aeromechanics. 2002. No.3, pp. 339–349.
2. Norden Huang et al. The empirical mode decomposition and the Hilbert spectrum for nonlinear and non-stationary time series analysis. Proc. of the Royal Society of London. A 454, 903–995, 1998.

METHOD FOR CALCULATION OF PROPELLER AERODYNAMIC CHARACTERISTICS AND ITS OPTIMIZATION WITH NOISE TAKING INTO ACCOUNT IN FRAMEWORK OF EWT-TSAGI APPLICATION PACKAGE

A.V. Lysenkov

Central Aerohydrodynamic Institute named after prof. N.E. Zhukovsky (TsAGI), Zhukovsky, Russia, lysenkov@tsagi.ru

The main method to obtain reliable propeller characteristics is an experiment in wind tunnels using special test benches. To investigate the characteristics of single and contrarotating propellers (including "open rotor" type), special test benches that permit to perform investigations in wide range of main flow velocities and of investigated propeller rotation frequency have been developed in TSAGI. During the experiment, thrust and momentum characteristics, flowfield after the propeller, pressure distributions on propeller blade (PSP method), blade deformations and acoustic characteristics are investigated.

In addition, the methodology of numerical experiment is used to investigate the propeller characteristics. In the investigations of both aircraft aerodynamic characteristics and propeller characteristics, the methodology includes several stages: preparation of investigated object mathematical model, calculation using multi-processor systems and result processing. To perform all these stage, a special application package (EWT-TsAGI [1]) has been performed in TsAGI. This application package has been verified and validated for a wide class of numerical aerodynamics problems in details.

To determine the aerodynamic characteristics of propellers, the application package uses solver RoS that is a modification of the solver ZEUS [2, 3]. Reynolds equation system closed by SST turbulence model is solved in rotating coordinate system. Godunov-Kolgan-Rodionov scheme and an explicit scheme with implicit smoother

$$u^{n+1} = u^n - \frac{\tau^n}{V_i}\left(\vec{F}^{\,n}_{i+\frac{1}{2}} - \vec{F}^{\,n}_{i-\frac{1}{2}}\right) + \left(-RM^n_{i-1}\Delta\vec{u}_{i-1} + RM^n_i\Delta\vec{u}_i + RM^n_{i+1}\Delta\vec{u}_{i+1}\right) - \vec{W}_{i,j,k}$$

are used. The rotation is taking into account by introducing the addition for convective fluxes and source terms. An exact solution of Godunov problem about arbitrary discontinuity at rotating grid is used. An additional restriction for the time step is introduced for the explicit scheme. The boundary conditions have been modified. Different methods of time step organization have been realized: global, local, fractional and dual.

RoS solver completes the verification and validation. The calculation results are compared with the experimental data and the calculation results obtained with the use of commercial software.

A sequence of operations that provides an automatic procedure of optimization cycle has been developed. It includes (Fig. 1): an optimization module, surface numerical model rebuilding, 3D computational mesh rebuilding, calculation run and integral characteristics calculation.

The objective function of optimization is propeller efficiency for given regime; the controlling parameters are setting angle of four profiles. Restrictions of the second order are following: the thrust of optimized propeller can't be less that the thrust of basic propeller and the noise estimated during the optimization with the use of empirical formula can't be more than the noise of the basic propeller. The propeller optimization has been performed in two formulations: without the restrictions of the second order and with taking them into account. It has been shown that, one has succeeded to improve the propeller model efficiency by 5% in the case of optimization without restrictions and by 1.2% in the case of optimization with restrictions.

The work was supported by Russian Ministry of Industry and Trade, the scientific work "Development of methodology for calculation of aerodynamic characteristics of the inlet for the turbofan engine of high thrust with simulation of gasdynamic fan-compressor interaction" (code "Inlet").

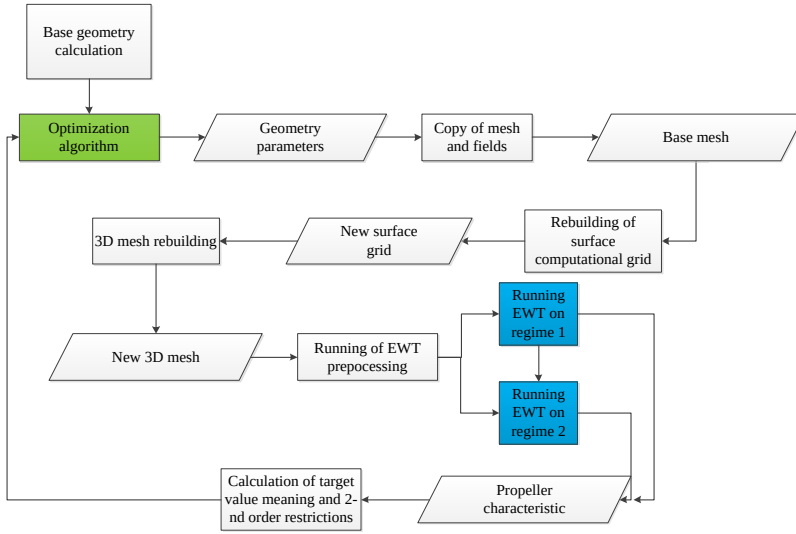

Fig. 1. Scheme of optimization cycle

References

1. V.Ya. Neyland, S.M. Bosnyakov, S.A. Glazkov, A.I. Ivanov, S.V. Matyash, S.V. Mikhailov, and V.V. Vlasenko. Conception of electronic wind tunnel and first results of its implementation. Progress in Aerospace Sciences, Vol. 37, No.2, 2001, pp. 121–145.
2. S. Bosnyakov, I. Kursakov, A. Lysenkov, S. Matyash, S. Mikhailov, V. Vlasenko, J. Quest. Computational tools for supporting the testing of civil aircraft configurations in wind tunnels. Progr. Aerospace Sci. 2008, Vol. 44, No.2, pp. 67–120.
3. E.V. Kazhan. Stability improvement of Godunov-Kolgan-Rodionov TVD scheme by a local implicit smoother, TsAGI Science Journal, Vol.43, 2012, Issue 6.

EXPERIMENTAL AERODYNAMIC AND ACOUSTIC DATABASE OF A 2D HIGH LIFT WING WITH AND WITHOUT SWEEP ANGLE

Eric Manoha[1], Michael Pott-Polenske[2]

[1]*Onera, Châtillon, France, eric.manoha@onera.fr*

[2]*DLR, Braunschweig, Germany, michael.pott-pollenske@dlr.de*

In LEISA2 (Silent Take-Off and Landing, 2010-2013) [1] and SWAHILI (Swept Airfoil with High Lift, 2014-2016), Onera and DLR are building experimental databases for the validation of CFD/CAA codes applied to the simulation of the unsteady flow and noise generation of high-lift wings. These activities are based on DLR's model F16, a two-dimensional (constant section in the span direction) high-lift profile with deployed slat and flap. The airfoil clean chord is close to 300 mm, and the nominal span is 800 mm, or 1400 mm with span extensions. In the LEISA2 project, the model was tested, without sweep angle, firstly in 2011 in F2, an aerodynamic wind tunnel located in Onera-Le Fauga, then in 2013 in AWB, an anechoic open-jet wind tunnel located in DLR-Braunschweig. In F2, intensive aerodynamic measurements were achieved using wall pressure steady/unsteady sensors, a hot wire probe and optical devices such as PIV and LDV. The reference velocity and the angle-of-attack were respectively set to 61.5 m/s and 6.15°. Acoustic measurements were also achieved with a wall microphone array (mounted beneath a wiremesh cloth in the windtunnel ceiling), despite the noisy and confined environment. In AWB, acoustic tests were conducted with another microphone array (Fig. 1).

Fig. 1. Top left : F16 airfoil section. Model in F2 (left) and AWB (right)

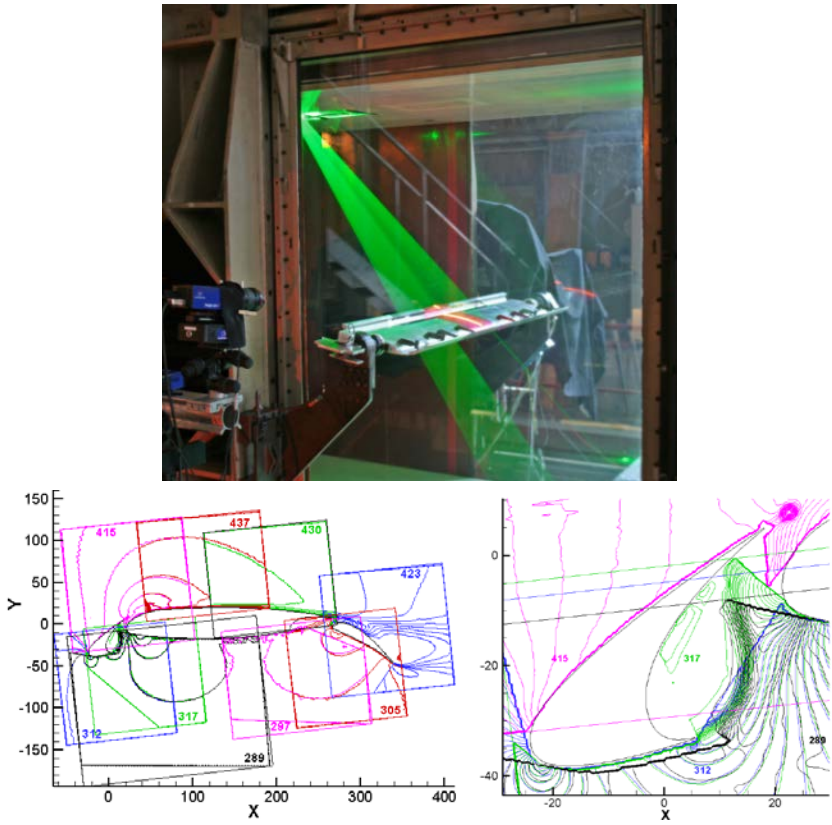

Fig. 2. PIV set-up in F2; iso-contours of velocity magnitude; PIV maps mosaic

Fig. 2 shows the 2-components (axial and vertical) PIV set-up in F2 and the mosaic of images that were necessary to cover the the largest possible flow area around the model.

Fig. 3 shows the 2-components (axial and vertical) LDV set-up in F2 and details of 1D surveys for steady velocity (mean flow) measurements in the slat cove and also isolated positions (right) where longer acquisitions were used to provide spectral information on velocity fluctuations in the fluid.

Fig. 4 shows profiles of the mean axial and vertical velocity components along the survey 11107-2 (see Fig. 3) in the slat cove, with comparison of LDV and three different PIV overlapped images. Fig. 4 also shows power spectral densities of U and V at several points along the shear layer which develops in the slat cove.

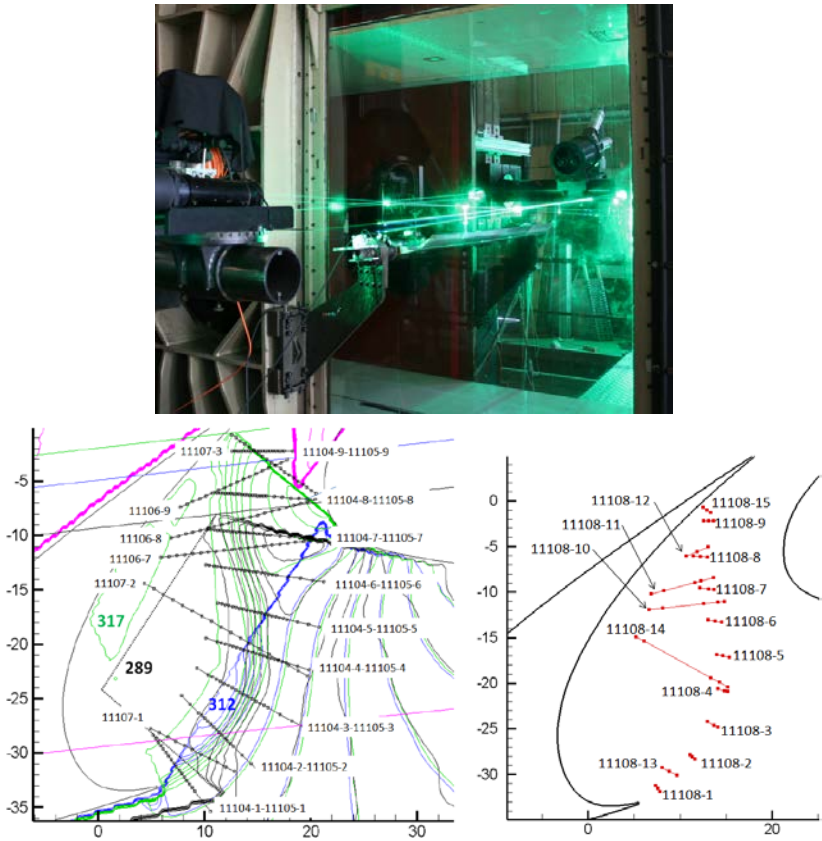

Fig. 3. LDV set-up in F2 (top); details of 1D surveys (left) and isolated points (right) for steady and unsteady velocity measurements in the slat cove

Acoustic measurements were achieved in both wind tunnels. Fig. 5 shows noise spectra measured in F2 and AWB with a single microphone, function of (i) the wind velocity (at given angle-of-attack) and (ii) the angle-of-attack (at given wind velocity). Result from F2 also shows the background noise obtained without model in the test section. Strong tones are observed in the 2-8 kHz range, especially in the AWB windtunnel, which amplitudes increase with the velocity and decrease with the AOA. Such tones are assumed to depend on installation effects and scale, they are not directly associated to slat noise.

The most interesting acoustic results were actually obtained with the microphone arrays. Fig. 6 shows noise maps obtained in F2 and AWB using the DAMAS process (De-convolution Approach for the Mapping of Acoustic Sources) at various frequencies in the range 1 – 6.3 kHz. In both windtunnels,

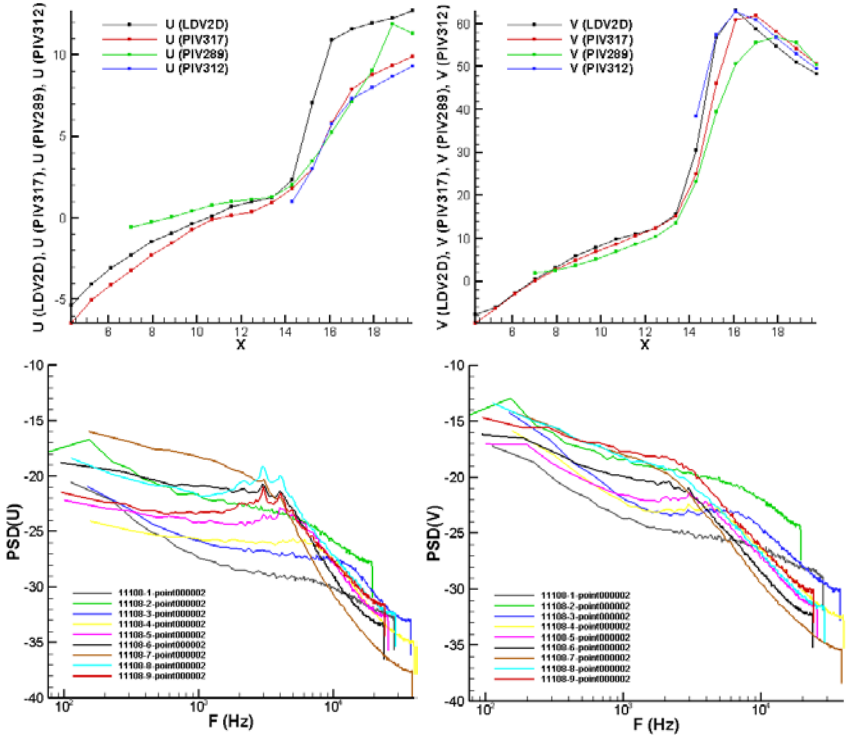

Fig. 4. Profiles of mean axial U and vertical V velocities along survey 11107-2 in the slat cove (top); PSD of U and V along the shear layer (bottom)

the flap is the main source below 2 kHz, whereas the slat becomes dominant at higher frequencies. With the DAMAS process, quantitative information on the noise radiated by a given area can be derived through simple integration of noise maps. Fig. 7 compares the spectra of noise radiated in both windtunnels by the same central region of the airfoil with a span of 0.24 m, a region where the mean flow is rather 2D. The agreement is quite good on the broadband levels, differences are only observed on the tones frequencies and amplitudes.

The LEISA2 database is now available to the aeroacoustic community in the framework of the Benchmark for Airframe Noise Computations (Category 6) [2].

More recently, in the SWAHILI program, the F16 model has been modified by DLR to account for a 30° sweep angle, requiring the manufacturing of new span extensions compatible with continuous incidence adjustment. The manufacture was completed by end of January 2016 and aerodynamic/acoustic tests were achieved in F2 between February and May 2016.

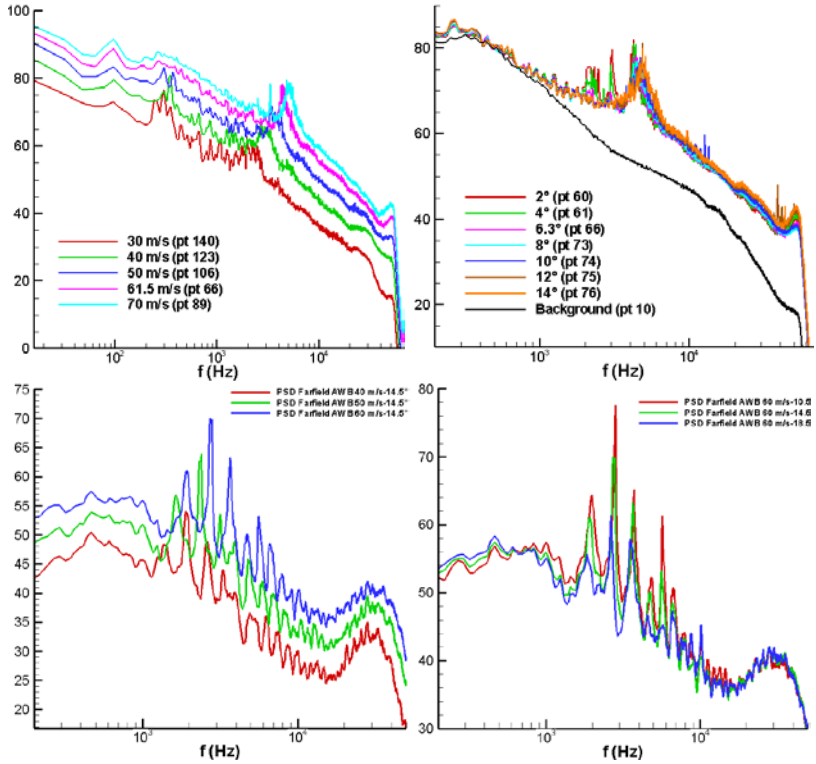

Fig. 5. Noise spectra measured by a single microphone in F2 (top) and AWB (bottom), function of wind velocity and angle of attack

Fig. 8 shows the model set-up in the F2 windtunnel. Again, the model is mounted upside down and the microphone array is visible in the windtunnel ceiling. The reference angle-of-attack and windtunnel velocity were respectively set to 5.3° and 71.0 m/s, ensuring that the velocity component normal to the leading edge is actually 61.5 m/s and the airfoil section in this direction recovers the 6.15° incidence w.r.t. the mean flow. Fig. 8 also shows an early acoustic result obtained with the microphone array, comparing the noise measured by a single microphone and the noise radiated by airfoil areas in the slat and flap regions.

Additional acoustic tests will be achieved in AWB in the second half of 2016. At mid-term, the SWAHILI database will also become public for sharing benchmarking activities inside the airframe noise community.

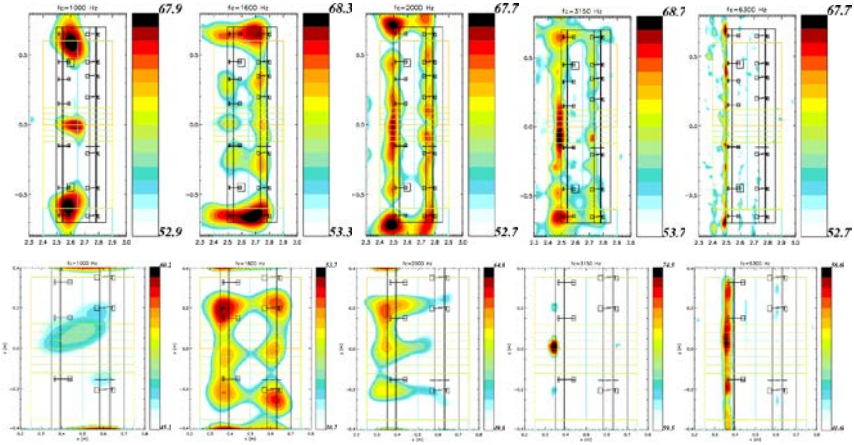

Fig. 6. DAMAS noise maps from F2 (61.5 m/s, 6.4°, top) and AWB (60 m/s, 14.5°, bottom) microphone arrays (flow is from left to right)

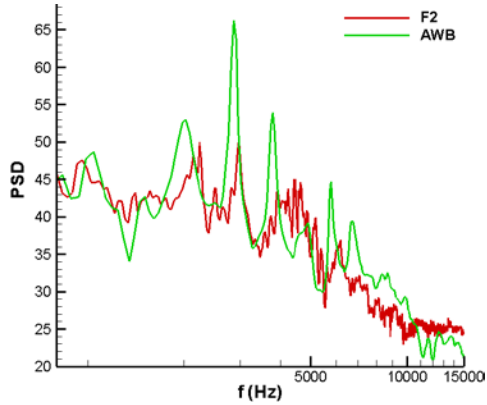

Fig. 7. Noise specra from a central airfoil section of span 0.24 m

References

1. E. Manoha and M. Pott-Polenske. “LEISA2: an experimental database for the validation of numerical predictions of slat unsteady flow and noise”. AIAA Paper 2015-3137, 21th AIAA/CEAS Aeroacoustics Conference 22–26 June 2015, Dallas, TX, 2015.
2. https://info.aiaa.org/tac/ASG/FDTC/DG/BECAN_files_/BANCIV.htm

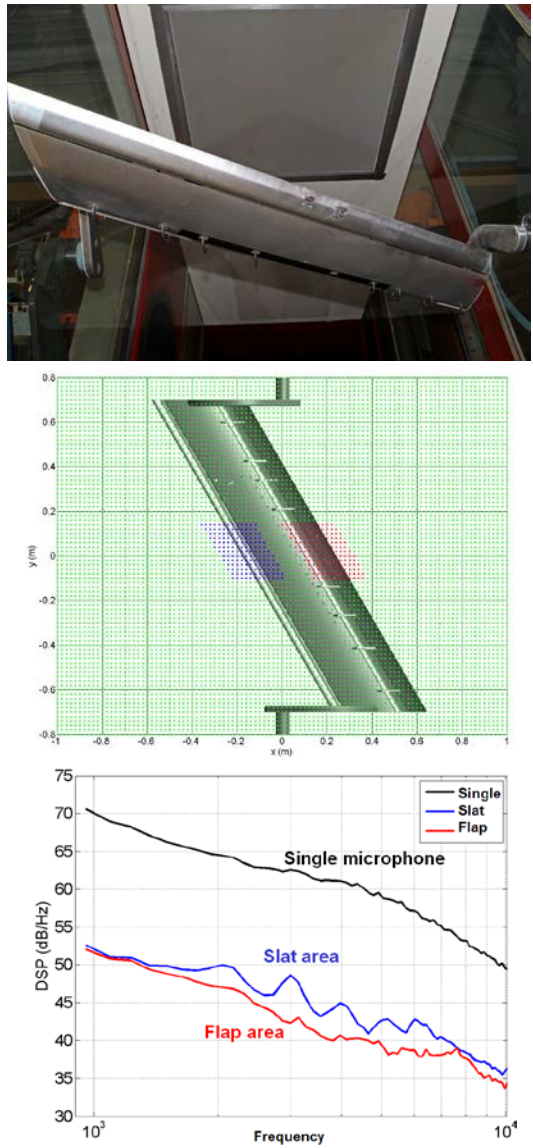

Fig. 8. F16 model in F2 with 30° sweep angle. Early acoustic result with the microphone array : noise radiated by airfoil areas in the slat and flap regions

ABNORMAL AMPLIFICATION OF SOUND REFRACTED BY AN OBLIQUE SHOCK WAVE

Igor Menshov[1], Keiichi Kitamura[2]
[1]*KIAM RAS, Moscow, Russia, menshov@mail.ru*[1]
[2]*Yokohama National University, Yokohama, Japan, kitamura@ynu.ac.jp*

The present paper addresses the problem of interaction of small flow disturbances in the form of a monochromatic plane wave with plane stationary oblique shock waves. There are three types of small disturbances that can propagate in uniformly moving compressible fluid. One represents isentropic pressure and density fluctuations that propagate with the speed of sound relatively to the fluid. The other two are fluctuations of vorticity and entropy that are carried with the fluid velocity. The impingement of such disturbances on a shock generates waves that are composed of all three types.

The problem of sound/shock interaction has been studied by several researches. Blokhintsev [1] solved the problem for the case of an acoustic wave normally striking by a plane shock wave in a perfect gas. Brillouin [2] investigated oblique incidence of a plane acoustic wave onto a normal shock, but obtained erroneous results. These results further have been corrected by Kontorovich [2], where an arbitrary compressible medium (with a general equation of state) has been also considered.

In the present paper we addresses the theoretical and numerical analysis of the interaction of plane sound with an oblique shock. Theoretical results concern the amplification factor as a function of the flow regime and incident angle. Basic conclusions from this study are as follows. (i) The regular sound/shock interaction exists provided that the angle of incidence does not exceed a critical angle; beyond this one no solution exists in the form of plane waves. (ii) Amplification of sound in the transmitted wave with respect to upstream Mach number is order of $O(M^2)$. (iii) Approaching the critical angle the amplification factor is abruptly grows up as $O(M^3)$. Numerical simulations of sound/shock interaction are carried out and compared with the linear theory.

The reported study was funded by JSPS and RFBR according to the research project № 15-51-50023.

References

1. D.I. Blokhintsev. Dokl.Akad.Nauk SSSR, v.47, p.22, 1945.
2. J. Brillouin. J. Acustica, v.5, p. 149, 1955.
3. V.M. Kontorovich. Sov. Phys. JETP, v.33, p.1180, 1958.

FREQUENCY DOMAIN METHOD OF MULTISTAGE TURBOMACHINE TONE NOISE CALCULATION

V.I. Mileshin, S.V. Pankov, **A.A. Rossikhin**
Central Institute of Aviation Motors (CIAM), Moscow, Russia, rossikhin@ciam.ru

Last decades essential efforts have been directed on the reduction of fan noise of aero-engines, and these efforts have led to impressive results. Wide-chorded fans of modern turbofans with small number of blades (≤ 18) and high by-pass ratio are significantly less noisy than narrow-chorded fans with high number of blades of earlier turbofans. At the same time the decrease of fan noise makes more important the contribution of other noise sources to the engine noise, such as low pressure turbine and booster stages.

Feature of the booster stages and low-pressure turbines as noise sources in comparison with the fan is that their tone noise is usually generated in the process of interaction of several blade rows. For example, even if we assume that the dominant contribution to the tone noise of the booster stages is provided by the first stage, we should consider interaction between the rotor of the stage and the inlet guide vanes of the booster, the rotor and the stator, and also consider interaction of noise of the stage with a fan rotor.

Thus, the method of calculation of a multistage turbomachine tone noise should take into account interaction between different rows of a turbomachine and describe noise propagation through the turbomachine duct. The simplest approach is direct full annulus unsteady calculation; however its computational cost is very high. Therefore there is a natural desire to use frequency domain methods, which are proven to be computationally efficient for the calculation of fan tone noise. Such approaches for multistage turbomachine tone noise calculation have indeed been developed and showed satisfactory cost of computations.

One of such methods was developed in CIAM. It is the linear frequency domain method of multistage turbomachines tone noise calculation based on the notion of harmonic fragment - component of flow which have definite frequency and phase lag between boundaries of blade channel [1]. In the framework of the method the solution in a row is represented by the set of harmonic fragments in one blade channel of the row. Calculations of flow fields of harmonic fragments in each blade row are performed independently. The link between the harmonic fragments in the adjacent rows is provided by interfaces on the boundaries between computational domains correspondent to these blocks. Interfaces provide the continuity of flow field on the boundary between rows for the prespecified set of harmonic functions of time and circumferential angle (circumferential modes).

The advantage of the method, which relies on the kinematic relations featuring dependence of flow fields in a turbomachine from time and circumferential angle, is the possibility of quite simple actuation of complex interactions between rows into the computation. Harmonic fragments calculated in the rows are determined by the choice of interactions under consideration, and boundary conditions are entirely specified by the sets of harmonic fragments in the adjacent rows.

By means of the given method unsteady interactions in several turbomachines were investigated. In the work [1] comparison of results of two-dimensional calculations of a two-stage turbomachine tone noise, performed with use of the method based on formalism of harmonic fragments, and the method based on direct unsteady calculation, is presented. In general satisfactory coincidence between the results of calculations is observed. In work [2] the results of numerical investigation of the first booster stage tone noise of a high bypass ratio turbofan, performed with the use of method under consideration are presented. Comparison of the results of calculation with the results of experiment at CIAM C-3A acoustic test facility has shown satisfactory coincidence between them.

At the same time the method based on the independent (within the limits of one sub step of the scheme) execution of calculation for each harmonic fragment, has an essential disadvantage: this method cannot be straightforwardly generalized to the nonlinear case.

The standard approach for calculation of nonlinear fluxes in frequency domain is organized as follows. At the first stage of computation flow field, represented in the form of a set of harmonics, is transformed from frequency domain to time domain, using discrete Fourier transformation for the calculation of unsteady flow fields on the specified number of time layers. Then on these time layers nonlinear components of fluxes are calculated. At the last stage there is a transformation of the calculated fluxes back in frequency domain. This method works well if all disturbances which should be treated independently, have different frequencies. However, different harmonic fragments can have identical frequencies, and in this case inverse transformation of fluxes from time domain to fluxes for a set of harmonic fragments is impossible.

In the paper the frequency domain numerical method, suitable for calculation of unsteady interaction between rows of a multistage turbomachine in nonlinear statement is presented. This method also makes a start from a formalism of harmonic fragments. In the framework of the method it is assumed that the flow field in a row is described by the specified set of harmonic fragments. At the same time calculation is conducted not for the specified numbers of harmonic fragments in one blade channel of each row, but for the specified numbers of frequencies and blade channels in rows. Boundary conditions on the external boundaries of computational domain corresponding to periodic boundaries of

blade channels are specified based on the data about flow fields on correspondent boundaries of blade channels inside computational domain, and data about sets of harmonic fragments which constitutes the required solution. In linear statement the presented method is completely equivalent to the method described earlier. It is possible to use in the calculations performed in a row for different frequencies unequal numbers of blade channels, coinciding with the numbers of harmonic fragments specified for those frequencies.

The given method, obviously, can be easily generalized on a nonlinear case using approach described above. The unique limitation necessary for that all blade channels are considered equally, is that the number of treated blade channels (and, hence, the number of harmonic fragments) is identical for all frequencies in one blade channel. This limitation is not a fundamental one but can be overcome only by the price of significant complication of the method.

The method under consideration is implemented in the CIAM 3DAS (3-Dimensional Acoustics Solver) in-house solver. The method of calculation used in the 3DAS solver is based on the decomposition of the unsteady viscous 3D flow into two parts - inhomogeneous viscous 3D steady flow field and 3D unsteady inviscid disturbances. The equations in our method are solved using numerical methods of computational aeroacoustics. For spatial approximation we use the fourth order DRP (Dispersion Relation Preserving) scheme, rewritten for the finite volume method. For time derivative approximation fourth order six stages Runge–Kutta scheme of HALE-RK (High-Accuracy Large-step Explicit Runge–Kutta) type was used in this work.

In the work a number of test examples showing, that the described method of calculation can be used for interaction calculation in a turbomachine, is presented. Its equivalence in a linear case to the method of calculation described in [1] is shown.

References

1. A.A. Osipov, A.A. Rossikhin. Calculation method for unsteady aerodynamic blade row interaction in a multistage turbomachine, TsAGI Science Journal, 45(3–4), 255–271, 2014.
2. A.A. Rossikhin, S.V. Pankov, V.I. Mileshin. Numerical investigation of the first booster stage tone noise of a high bypass ratio turbofan. GT2016-57352. ASME Turbo Expo 2016, Seoul, South Korea, June 13-17, 2016.

A COMBINED FEM/BEM DISCRETE NUMERICAL METHOD FOR SOLVING EXTERNAL SCATTERING PROBLEMS IN ACOUSTICS

J. Poblet-Puig[1], **A.V. Shanin**[2]

[1]*Universitat Politècnica de Catalunya, Barcelona, Spain, jordi.poblet@upc.edu*

[2]*M.V. Lomonosov Moscow State University, Moscow, Russia, a.v.shanin@gmail.com*

Recently [1,2] a combined approach of CFIE–BAE has been proposed by authors for solving external scattering problems in acoustics. CFIE stands for combined-field integral equations, and BAE is the method of boundary algebraical equation. The combined method is, essentially, a discrete analogue of the boundary equations method (BEM), having none of its disadvantages. Namely, due to the discrete nature of BAE one should not compute quadratures of oversingular integrals. Moreover, due to CFIE formulation, the method does not possess spurious resonances.

However, the CFIE–BAE method has an important drawback. Since the modelling is performed in a regular discrete space, the shape of the obstacle should be assembled of elementary "bricks", so smooth scatterers (like spheres, cylinders, etc) are approximated with a poor accuracy. This loss of accuracy becomes the bottleneck of the method. Here this disadvantage is overcome. The CFIE–BAE method developed for regular meshing of the outer space is coupled in a standard way with a relatively small irregular mesh enabling one to describe the shape of the obstacle accurately enough. The process on the irregular mesh is modeled by the finite element method (FEM).

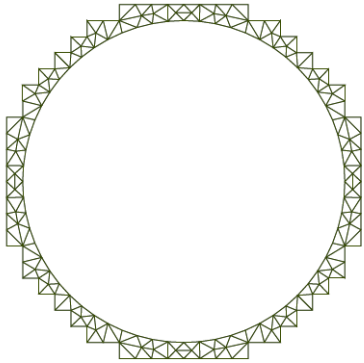

Fig. 1. An example of irregular FEM mesh used in the method

The scheme of the method is as follows. Consider a stationary 2D problem of diffraction by an acoustically hard circle as an example. Embed the scat-

terer (circle) into a FEM mesh, whose outer boundary is “regular”. By “regular” we mean that the nodes and the edges belong to a regular periodic square mesh. An example of such a FEM mesh is shown in Fig. 1. One can see that the amount of elements may be quite small since it is necessary to fill only the space between the scatterer and the outer boundary. There is no need to fill big spaces or add absorbing layers.

The irregular FEM mesh is processed by the usual finite element method. The internal boundary bears a natural (Neumann) boundary condition. For the external boundary, a non-local boundary condition is formulated. This condition should be equivalent to the absence of waves coming from infinity, so it is a radiation condition. Generally, such a condition has form

$$\Pi L u = D u \,, \qquad (1)$$

where u is the vector of nodal values of the field variable, L is the matrix of the FEM operator on the mesh (the FEM equation is

$$L u = f \qquad (2)$$

for the internal nodes of the mesh), Π is the projector on the external boundary, D is the matrix playing the role of the Dirichlet-to-Neumann operator on the external boundary.

The operator D is found by applying the method of CFIE-BAE described in [1,2]. For this, an analog of CFIE boundary integral equation is constructed in a discrete space. Equation (2) is solved with boundary condition (1) providing the field at the nodes of the FEM mesh. After postprocessing, one can obtain the directivity of the field.

The talk presents the details of the realization of the method, numerical results and the error analysis.

The authors acknowledge the Euro-Russian Academic Network-Plus program (grant number 2012-2734/001-001-EMA2). In addition, J.Poblet-Puig is grateful for the sponsorship/funding received from Generalitat de Catalunya (Grant number 2014-SGR-1471). A.V.Shanin has been also supported by Russian Scientific school grant 7062.2016.2 and the Russian Foundation for Basic Research grant 14-02-00573.

References

1. J. Poblet-Puig, A.V. Shanin, V.Yu.Valyaev, BEM method initially based on FEM approximation. International workshop “Computational experiment in aeroacoustics”, September 19-22 2012, Svetlogorsk, Russia, p.105.
2. J. Poblet-Puig, V.Yu. Valyaev, and A.V. Shanin, Suppression of spurious frequencies in scattering problems by means of boundary algebraic and combined field equations. J. Integr. Eq. Appl. v.27, 2015, pp.233–272.

A FAR-FIELD CALIBRATION-FREE LOW-ORDER MODEL FOR JET NOISE PREDICTIONS

Vasily A. Semiletov[1], Sergey A. Karabasov[2]

[1]*University of Cambridge, Engineering Department, Whittle laboratory, 1 JJ Thomson Avenue, Cambridge, CB1 8QH, UK, vs346@cam.ac.uk*

[2]*Queen Mary University of London, Mile End Rd, London, E1 4NS, UK, s.karabasov@qmul.ac.uk*

Many jet noise prediction codes are based on the acoustic analogy approaches of Lighthill (1952) and Lilley (1974), where both the mean flow and the turbulence fields are modelled statistically based on Reynolds Averaged Navier-Stokes (RANS) calculations. Examples of such codes that are currently used by industry include the MGBK code from Mani et al (1978) and the JeNo code of Khavaran et al (2002). An important advantage of the RANS based methods is short turn-around times which allow the user to consider a wide range of operating conditions and nozzle designs. However, there is not enough experimental data to validate various assumptions made in these models about the functional dependencies involved in the source modelling such as in the modelling of cross-correlation functions of fluctuating turbulent stresses.

Here, we suggest a new low-order jet noise model based on an implementation of the Goldstein generalized acoustic analogy with parameters calibrated from a Large Eddy Simulation flow solution. An extensive analysis of cross-correlation functions of turbulent stress components, R_{1111}, R_{1212}, R_{2222}, which are most important source sources for isothermal jets, has been conducted. The relationships between velocity fluctuations, dissipation tensor components and noise sources amplitudes, temporal and spatial scales are established. Using these relations, a low-order model for jet noise predictions is developed, its far-field noise predictions are compared with the experiment and a sensitivity study to different model parameters is performed.

References

1. M.E. Goldstein. A unified approach to some recent developments in jet noise theory. Int. Journ. Aeroacoustics, 1(1), 2002, pp. 1–16.
2. M.E. Goldstein. A generalized acoustic analogy. J. Fluid Mech., 488, 2003, pp. 315–333.
3. M.E. Goldstein and S.J. Leib. The Aero-acoustics of slowly diverging supersonic jets. J. Fluid Mech., 600, 2008, pp.291–337.

4. V.A. Semiletov, S.A. Karabasov, A. Chintagunta, and A.P. Markesteijn. “Empiricism-free noise calculation from LES solution based on Goldstein generalized acoustic analogy: volume noise sources and meanflow effects”. 21st AIAA/CEAS Aeroacoustics Conference, AIAA Aviation, (AIAA 2015-2536).
5. V.A. Semiletov, S.A. Karabasov. Adjoint Linearised Euler solver and Source Modelling for Goldstein acoustic analogy equations for 3D jet flow problems: verification and capability study. 20th AIAA/CEAS Aeroacoustics Conference, AIAA, 2014.

COMPUTATIONAL MODELLING OF DUAL STREAM JET USING CABARET GPU SOLVER: AERODYNAMIC AND AEROACOUASTIC VALIDATION

Vasily A. Semiletov[1], Anton P. Markesteijn[2], Georgy A. Faranosov[3,4], Sergey A. Karabasov[2], Victor F. Kopiev[3,4]

[1]*University of Cambridge, Engineering Department, Whittle laboratory, 1 JJ Thomson Avenue, Cambridge, CB1 8QH, UK, vs346@cam.ac.uk*

[2]*Queen Mary University of London, Mile End Rd, London, E1 4NS, UK, s.karabasov@qmul.ac.uk*

[3]*Central Aerohydrodynamic Institute, Moscow, 17, Radio Street, Russia*

[4]*Perm National Research Polytechnic University, 29, Komsomolsky Pr., Perm, Russia*

A new GPU implementation of the CABARET solver coupled with the Ffowcs Williams – Hawkings integral surface method [1] is applied for the flow and noise predictions of a dual-stream jet case. There are two configurations considered: a co-planar nozzle and a short cowl nozzle with a central body.

Aerodynamic and aeroacoustic predictions are obtained on several computational grids and compared with the experimental data from the QinetiQ facility [2]. Effects of the central body and inflow conditions on noise spectra are discussed.

References

1. A.P. Markesteijn, V.A. Semiletov, S.A. Karabasov. GPU CABARET solutions for the SILOET jet noise experiment: flow and noise modelling. AIAA Aeracoustics 2016.
2. C.J. Mead, C.M. Wrighton and K.M. Britchford. An Experimental Study of Co-Axial Jets Using Acoustic, PIV & LDA Methods (CoJeN). Aeracoustics 2015, AIAA 2015-3122.

NUMERICAL SIMULATIONS OF LEISA2 HIGH-LIFT CONFIGURATION AT ONERA

Marc Terracol[1], Thomas Le Garrec[1], **Daniel-Ciprian Mincu**[1], Eric Manoha[1], Damiano Casalino[2], André Ribeiro[2]

[1]*Onera, The French Aerospace Lab, Châtillon, France, daniel-ciprian.mincu@onera.fr*

[2]*Exa GmbH, Stuttgart, Germany, damiano@exa.com*

For aircraft in approach and landing operations, when the engines are in idle regime, airframe noise becomes predominant. High lift devices, namely the leading edge slats and the trailing edge flaps, deployed to increase lift at low speed, represent one of the main contributor to the airframe noise.

A large number of numerical studies have addressed such configurations in the past, using unsteady computations based on either zonal RANS/LES [1-4] or hybrid RANS/LES [5-12] approaches. However, despite the advanced understanding of flow features, these studies suffered from the lack of mixed experimental measurements to validate conjunctively the aerodynamics and the aeroacoustics. Among the reasons, one can point out the different stream deflections, with direct consequences on the flow around the wing, when such deployed configuration is measured in a closed test section (for aerodynamics) or open test section (for aeroacoustics) measurement wind tunnels.

With a view to fill this gap, the French (ONERA) and German (DLR) Aerospace Research Centers unified their competences to address this last topic, and provide, a complete measurement database (with both aerodynamics and acoustics data) to validate computations and to explore in details such configuration. Fig. 1 shows some results of this experimental campaign, named LEISA2. Recently, Onera and DLR made this database available to the community, within the framework of the NASA BANC workshop – Category 6 [13].

In parallel, several numerical computations were conducted or are still under progress at Onera to perform a detailed numerical flow analysis and to identify the noise mechanisms at approach. Fig. 2 shows several results about the acoustic near field and flow features in the slat cove and over the flap using the in-house research CFD/CAA code FUNk working with a structured multi-blocks grid [14].

Furthermore, recently Onera started to invest in the Lattice Boltzmann methods, firstly through a fruitful cooperation [15] with Exa Corporation, with the objective of evaluating their numerical solution PowerFLOW (Fig. 3, top) and, secondly, by joining the French consortium LaBS, which also develops a LBM solver (Fig. 3, bottom).

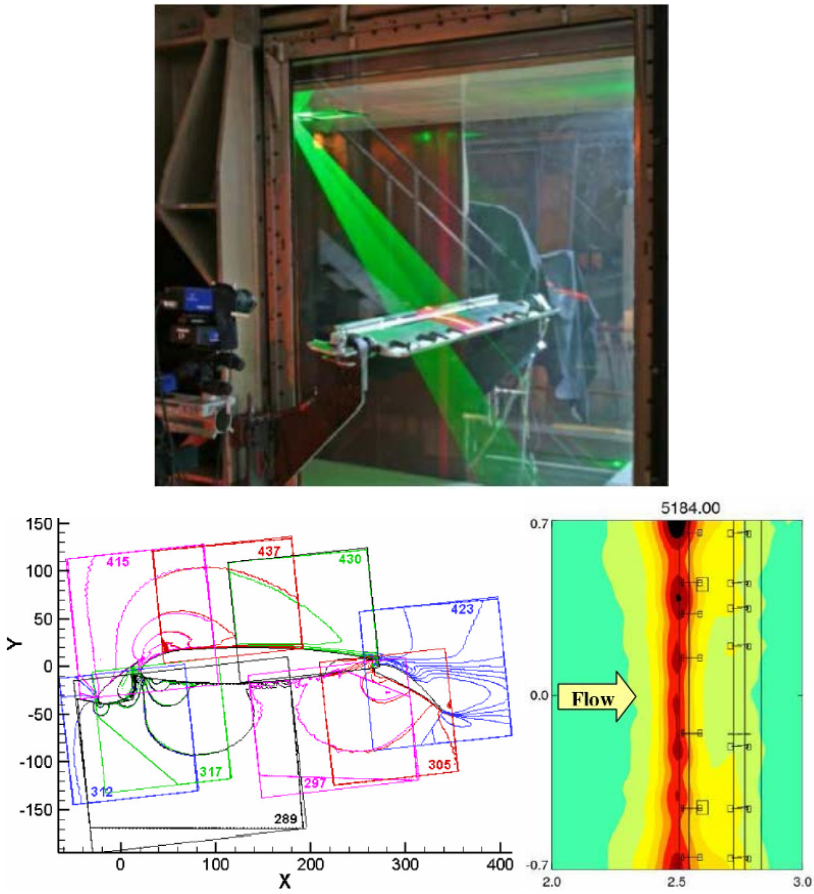

Fig. 1. LEISA2 experiments in F2 Onera closed wind tunnel. Top: 2D PIV test set-up in; left: mean flow PIV map; right: example of a noise source map at a given frequency obtained using classical acoustic beamforming

The final presentation will include a detailed comparison of Onera's numerical simulations (LES, LBM) with the experimental LEISA2 database for both aerodynamics and acoustics features. The feasibility of alternative methods, such as the Lattice-Boltzmann method, will be discussed to address aeroacoustics simulations of profiled bodies, after setting state of the art of such computations at Onera.

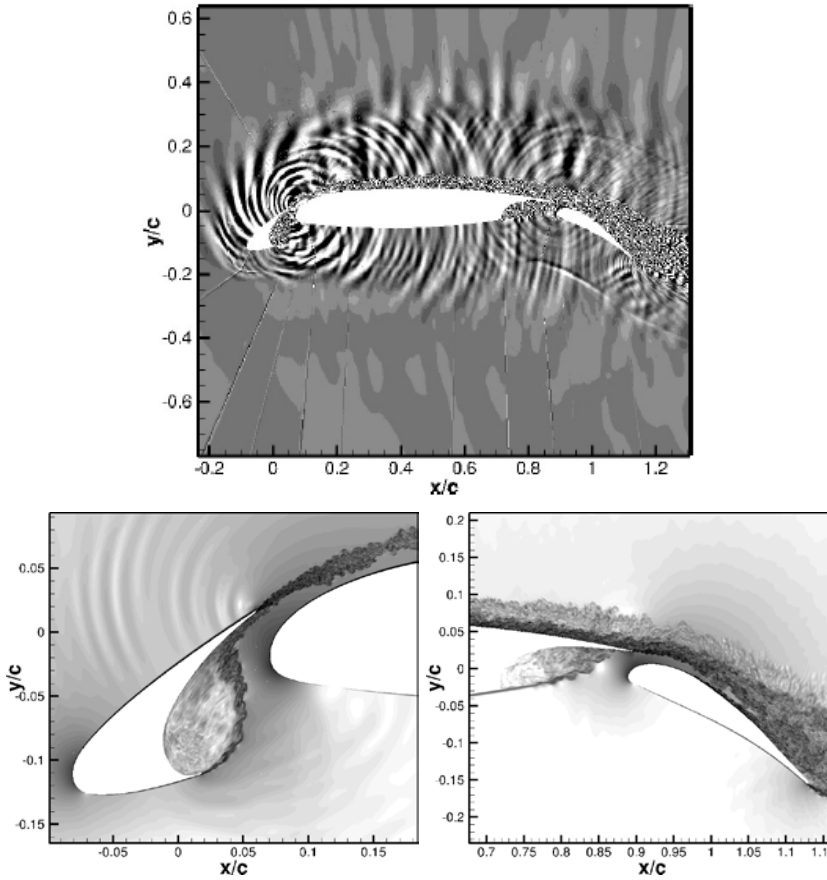

Fig. 2. FUNk computation, flow visualizations in the mid plane in the spanwise direction. Top: instantaneous view of the dilatation field; slat (left) and flap (right) numerical Schlieren visualizations

References

1. T. Imamura, S. Enomoto, Y. Yokokawa, and K. Yamamoto. Three-dimensional unsteady flow computations around a conventional slat of high-lift devices. AIAA Journal, 46:1045-1053, 2008.
2. M. Terracol, E. Manoha, and B. Lemoine. Investigation of the unsteady flow and noise sources generation in a slat cove: hybrid zonal RANS/LES simulation and dedicated experiment. AIAA Paper 2011-3203, 41st AIAA Fluid Dynamics Conference and Exhibit, Honolulu, Hawaii, 2011.

3. M. Terracol, E. Labourasse, E. Manoha, and P. Sagaut. Simulation of the 3D unsteady flow in a slat cove for noise prediction. AIAA paper 2003-3110, 9th AIAA/CEAS Aeroacoustics Conference and Exhibit, 2003.
4. M. Terracol, E. Manoha, C. Herrero, E. Labourasse, S. Redonnet, and P. Sagaut. Hybrid methods for airframe noise numerical prediction. Theor. Comput. Fluid Dyn., 19(3):197-227, 2005.
5. M. Choudhari and M.R. Khorrami. Effect of three-dimensional shear-layer structures on slat cove unsteadiness. AIAA Journal, 45:2174-2186, 2007.
6. S. Deck. Zonal detached-eddy simulation of the flow around a high-lift configuration. AIAA journal, 43:2372-2384, 2005.
7. S. Deck and R. Laraufie. Numerical investigation of the flow dynamics past a three-element airfoil. Journal of Fluid Mechanics, 732:401-444, 2013.
8. T. Knacke and F. Thiele. Time-resolved 3D simulation of an aircraft wing with deployed high-lift system. In P. Sagaut, T.H. Le, and Springer M. Deville, editors, Turbulence and Interactions Proceedings the TI 2009 Conference, pages 223-230, 2010.
9. T. Knacke and F. Thiele. Numerical analysis of slat noise generation. AIAA Paper 2013-2162, 19th AIAA/CEAS Aeroacoustics Conference, Berlin, Germany, 2013.
10. D.P. Lockard and M. Choudhari. Noise radiation from a leading-edge slat. AIAA paper 2009-3101, 15th AIAA/CEAS Aeroacoustics Conference, Miami, FL, USA, 11-13 May, 2009.
11. D.P. Lockard and M. Choudhari. The effect of cross flow on slat noise. AIAA paper 2010-3835, 16th AIAA/CEAS Aeroacoustics Conference, 2010.
12. B. Zhong, F. Scheurich, V. Titarev, and D. Drikakis. Turbulent flow simulations around a multi-element airfoil using URANS, DES and ILES approaches. AIAA paper 2009-3799, 19th AIAA Computational Fluid Dynamics Conference, 2009.
13. www.aiaa.com, AIAA Info > Technical Activities > Aerospace Sciences Group > Fluid Dynamics Technical Committee > DG > BECAN_files_ > BANCII_category6 > Summary_BANCII_Category_6_Slat_Noise_DLR_ ONERA DG: Summary_BANCII_Category_6_Slat_Noise_DLR_ ONERA
14. M. Terracol and E. Manoha, Wall-resolved Large Eddy Simulation of a high-lift airfoil: detailed flow analysis and noise generation study, AIAA paper 2014-3050, 20th AIAA/CEAS Aeroacoustics Conference, Atlanta, , USA, 16-19 June, 2014.
15. T. Le Garrec, D.C. Mincu, M. Terracol, D. Casalino, A. Ribeiro, Aeroacoustic prediction of the LEISA2 high lift airfoil : Lattice Boltzmann method vs. Navier-Stokes finite volume method and experiments, TI 2015 Conference, 2-6 November 2015.

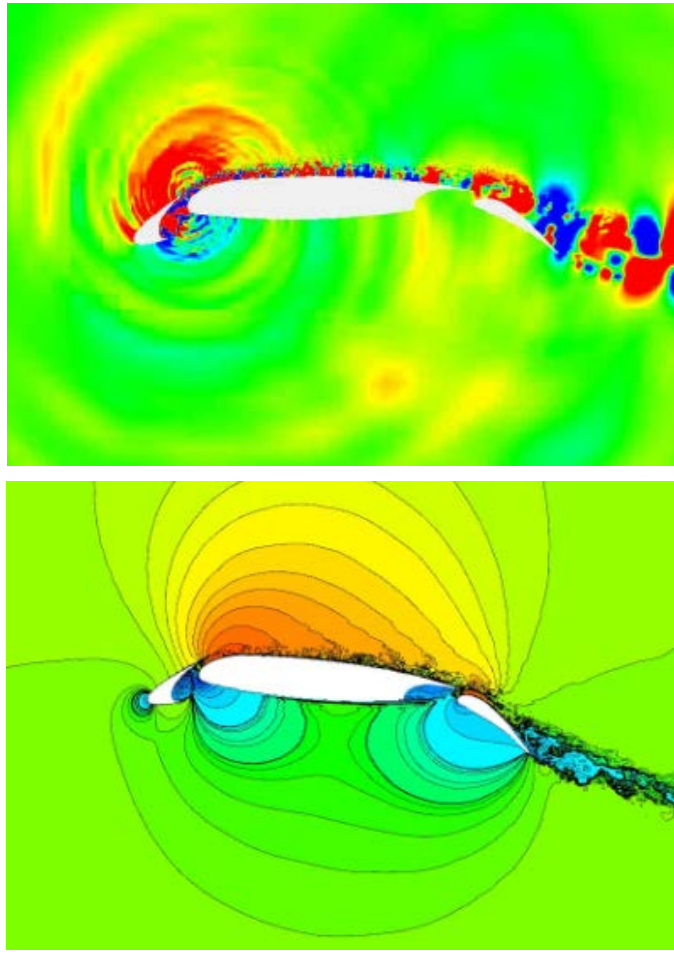

Fig. 3. Flow computations of the LEISA2 configuration with LBM solvers. Top: instantaneous view of the acoustical pressure field - PowerFLOW; bottom: Streamwise flow field - LaBS

NUMERICAL MODELING OF TURBOMACHINERY TONAL NOISE IN SPACE WITH COMPLEX ACOUSTIC IMPEDANCE BOUNDARY CONDITIONS

S.F. Timushev[1], V.N. Gavrilyuk[1], K.I. Volosenko[1], A.A. Aksenov[2]

[1]*Rocket Engines Department of the Moscow Aviation Institute (National Research University),125993, Moscow, 4, Volokolamskoye Highway, Russia, irico.harmony@gmail.com*

[2]*TESIS Ltd.127083 Moscow, 18/706, Unnatov st., Russia, andrey@tesis.com.ru*

Noise reduction in order to minimize its negative effects on the human ability to live in an open areas, residential, office and industrial buildings, cultural and religious institutions, car interiors, trains, planes and spaceship interiors, etc. is becoming more urgent issue. In developed countries it is given sustained attention, which is reflected in a significant tightening of the requirements for limiting the noise level in accordance with ISO standards [1,2].

For the practical solution of this problem this work proposes a new high-performance numerical simulation method of three-dimensional acoustic field of a tonal component on blade passing frequency and its higher and combined harmonics produced by blade machines in computer devices, air conditioning systems and in aircraft engines. This method is based on the direct solution by finite volume method of Fourier-transformed convective wave equation [5], that describes the propagation of sound in adiabatic and thermodynamically uniform irrotational stationary flow with respect to pressure perturbations in the form of Fourier transform

$$\frac{1}{c^2}\left(i\omega + U_k \frac{\partial}{\partial x_k}\right)^2 p = \frac{\partial^2 p}{\partial x_k^2} + F \quad , \qquad 1)$$

where c is the adiabatic speed of sound, U_k averaged flow velocity, F source term determined from the energy relation

$$\frac{1}{\sqrt{2\pi}} \int_S \int_{-\infty}^{+\infty} p(\omega - \xi) u_n(\xi) d\xi \cdot dS = W_l \delta(\omega - \omega_l) \qquad 2)$$

by the method of simple iteration in the co-solution of (1, 2) equations. Here S is the surface surrounding the source of acoustic disturbances at the distance of attenuation of vortex perturbations created by the source, ω_l is l-th Blade Passing Frequency (BPF) harmonic number, W_l known sound power at the l-frequency, obtained by acoustic-vortex method [8, 9].

Boundary conditions for (1) are defined on sound absorbing boundaries in the complex impedance form, taking into account both active and reactive component of the boundary impedance.

Noise reduction is achieved by the spatial redistribution of the tonal sound, which ensures its essential reduction in the areas of people location. Actually, the most effective technical means are multi-layered sound-absorbing cellular structures (SAS) [3], which can be installed on the inner surfaces of noise sources, and on the walls, ceilings and partitions of buildings. Optimal parameters of sound-absorbing structures (SAS) and their location can be determined by multi-parametric computations of spatial sound fields for each tonal components of interest using developed method [4].

Practical solution of the tonal noise control problem can only be dealt under the condition of correct setting of impedance boundary conditions on the SAS outer surfaces. In this paper, a new semi-empirical model proposed for the single-layer SAS, which is based on the original model Munin [6] and new experimental data obtained for a plate of plasterboard and plexiglass with different thickness, diameter and length of holes. The measurements were made in the impedance tube according to standard ISO 10534-2: 1998. The measuring system uses calibrated pair of microphones. The tube is excited by the white noise; the signals from the installed microphones are recorded in a file and are subject to subsequent computer processing using the correlation method.

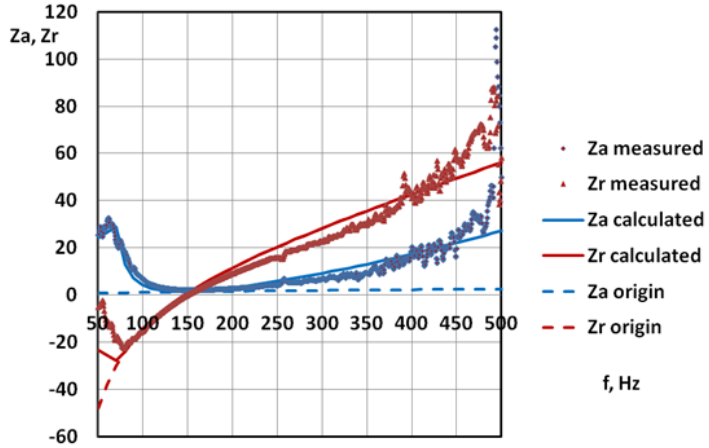

Fig. 1. Impedance of SAS; measurements and calculations using the new, modified model of SAS by Munin, and the original model

Fig. 1 shows the obtained experimental data and calculations of the active Za and reactive Zr components of impedance using the original model Munin (origin) and the new modified model (calculated) in the case of plates of plasterboard with a degree of perforation of F = 0.0025, hole diameter d = 5 mm, thickness t = 12 mm and volume length h = 20 mm.

Features of the new calculation method illustrated in the examples of calculation of the suppression of tonal noise at a frequency of 222.5 Hz in the room with a partition [4], as well as the simulation of the installation on the wall of the reverberation room with a given SAS impedance [10].

The proposed method allows determining the optimal parameters of SAS to ensure minimum sound radiation at a given frequency. This is shown by the example of reducing the tonal noise of the gas turbine unit by 5.39 dB at a frequency of 2100 Hz when using SAS with the specific impedance $Z = 4.0 - 4.0$ i.

Im Z \ Re Z	0.8	2	4	6	8
1			–3.52		
–0.5	–2.82	–3.94	–4.35	–4.04	–3.60
–2			–5.13		
–4			**–5.39**		
–5			–4.99		
–8			–3.08		

Table 1. Reduction of the sound power radiation dB as a function of SAS specific impedance Z

The acoustic calculations performed using the Cartesian grid (150x90x90) with the number of cells 662544 by adapting to the boundary of computational domain. The processing time for one case on the processor i7 is 44 minutes.

The proposed method of modeling the acoustic fields is very efficient in terms of minimization of computer and human resources and calculation accuracy. It can be used for optimization of impedance characteristics and location of SAS.

References

1. ISO 3740-1980 Acoustics – Determination of sound power levels of noise sources – Guidelines for the use of basic standards and for the preparation of noise test codes.
2. ISO 11690-1 (1996), ‘Acoustics – Recommended practice for the design of low-noise workplaces containing machinery – Part 1: Noise-control strategies’.
3. Siner A.A. Method of selection of sound-absorbing structures for turbomachinery based on mathematical modeling. (Thesis for the degree of Candidate of Technical Sciences, 2010) [in Russian].

4. A.A. Aksenov, V.N. Gavrilyuk and S.F. Timushev. Numerical Simulation of Tonal Fan Noise of Computers and Air Conditioning Systems. ISSN 1063_7710, Acoustical Physics, 2016, Vol. 62, No. 4, pp. 447–455. © Pleiades Publishing, Ltd., 2016. Original Russian Text © A.A. Aksenov, V.N. Gavrilyuk, S.F. Timushev, 2016, published in Akusticheskii Zhurnal, 2016, Vol. 62, No. 4, pp. 442–450.
5. J.M. Tyler, T.G. Sofrin, Axial flow compressor noise studies. Transactions of the society of automotive engineers, Vol.70, 1962, pp. 309–332.
6. A.G. Munin, V.M. Kuznetsov, E.A. Leontiev, Aerodynamic Noise Sources (Mashinostroenie, Moscow, 1981) [in Russian].
7. A.A. Aksenov, A.A. Dyad'kin, V.A. Kutin, I.V. Moskalev, G.B. Sushko, and S.A Kharchenko, in Proc. All-Russia Sci. Conf. "Scientific Service in INTERNET Net: Solution of Large Problems", Novorossiisk, 2008, pp. 22–27.
8. K.I. Artamonov, Thermohydroacoustical Stability (Mashinostroenie, Moscow, 1982) [in Russian].
9. Timouchev S., Tourret J., Pavic G., Aksenov A. Numerical 2-D and 3-D methods for computation of internal unsteady pressure field and near-field noise of fans (Conference Paper) Noise Control Engineering Journal, Vol.54, Issue 1, January 2006, Pages 15–20.
10. V.N. Gavrilyuk, S.F. Timushev, A.A. Aksenov, Efficient Numerical Method for Spatial Tonal Noise Computation. International Conference on the Methods of Aerophysical Research, June 27 – July 3, 2016, Perm, Russia: Abstracts. Pt. II, pp. 74–75.

BUILDING A NEW SUBGRID CHARACTERISTIC LENGTH FOR LES

F.X. Trias[1], A. Gorobets[1,2], A.P. Duben[2] and A. Oliva[1]
[1]*CTTC UPC, ETSEIAT, C/Colom 11, 08222 Terrassa, Spain*
[2]*KIAM RAS, 4A, Miusskaya Sq., Moscow 125047, Russia*

1. Introduction

We consider the numerical simulation of the incompressible Navier–Stokes (NS) equations. In primitive variables they read

$$\partial_t \mathbf{u} + \left(\mathbf{u}\cdot\nabla\right)\mathbf{u} = \nu\nabla^2\mathbf{u} - \nabla p, \quad \nabla\cdot\mathbf{u} = 0, \tag{1}$$

where $\mathbf{u}$ denotes the velocity field, p represents the kinematic pressure and ν is the kinematic viscosity. Direct simulations at high Reynolds numbers are not feasible because the convective term produces far too many scales of motion. Hence, in the foreseeable future, numerical simulations of turbulent flows will have to resort to models of the small scales. The most popular example thereof is the Large-Eddy Simulation (LES). Shortly, LES equations result from applying a spatial commutative filter, with filter length δ, to the NS Eqs. (1)

$$\partial_t \overline{\mathbf{u}} + \left(\overline{\mathbf{u}}\cdot\nabla\right)\overline{\mathbf{u}} = \nu\nabla^2\overline{\mathbf{u}} - \nabla\overline{p} - \nabla\cdot\tau(\overline{\mathbf{u}}), \quad \nabla\cdot\overline{\mathbf{u}} = 0, \tag{2}$$

where $\overline{\mathbf{u}}$ is the filtered velocity and $\tau(\overline{\mathbf{u}})$ is the subgrid stress tensor and aims to approximate the effect of the under-resolved scales, i.e. $\tau(\overline{\mathbf{u}}) \approx \overline{\mathbf{u}\otimes\mathbf{u}} - \overline{\mathbf{u}}\otimes\overline{\mathbf{u}}$. Because of its inherent simplicity and robustness, the eddy-viscosity assumption is by far the most used closure model

$$\tau(\overline{\mathbf{u}}) \approx -2\nu_e S(\overline{\mathbf{u}}), \tag{3}$$

where ν_e denotes the eddy-viscosity. Following the same notation as in [1], the eddy-viscosity can be modeled as follows

$$\nu_e = (C_m\delta)^2 D_m(\overline{\mathbf{u}}). \tag{4}$$

In the last decades most of the research has primarily focused on either the calculation of the model constant, C_m (e.g. the dynamic modeling approach), or the development of more appropriate model operators $D_m(\overline{\mathbf{u}})$ (e.g. WALE, Vreman's, Verstappen's, σ-model, S3PQR, ...). Surprisingly, little attention has been paid on the computation of the subgrid characteristic length, δ, which is also a key element of any eddy-viscosity model. Despite the fact that in some situations it may provide very inaccurate results, three and a half decades later, the approach proposed by Deardoff [2], i.e., the cube root of the cell volume (see Eq. 5), is by far the most widely used to computed the subgrid characteris-

tic length, δ. Its inherent simplicity and applicability to unstructured meshes is probably a very good explanation for that. Alternative methods to compute δ are summarized and classified in Table 1 according to a list of desirable properties for a (correct) definition of δ. Namely,

$$\delta_{\mathrm{vol}} = (\Delta x \Delta y \Delta z)^{1/3}, \qquad \delta_{\mathrm{Sco}} = f(a_1, a_2)\delta_{\mathrm{vol}}, \tag{5}$$

$$\delta_{\mathrm{max}} = \max(\Delta x, \Delta y, \Delta z), \qquad \delta_{L^2} = \sqrt{(\Delta x^2 + \Delta y^2 + \Delta z^2)/3}, \tag{6}$$

$$\delta_{\boldsymbol{\omega}} = \sqrt{(\omega_x^2 \Delta y \Delta z + \omega_y^2 \Delta x \Delta z + \omega_z^2 \Delta x \Delta y)/|\boldsymbol{\omega}|^2}, \quad \tilde{\delta}_{\boldsymbol{\omega}} = \frac{1}{\sqrt{3}} \max_{n,m=1,\ldots,8} |\mathbf{l}_n - \mathbf{l}_m|, \tag{7}$$

$$\delta_{\mathrm{SLA}} = \delta_{\boldsymbol{\omega}} F_{\mathrm{KH}}(VTM), \tag{8}$$

where $\boldsymbol{\omega} = (\omega_x, \omega_y, \omega_z) = \nabla \times \mathbf{u}$ is the vorticity and $f(a_1, a_2) = \cosh\sqrt{4/27[(\ln a_1)^2 - \ln a_1 \ln a_2 + (\ln a_2)^2]}$ ($a_1 = \Delta x / \Delta z$, $a_2 = \Delta y / \Delta z$, assuming that $\Delta x \le \Delta z$ and $\Delta y \le \Delta z$) is the correcting function proposed by Scotti [3].

	δ_{vol}	δ_{Sco}	δ_{max}	δ_{L^2}	$\delta_{\boldsymbol{\omega}}$	$\tilde{\delta}_{\boldsymbol{\omega}}$	δ_{SLA}	δ_{lsq}
Reference	[2]	[3]	[6]		[7]	[5]	[4]	
Formula	Eq.5	Eq.5	Eq.6	Eq.6	Eq.7	Eq.7	Eq.8	Eq.13
P0	Yes	Yes	Yes	Yes	Yes	Yes	Yes	Yes
P1	Yes	Yes	Yes	Yes	Yes	Yes	Yes	Yes
P2	No	No	No	No	Yes	Yes	Yes	Yes
P3	Yes	No	No	No	No*	Yes	Yes	Yes
P4	+++	++	++++	+++	++	+	+	+++

Table. 1. Properties of different definition of the subgrid characteristic length δ. Namely, **P0**: $\delta \ge 0$, locality and frame invariant; **P1**: boundedness, i.e., given a structured Cartesian mesh where $\Delta x \le \Delta y \le \Delta z$, $\Delta x \le \delta \le \Delta z$; **P2**: sensitive to flow orientation; **P3**: applicable to unstructured meshes; **P4**: well-conditioned and low computational cost. *Deck [8] proposed a generalization for unstructured meshes.

The function $0 \le F_{\mathrm{KH}}(VTM) \le 1$ has been recently proposed by Shur et al. [4] to correct the δ_ω definition proposed by Mockett et al. [5], both in the context of Detached Eddy Simulation (DES). These properties are based on physical, numerical, and/or practical arguments. This list is completed with the definition of δ_{lsq} given in Eq.(13) and introduced in this section. According to property **P2**, they can be classified into two main families; namely, (i) definitions of δ that solely depend on geometrical properties of the mesh, and (ii) definitions of δ that are also dependent on the local flow topology. The latter is characterized by the gradient of the resolved velocity field, $G \equiv \nabla \overline{\mathbf{u}}$. This is a second-order

traceless tensor, $tr(G) = \nabla \cdot \overline{\mathbf{u}} = 0$. Therefore, it seems logical that a flow-dependent definition of δ should be based on the tensor G. On the other hand, the local mesh geometry for a Cartesian grid is contained in the following second-order diagonal tensor,

$$\Delta \equiv \mathrm{diag}(\Delta x, \Delta y, \Delta z). \tag{9}$$

Hereafter, we take $\Delta x \le \Delta y \le \Delta z$ without loss of generality. Therefore, methods solely based on the geometrical properties of the mesh are fully characterized by the tensor Δ. Apart from the geometric information contained in Δ, the other methods are also dependent on the flow topology, i.e., G.

2. Building a new subgrid characteristic length

The subgrid characteristic length δ appears in a natural way when we consider the leading term of the Taylor series expansion of the subgrid stress tensor,

$$\tau(\overline{\mathbf{u}}) = \frac{\delta^2}{12} GG^T + O(\delta^4). \tag{10}$$

This is the gradient model proposed by Clark et at. [9], where in this case δ denotes the filter length. The local dissipation of gradient model is then proportional to $-GG^T : S = -tr(^T) = 1/3(tr(G^3) - 4tr(S^3)) = R_G - 4R_S$ (refer to our previous work [10] for a definition of the tensor invariants R_G and R_S). Hence, the local dissipation introduced by the model, i.e., $(\delta^2/12)(R_G - 4R_S)$, can take negative values; therefore, the gradient model cannot be used as a standalone LES model, since it produces a finite-time blow-up of the kinetic energy [11]. For anisotropic filter lengths, the Taylor expansion of the subgrid stress tensor gives

$$\tau(\overline{\mathbf{u}}) = \frac{\delta^2}{12} G_\delta G_\delta^T + O(\delta^4), \tag{11}$$

where $G_\delta \equiv G\Delta$. Therefore, in this case the subgrid dissipation can be approximated as $-(1/12)G_\delta G_\delta^T : S$. Then, equating the dissipations of the leading terms of Eqs. (10) and (11), i.e., $-(\delta^2/12)GG^T : S = -(1/12)G_\delta G_\delta^T : S$, leads to the following definition of δ

$$\delta_{\mathrm{diss}} = \sqrt{\frac{G_\delta G_\delta^T : S}{GG^T : S}}. \tag{12}$$

Another possibility consists on minimizing the difference between the leading term tensors of Eqs. (10) and (11), i.e. $(\delta^2/12)GG^T \approx (1/12)G_\delta G_\delta^T$. A least-square minimization leads to

$$\delta_{\text{lsq}} = \sqrt{\frac{G_\delta G_\delta^T : GG^T}{GG^T : GG^T}}. \tag{13}$$

The expression given in Eq. (12) does not constitute a proper definition of δ since basic properties **P0**, **P1** and **P4** are not guaranteed (see Table 1). Namely, as mentioned above, (minus) the denominator, $-GG^T : S = R_G - 4R_S$ may take non-positive values. The numerator is not bounded either and it may eventually have a different sign than the denominator. On the other hand, the definition of δ does not suffer all these pathologies. It is locally defined and well bounded, $\Delta x \le \delta_{\text{lsq}} \le \Delta z$; therefore it meets properties **P0** and **P1**. Moreover, it is obviously sensitive to flow orientation (property **P2**) and applicable to unstructured meshes (property **P3**). In this regard, for purely rotating flows, i.e., $S = 0$ and $G = \Omega$, quantity δ_{lsq} reduces to

$$\delta_{\text{lsq}} = \sqrt{\frac{\omega_x^2(\Delta y^2 + \Delta z^2) + \omega_y^2(\Delta x^2 + \Delta z^2) + \omega_z^2(\Delta x^2 + \Delta y^2)}{2\,|\boldsymbol{\omega}|^2}}, \tag{14}$$

which resembles the definition of δ_ω given in Eq.(7) proposed by Chauvet et al [7]. Actually like the definition δ_ω given in Eq.(7) proposed by Mockett et al [5] it is $O(\max\{\Delta x, \Delta y\})$ instead of $\delta_\omega = \sqrt{\Delta x \Delta y}$; therefore, it also avoids a strong effect of the smallest grid spacing.

3. Conclusions and preliminary results

The objective of this work is to test the influence of the definition of δ on highly anisotropic meshes. To do so, different approaches will be tested and compared using (artificially) anisotropic meshes with the aim to answer the following research question: *can we find a simple and robust definition of the subgrid characteristic length that minimizes the effect of mesh anisotropies on the performance of subgrid-scale models?* In this regard, we consider the novel definition of δ_{lsq} proposed in Eq.(13) as a very good candidate. Preliminary results displayed in Fig. 1 correspond to the classical experimental results obtained by Comte-Bellot and Corrsin [12]. Two different anisotropic meshes have been considered; namely, $32 \times 128 \times 32$ and $128 \times 128 \times 32$. As expected, $\delta_{\max}$ introduces too much subgrid dissipation specially for the second test-case. It is remarkable that the definition δ_{lsq} proposed in Eq.(13) performs similarly (or even slightly better) than the δ_ω and δ_{SLA} proposed in the context of DES. Therefore, we consider that the here proposed definition of the subgrid charac-

teristic of the filter length is a good option to be used for LES in complex geometries (with unstructured grids too) but also in the context of DES.

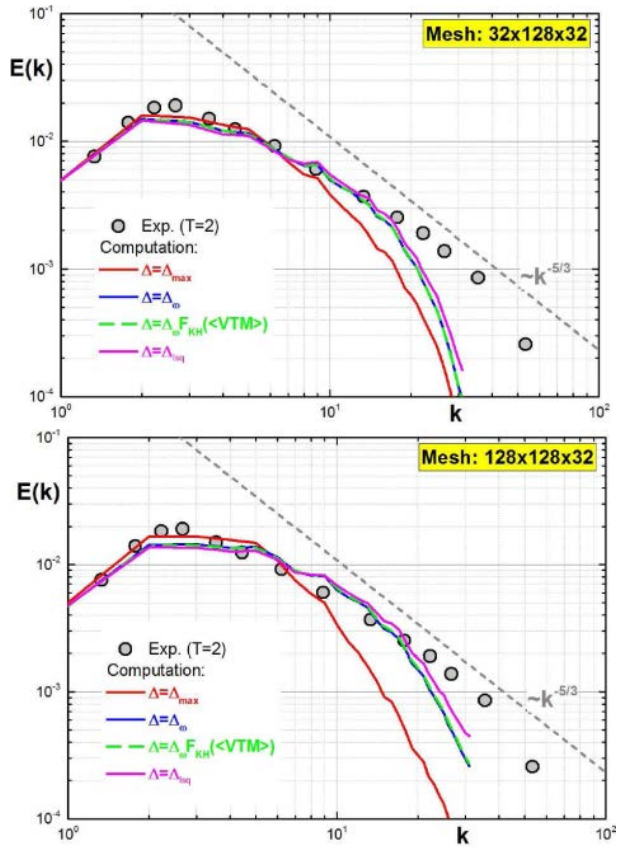

Fig. 1. Three-dimensional energy spectra for the decaying isotropic turbulence corresponding to the Comte-Bellot and Corrsin [12] experiment. LES results have been obtained with two different anisotropic meshes using Smagorinsky model and different definitions of the filter length, δ.

References

1. F. Nicoud, H.B. Toda, O. Cabrit, S. Bose, and J. Lee. Using singular values to build a subgrid-scale model for large eddy simulations. Physics of Fluids, 23(8):085–106, 2011.
2. J. W. Deardorff. Numerical study of three-dimensional turbulent channel flow at large Reynolds numbers. J. of Fluid Mechanics, 41:453–480, 1970.

3. A. Scotti, C. Meneveau, and D.K. Lilly. Generalized Smagorinsky model for anisotropic grids. Physics of Fluids A, 5(9):2306–2308, 1993.
4. M.L. Shur, P.R. Spalart, M.K. Strelets, and A.K. Travin. An Enhanced Version of DES with Rapid Transition from RANS to LES in Separated Flows. Flow, Turbulence and Combustion, 95:709–737, 2015.
5. C. Mockett, M. Fuchs, A. Garbaruk, M. Shur, P. Spalart, M. Strelets, F. Thiele, and A. Travin. Two Non-zonal Approaches to Accelerate RANS to LES Transition of Free Shear Layers in DES. In Progress in Hybrid RANS-LES Modelling, volume 130 of Notes on Numerical Fluid Mechanics and Multidisciplinary Design, pages 187–201. Springer Intl. Publishing, 2015.
6. P.R. Spalart, W.H. Jou, M. Strelets, and S.R. Allmaras. Comments on the feasibility of LES for wings, and on a hybrid RANS/LES approach. In: C. Liu & Z. Liu (eds.) Advances in DES/LES. Greyden Press, 1997.
7. N. Chauvet, S. Deck, and L. Jacquin. Zonal detached eddy simulation of a controlled propulsive jet. AIAA Journal, 45(10):2458–2473, 2007.
8. S. Deck. Recent improvements in the Zonal Detached Eddy Simulation (ZDES) formulation. Theoretical and Computational Fluid Dynamics, 26(6):523–550, 2012.
9. R.A. Clark, J.H. Ferziger, and W.C. Reynolds. Evaluation of subgrid-scale models using an accurately simulated turbulent flow. Journal Fluid Mechanics, 91:1–16, 1979.
10. F.X. Trias, D. Folch, A. Gorobets, and A. Oliva. Building proper invariants for eddy-viscosity subgrid-scale models. Physics of Fluids, 27(6):065103, 2015.
11. B. Vreman, B. Geurts, and H. Kuerten. Large-eddy simulation of the temporal mixing layer using the Clark model. Theoretical and Computational Fluid Dynamics, 8:309–324, 1996.
12. G. Comte-Bellot and S. Corrsin. Simple Eulerian time correlation of full- and narrow-band velocity signals in grid-generated, isotropic turbulence. Journal of Fluid Mechanics, 48:273–337, 1971.

APPLICATION EXPERIENCE OF LARGE EDDY SIMULATION FOR THE TASK OF AIRPLANE VORTEX WAKE

I.S. Bosnyakov[1, 2], G.G. Soudakov[1]

[1] *Central Aerohydrodynamic Institute named after prof. N.E. Zhukovsky (TsAGI), Zhukovsky, Russia, e-mail: bossig@yandex.ru*

[2] *Moscow Institute of Physics and Technology (state university), Dolgoprudhy, Russia*

Setup for the tasks of airplane vortex wake varies sufficiently both in structure and in key parameters that are defined by flight regime. Two sets of tasks could be conditionally marked out: cruise flight and flight in ground proximity. The vortex wake in cruise flight conditions is formed mainly by tip vortices with very small core radius (~0.2-0.5m). The situation is different in ground proximity due to the presence of flaps that generate additional vortices and alter radius of tip vortex core to the values of 1.5-3.5m as well. This essentially changes the flow structure. In addition, the circulation of wake vortices varies due to different flight speeds and air density at different altitudes, not sufficiently however.

In this paper the tasks are solved numerically, in non-linear setup by means of large eddy simulation (LES) method [1]. The study is held using ANSYS application software complex. Second order schemes, both in space and time, are adopted, with sufficient resources having been involved. The CPU time for computation of one case is estimated by the value of 3 weeks of continuous work on compact supercomputer, with dense computational grid of 100 million cells being used.

Preliminary testing has been held. It involves estimations of numerical method dissipative properties and assertion of computation results accuracy, which is tested on the tasks that have analytical or reference solutions. Among such tasks the dissipation of homogeneous isotropic turbulence case should be mentioned. Different ways of computational mesh generation and task adaptation to the architecture of available computer are discussed as well. The special attention is paid to the validity of results in cases where scheme viscosity could distort the task physics.

A part of the study is devoted to discussion of the results obtained with engineering methodologies. Numerical and approximate solutions have been matched and conclusions on the accuracy of utilized engineering models have been outlined.

The resultant part of the study contains data about evolution of vortex wake in time. The series of computations of practical importance has been held. Their initialization involves velocity field from vortex wake behind big aircraft obtained from model [2] and background turbulence. Studied are two suffi-

ciently different cases: 1) uniform and isotropic turbulence at cruise flight and 2) ground boundary layer with side gradient wind. Analysis and comparison of experimental and numerical data has been held.

The work was supported by Russian Ministry of Education and Science within the Federal Target Program “Studies and Designs on Priority Directions of the Russian Science-Technology Complex Development in 2014-2020” No. 14.628.21.0005, unique project identifier: RFMEFI62815X0005.

References

1. Garnier E. et al., Large Eddy Simulation for Compressible Flows, Scientific Computation, Springer Science + Business Media B.V., 2009
2. Shen S. H., Ding F., Han J., Lin Y. L., Arya S. P., Proctor F. H. Numerical modeling studies of wake vortices: real case simulations, 1999, AIAA Paper 0755.

Authors Index

Scientific publication

Fourth International Workshop

COMPUTATIONAL EXPERIMENT
IN AEROACOUSTICS

Book of abstracts

September 20-24, 2016
Svetlogorsk
Kaliningrad region
Russia

Makeup: *L.V. Dorodnitsyn*
Cover: *A.V. Gorobets*

Подписано в печать 05.09.2016. Формат 60x84/16. Усл. печ. л. 8,7. Тираж 155 экз. Заказ С-6.
ИПМ им. М.В. Келдыша РАН, 125057, Москва, Миусская пл., 4